

**For Reference**

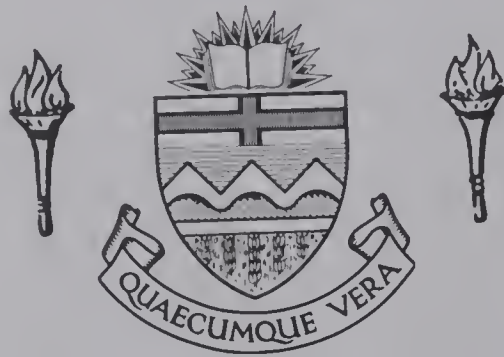
---

**NOT TO BE TAKEN FROM THIS ROOM**

# For Reference

NOT TO BE TAKEN FROM THIS ROOM

Ex LIBRIS  
UNIVERSITATIS  
ALBERTAENSIS











THE UNIVERSITY OF ALBERTA

THE  $^{40}\text{Ca}(\text{d},\text{d})^{40}\text{Ca}$  AND  $^{40}\text{Ca}(\text{d},\text{p})^{41}\text{Ca}$  REACTIONS

by

Henry George Leighton



A THESIS

SUBMITTED TO THE FACULTY OF GRADUATE STUDIES  
IN PARTIAL FULFILLMENT OF THE REQUIREMENTS FOR THE DEGREE  
OF DOCTOR OF PHILOSOPHY

DEPARTMENT OF PHYSICS  
EDMONTON, ALBERTA

March, 1968





UNIVERSITY OF ALBERTA

FACULTY OF GRADUATE STUDIES

The undersigned certify that they have read, and recommend to the Faculty of Graduate Studies for acceptance, a thesis entitled THE  $^{40}\text{Ca}(\text{d},\text{d})^{40}\text{Ca}$  AND  $^{40}\text{Ca}(\text{d},\text{p})^{41}\text{Ca}$  REACTIONS, submitted by Henry George Leighton in partial fulfillment of the requirements for the degree of Doctor of Philosophy.



## ABSTRACT

The absolute cross-sections for the elastic scattering of deuterons from calcium were measured for incident deuteron energies of 5.0, 6.0 and 6.5 MeV. Using the parameters obtained from optical model analyses of these distributions, the predictions of distorted wave Born approximation calculations were compared with measured  $^{40}\text{Ca}(d,p)^{41}\text{Ca}$  stripping distributions leaving  $^{41}\text{Ca}$  in the ground, 1.95, 2.47 and 3.95 MeV states. In addition, the polarization of the protons from the ground state reaction was also measured and compared with the results of the DWBA calculations. The code DWUCK (Ku 67) was used for the DWBA calculations. Fair agreement was found between the calculations and stripping distributions, however, the predicted polarization was opposite in sign to that measured.

This work was part of a cooperative study by a number of groups at this laboratory to extend to lower energy and to extend in scope the experimental information available from deuteron induced reactions on calcium. The  $^{40}\text{Ca}(d,n)^{41}\text{Sc}_{g.s.}$  angular distributions and polarization have been measured previously (Gr 67, Ge 67) and the data from these experiments have also been compared with DWBA calculations. Similar conclusions to those found in the proton experiments apply here also.



## ACKNOWLEDGEMENTS

I wish to express my gratitude to my supervisor Dr. G. Roy.

Apart from the effort he spent on designing both the target chamber and the polarimeter, I am grateful for the advice, encouragement and enthusiasm that he has communicated to me over the last two and one half years.

The deep involvement of Mr. David Gurd in these experiments is greatly appreciated. Although he was primarily concerned with a similar series of experiments on silicon, the dividing line was often very fine. His help, advice and good humour were basic in the successful completion of this work.

I would like to thank Mr. Jan Bogaards and Mr. Bob Humphries for their help in the data taking, particularly during the seemingly never ending week of running during which most of the polarization data were accumulated.

I am also grateful to Dr. P.D. Kunz for making his DWBA code available to us, and to Drs. G.M. Stinson, S.M. Tang and S.S.M. Wong for adapting it for use on the University of Alberta IBM 360 computer.

Discussions with Dr. Dale Gedcke and Dr. Tom Grandy, as well as with Drs. Stinson, Tang and Wong concerning aspects of the analysis, are appreciated.

Thanks are also due to Mr. Norman Davison who was kind enough to supply the Hauser-Feshbach calculations.





The care of Mr. Nick Riebeck and his staff in machining the target chamber and polarimeter is gratefully acknowledged.

I would also like to thank Mr. Jock Elliott and the other members of the laboratory technical staff for the excellent support they have provided.

Miss Elsie Hawirko is to be commended on her great care in typing this thesis, and Mr. Jock Elliott for transcribing what were little more than free hand sketches into the drawings contained in this report.

I appreciate the financial support provided by the University of Alberta throughout the course of this work.

Finally, I wish to thank my wife for her patience and understanding during the long years of graduate study.





## TABLE OF CONTENTS

	Page
CHAPTER 1      INTRODUCTION	1
1.1      Background and Motivation	1
1.2      Optical Model Theory	8
1.3      DWBA Theory of Stripping Reactions	10
CHAPTER 2      EXPERIMENTAL METHODS	15
2.1      Elastic Scattering and (d,p) Stripping Distribu- tions	15
2.2      The Proton Polarimeter	21
2.3      Polarimeter Tests	28
2.4      Calibration of the Polarimeter	31
CHAPTER 3      RESULTS AND ANALYSIS	38
3.1      Yield Curves	38
3.2      Elastic Scattering	40
3.3      Stripping Distributions	61
3.4      Polarization Distributions	82
CHAPTER 4      CONCLUSIONS	89
REFERENCES	92



# LIST OF TABLES

	Page
Table 2.1 The polarimeter analyzing power	36
Table 3.1 Elastic scattering cross-sections	41
Table 3.2 Set I potential parameters	50
Table 3.3 Set II potential parameters	52
Table 3.4 Set III potential parameters	53
Table 3.5 $\chi^2$ as a function of normalizing factor	56
Table 3.6 Set IV potential parameters	60
Table 3.7 $^{40}\text{Ca}(d,p)^{41}\text{Ca}$ cross-sections	63
Table 3.8 Captured neutron well depths	69
Table 3.9 Spectroscopic factors for the ground states of $^{41}\text{Ca}$ and $^{41}\text{Sc}$	78
Table 3.10 Spectroscopic factors for states in $^{41}\text{Ca}$	79
Table 3.11 Polarization distribution	83
Table 3.12 Potentials used in polarization calculations	86



## LIST OF FIGURES

	Page
Fig. 1.1      The lower energy levels of $^{41}\text{Ca}$ and $^{41}\text{Sc}$	6
Fig. 2.1      A typical step wedge spectrum	17
Fig. 2.2      Plot of counting rate against Rutherford scattering cross-section	20
Fig. 2.3      Schematic diagram of experimental apparatus	22
Fig. 2.4      Inside view of polarimeter	25
Fig. 2.5      Photograph of the polarimeter	26
Fig. 2.6      Block diagram of electronics	27
Fig. 2.7      Sensitivity test of polarimeter	30
Fig. 2.8      Effect of $\frac{dE}{dX}$ detector on polarimeter spectrum	33
Fig. 2.9      Polarimeter calibration measurement	34
Fig. 3.1      Excitation functions	39
Fig. 3.2      Elastic scattering distributions and optical model fits	42
Fig. 3.3      Results of optical model searches on 5 MeV elastic scattering data	46
Fig. 3.4      Results of optical model searches on 6 MeV elastic scattering data	47
Fig. 3.5      Results of optical model searches on 6.5 MeV elastic scattering data	48
Fig. 3.6      Results of optical model searches on 7 MeV elastic scattering data	49
Fig. 3.7      Set III and 'best Z' parameters as a function of deuteron energy	55



Fig. 3.8	Optical model fits to renormalized 6 and 6.5 MeV elastic scattering data	57
Fig. 3.9	Compound elastic scattering distributions	62
Fig. 3.10	$^{40}\text{Ca}(\text{d},\text{p})^{41}\text{Ca}_{\text{g.s.}}$ distribution, $E_{\text{d}} = 5$ MeV, including Set III and Set IV DWBA calculations	64
Fig. 3.11	$^{40}\text{Ca}(\text{d},\text{p})^{41}\text{Ca}_{\text{g.s.}}$ distribution, $E_{\text{d}} = 6$ MeV, including Set III and Set IV DWBA calculations	65
Fig. 3.12	$^{40}\text{Ca}(\text{d},\text{p})^{41}\text{Ca}^*$ distributions, $E_{\text{d}} = 5$ MeV, including Set III DWBA calculations	66
Fig. 3.13	Comparison of $^{40}\text{Ca}(\text{d},\text{p})^{41}\text{Ca}_{\text{g.s.}}$ distribution with the Set I and Set II DWBA calculations	74
Fig. 3.14	Comparison of $^{40}\text{Ca}(\text{d},\text{n})^{41}\text{Sc}_{\text{g.s.}}$ distributions with the Set I and Set II DWBA calculations	75
Fig. 3.15	Comparison of $^{40}\text{Ca}(\text{d},\text{n})^{41}\text{Sc}_{\text{g.s.}}$ distributions with the Set III and Set IV DWBA calculations	76
Fig. 3.16	$^{40}\text{Ca}(\text{d},\text{p})^{41}\text{Ca}$ and $^{40}\text{Ca}(\text{d},\text{n})^{41}\text{Sc}$ polarization distributions	84
Fig. 3.17	Comparison of DWBA calculations with proton polarization distribution	87







## CHAPTER 1

### INTRODUCTION

#### 1.1 Background and Motivation

Deuteron stripping reactions provide an extremely useful tool for obtaining spectroscopic information about nuclei. The earliest analysis of such reactions was in terms of Butler's Plane Wave Theory (Bu 50, 51, 52, 57) in which the incoming deuteron and outgoing nucleon were described by plane waves. This theory enjoyed considerable success in predicting the angular momentum of the transferred nucleon, that is in predicting relative parities of the initial and final states and the range of possible  $\ell$ -values for the final state. The main failings of the theory were that for heavy nuclei the assignment of  $\ell$ -values was often ambiguous, and more serious, that for the whole range of nuclei the magnitude of the absolute cross-section was often overestimated by an order of magnitude or more. The ratio of the experimental to theoretical stripping cross-sections, the spectroscopic factor, provides a measure of the single particle strength of a state and so is important in understanding the structure of the nucleus.

These discrepancies led to the proposal of the distorted wave Born approximation (DWBA) theory (Au 63, To 61, Sa 64). In this theory, the plane waves are replaced by waves that are distorted by the nuclear



potential. In practice, the distorted waves are generated by the optical potentials that are used to describe the elastic scattering of the deuteron from the target nucleus and the scattering of the outgoing nucleon from the residual nucleus. So in principle, to apply the theory correctly, one should first measure the corresponding elastic scatterings and then carry out optical model fits in order to generate the correct potentials. It is in the spirit of the optical model, however, that the potential should be smoothly varying as a function of energy and mass number. This has meant, in the case of the nucleon potential, that it has been possible to generate an average potential that provides good agreement to almost the whole body of elastic scattering and the corresponding polarization distributions (Ro 65, Ro 66, Pe 62, Pe 63a, Pe 66a). The same is not true for the deuteron optical potential. Perey has found large fluctuations in the potential parameters as a function of both mass and energy (Pe 63b, 66b). One of the reasons for this may be the sensitivity of the parameters to the absolute normalization of the scattering distribution, especially when the diffraction pattern is not well pronounced (Di 65). Thus at present, it is still necessary to measure the deuteron elastic scattering.

The situation is unfortunately complicated even further. The optical model analysis of deuteron elastic scattering is not unique. It has been found (Pe 63b, Ha 64, Pe 66b) that families of potentials characterized by the real potential well depth exist, that give the same elastic scattering distributions. At one time, it appeared that





the best overall agreement resulted from using a potential with a well depth of approximately 60 MeV. The most recent indications (Le 64, Pe 66b) are that the most satisfactory well depth is of the order of 100 MeV, that is the sum of the two nucleon potentials. This value is corroborated by the results of calculations of the deuteron optical potential starting from the nucleon potentials (Co 67, Pe 67).

In addition to the above type of ambiguity, there are also ambiguities in the potentials resulting from correlations in the parameters. Examples of this would be the well-known  $Vr^n = \text{const.}$  and  $W_D a' = \text{const.}$  relations. Other more complicated correlations also exist and these almost certainly contribute to some of the fluctuations found in deuteron optical potential parameters. Part of the motivation for performing the experiments reported here in conjunction with the related neutron experiments was the hope of removing some of the ambiguities in the optical model by requiring that the same potentials describe all of the experimental results.

DWBA theory has been highly successful in predicting the angular distributions and absolute cross-sections of deuteron stripping reactions. However, in recent years, some limitations of the theory in its present form have become more apparent. The comprehensive study of the  $^{40}\text{Ca}(d,p)^{41}\text{Ca}$  reaction in the energy range 7 - 12 MeV by Lee (Le 64) shows a lack of agreement between theory and experiment for the ground state  $\ell = 3$  reaction. From a study of the  $^{52}\text{Cr}(d,p)^{53}\text{Cr}$  reaction, Legg et al. (Le 66) find that the  $\ell = 1$  stripping distributions are



fit reasonably well by DWBA calculations whereas the  $\ell = 3$  distribution leading to the 1.01 MeV state of  $^{53}\text{Cr}$  is not. The most serious disagreements between experiment and theory, however, are for polarization distributions. Hjorth (Hj 65) found no satisfactory agreement in the study of the  $^{40}\text{Ca}(d,p)^{41}\text{Ca}$  reaction at 14.3 MeV. Toosi and Ivash (To 68) in an attempt to fit the cross-sections and polarizations for 13 different reactions in a study involving the calculations of approximately 6000 distributions achieved only fair agreement in many cases.

The inadequacies of the theory have led to different approaches. On the one hand, there have been efforts to improve the present form of DWBA theory. Johnson and Santos, for instance, (Jo 67) have shown that inclusion of the deuteron D-wave in the calculations can improve the theoretical distributions for the higher  $\ell$ -values. These calculations may also have a significant effect on the polarization distribution. Without a doubt, other refinements to the theory will also be introduced. It is also argued (Hj 65) that the deuteron optical potential is not sufficiently well-known, with particular reference to the spin-orbit part where tensor interactions may be required, and improved agreement to polarizations may result when some of the ambiguities are resolved.

The other approach has been to formulate entirely new stripping theories, namely the BHMM theory of Butler et al. (Bu 65, Mo 65, Bu 67) and the WBP model of Pearson and Coz (Pe 66c Ba 67a,b). The BHMM theory has shown surprising success at fitting both angular distributions and polarizations with very few adjustable parameters.





In testing such theories, both DWBA and new stripping theories, it is useful to have large amounts of data from the same target nucleus and covering a wide range of energies. The studies of the  $^{52}\text{Cr}(d,p)^{53}\text{Cr}$  reaction from 8 - 11 MeV by Alty et al. (Al 66), and from 4.3 to 6.3 MeV by Legg et al. (Le 66) comprise one such large body of data. Another extensive study is that of the  $^{40}\text{Ca}(d,d)^{40}\text{Ca}$  and  $^{40}\text{Ca}(d,p)^{41}\text{Ca}$  reactions by Bassel et al. (Ba 64) and Lee et al. (Le 64) in the energy range 7 to 12 MeV, and by Hjorth, Saladin and Satchler (Hj 65) at 14.3 MeV. The latter study also included polarization measurements.

The second motivation for this work was to provide further experimental information which would be useful in testing theories of deuteron stripping reactions. To achieve this, a number of experimental groups at this laboratory have cooperated to increase the experimental information on  $d-^{40}\text{Ca}$  reactions. The neutron angular distributions have been measured at 5.0, 6.0 and 6.5 MeV by Grandy et al. (Gr 67, 68), and the neutron polarization distributions have been measured by Gedcke et al. (Ge 67, 68, Ro 67). This report describes the measurement and analysis of the elastic scattering at 5, 6 and 6.5 MeV, the proton distributions leading to the ground state for deuteron energies of 5 and 6 MeV and to the 1.95, 2.47 and 3.95 MeV states at 5 MeV only (Le 67, 68a), and finally, the polarization of the protons from the ground state at 5 MeV (Ro 67, Le 68b).

$^{40}\text{Ca}$  has a number of advantages as its choice of the nucleus under investigation. It is doubly magic so that the low-lying levels of  $^{41}\text{Ca}$  and  $^{41}\text{Sc}$  should be mirror states. Therefore, the  $(d,n)$  and  $(d,p)$



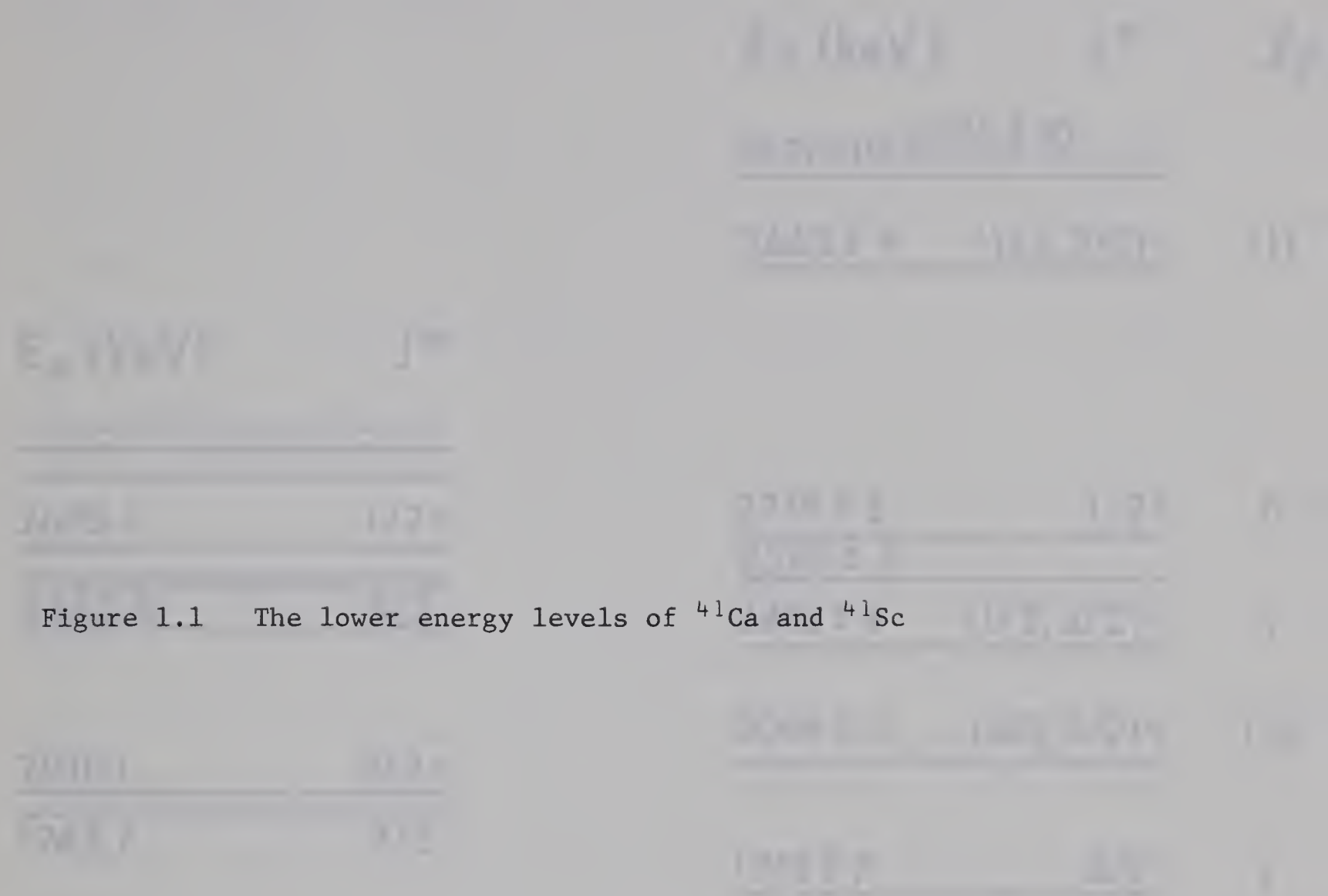


Figure 1.1 The lower energy levels of  $^{41}\text{Ca}$  and  $^{41}\text{Sc}$



$E_x$ (keV)	$J^\pi$	$\ell_p$
-------------	---------	----------

<u><u><math>3721 \pm 10</math></u></u>	<u><u><math>3776 \pm 10</math></u></u>	
--	--	--

<u><u><math>3463 \pm 9</math></u></u>	<u><u><math>(1/2, 3/2)^-</math></u></u>	(1)
---------------------------------------	---	-----

$E_x$ (keV)	$J^\pi$
-------------	---------

<u><u> </u></u>	
<u><u> </u></u>	
<u><u> </u></u>	

<u><u>2670.1</u></u>	<u><u><math>1/2^+</math></u></u>
----------------------	----------------------------------

<u><u>2462.5</u></u>	<u><u><math>3/2^-</math></u></u>
----------------------	----------------------------------

<u><u><math>2719 \pm 8</math></u></u>	<u><u><math>1/2^+</math></u></u>	0
---------------------------------------	----------------------------------	---

<u><u><math>2593 \pm 9</math></u></u>		
---------------------------------------	--	--

<u><u><math>2415 \pm 8</math></u></u>	<u><u><math>(1/2, 3/2)^-</math></u></u>	1
---------------------------------------	---	---

<u><u><math>2096 \pm 7</math></u></u>	<u><u><math>(3/2, 5/2)^+</math></u></u>	(2)
---------------------------------------	---	-----

<u><u>2010.1</u></u>	<u><u><math>3/2^+</math></u></u>
----------------------	----------------------------------

<u><u>1942.7</u></u>	<u><u><math>3/2^-</math></u></u>
----------------------	----------------------------------

<u><u><math>1718 \pm 7</math></u></u>	<u><u><math>3/2^-</math></u></u>	1
---------------------------------------	----------------------------------	---

<u><u>0</u></u>	<u><u><math>7/2^-</math></u></u>
-----------------	----------------------------------

$^{41}\text{Ca}$

<u><u>0</u></u>	<u><u><math>7/2^-</math></u></u>	3
-----------------	----------------------------------	---

$^{41}\text{Sc}$



reactions should be identical except for Coulomb and kinematic effects. Furthermore, since  $^{40}\text{Ca}$  is expected to be an inert core for the addition of a single proton or neutron, the spectroscopic factors for the low-lying states of  $^{41}\text{Ca}$  and  $^{41}\text{Sc}$  would be expected to have  $S = 1$ . The assumption that  $^{40}\text{Ca}$  is an inert core is an oversimplification. This can be seen by looking at the energy level diagram in fig. 1.1. Instead of a single low-lying  $3/2^-$  state as would be expected from a simple shell model picture, there are actually two  $3/2^-$  states separated by 0.52 MeV in  $^{41}\text{Ca}$  and 0.7 MeV in  $^{41}\text{Sc}$ . It is also observed that both of these levels are strongly excited in single nucleon transfer reactions (Bo 57). Gerace and Green (Ge 67a) explained the low-lying levels of  $^{41}\text{Ca}$  and  $^{41}\text{Sc}$  as mixtures of shell model and deformed states, the states being mixed with the single 2p  $3/2$  level being a 3p-2h state and a 5p-4h state. Nevertheless, they show that the single particle strength for the  $j = \frac{7}{2}$  levels is still expected to be almost entirely in the ground state, that is the spectroscopic factor should still be close to 1, and the sum of the spectroscopic factors for the two  $3/2^-$  states is also expected to be close to 1. A further advantage in the choice of  $^{40}\text{Ca}$  is that the present work extends the energy range over which the reaction has been studied in some detail. It is satisfying that extending the study of this reaction to lower energies has already raised some interesting questions in the coupled channels calculations of the energy dependence of the deuteron optical potential and the effect of this on stripping calculations (Ra 67, 68b).







## 1.2 Optical Model Theory

No attempt is going to be made in this or the following section to develop the theories used later in this report to analyze the experimental results. In the case of the optical model in general the reader is referred to the book by Hodgson (Ho 63) and for discussions on the optical model as applied to elastic deuteron scattering, to the work of Halbert (Ha 64) and of C.M. Perey and F.G. Perey (Pe 63b and Pe66b). Attempts have also been made to arrive at a deuteron optical model potential derived in terms of nucleon optical potentials (Pe 67, Co 67). Good agreement was found with the real part of the potential derived from phenomenological analyses of deuteron elastic scattering, but the agreement to the imaginary part of the potential was less satisfactory.

There are a number of limitations of the optical model and these will be discussed now with particular reference to the case of 5 MeV deuterons on calcium. First of all, at low energies, the compound nucleus may exist in a series of discrete states. If the energy resolution of the beam is less than the mean spacing between compound nucleus states, the elastic distributions could show structure not considered in the optical model description. However, for the case of interest here the compound nucleus  $^{42}\text{Sc}$  is formed at 15 MeV excitation where the density of states is estimated to be approximately 4/keV (Da 68). Consequently, this effect is not expected to cause problems in the present analysis. Similar to the first consideration is the possibility that as the incident energy is changed by a small amount,



the number of inelastic channels may change significantly. Again, this is not the case here where the number of exit channels is already very large. A small number of exit channels for the compound nucleus would imply the possibility of a compound elastic cross-section which would be indistinguishable experimentally from the shape elastic cross-section, but which is not included in the optical model calculations of the elastic cross-section. Because of the large number of possible exit channels, this is not expected to be a significant problem. This was, in fact, verified by Hauser-Feshbach calculations (Da 68) the results of which are shown in section 3.2. One would also expect the optical model to be less applicable for very light nuclei where the assumption of describing the nucleus by uniform nuclear matter is not justified. The mass region around 40, however, does not fall into this category.

Inherent in the optical potential of section 3.2 is the assumption that the deuteron is a point particle. In fact, the deuteron is a loosely-bound system of a neutron and a proton, and the centre of mass and the centre of charge may be separated appreciably. One might expect at deuteron energies close to the Coulomb barrier, as is the case in the experiments reported here, that the effect of the nuclear electric field might seriously affect the distributions. Dickens and Perey have shown (Di 65) by including a potential due to the deuteron electric polarizability of the form  $V_p = -\frac{1}{2} \left[ \frac{Z^2 e^2 \alpha}{R^4} \right]$  with  $\alpha \sim 0.5 F^3$  that the effect





is small but not negligible. However, Dickens points out that it would be inconsistent to include deuteron polarizability into the calculations without also treating the electric breakup of the deuteron, which at present, cannot be simply incorporated into an optical model formalism.

### 1.3 DWBA Theory of Stripping Reactions

The DWB approximation as applied to stripping calculations has been described in detail by Tobocman (To 61) and Satchler (Sa 64) and further discussion is available in the references quoted in these two works.

The distorted wave transition amplitude for a reaction of the form  $A(d,p)B$  can be written

$$T = \iiint \chi_p^{(-)*}(\vec{k}_p, \vec{r}_p) \langle B | V | A \rangle \chi_d^{(+)}(\vec{k}_d, \vec{r}_d) d\vec{r}_p d\vec{r}_d \quad 1.1$$

where  $\chi_p^{(-)}$  describes the elastic scattering of a proton from the residual nucleus B with energy equal to the proton energy in the  $A(d,p)B$  reaction, and  $\chi_d^{(+)}$  is the elastic scattering wave function for deuterons from the target nucleus A at the incident deuteron bombarding energy. The superscripts indicate the asymptotic boundary conditions of the wave functions, the (+) and (-) indicate incoming and outgoing waves, respectively.  $|A\rangle$  contains the deuteron internal wave function and the target nucleus wave function, similarly  $\langle B|$  contains the proton wave function and the residual nucleus wave function.  $V$  is the final state interaction



potential. There is an inherent assumption in writing the transition amplitude in the form of equation (1.1). Strictly  $\chi_d^+$  represents the relative motion of the deuteron and the target nucleus. If the cross-section for all reactions is small compared to the elastic scattering cross-section then we can approximate the wave function for the relative motion by the elastic scattering wave function. Similar conditions have to be true in order to write for  $\chi_p^-$  the corresponding proton elastic scattering wave function. The interaction potential  $V$  is the interaction of the proton with all the nucleons of  $B$  minus the optical potential, i.e.

$$V = V_{pB} - U_{pB} = V_{pn} + (V_{pA} - U_{pB}) \quad 1.2$$

It is then argued (Le 64) that  $V_{pn}$ , the neutron-proton interaction, dominates the term in brackets. This term is never identically zero,  $V_{pA}$  having off-diagonal matrix elements, consequently this step involves a further approximation. Even the full neutron-proton interaction would be too complicated to include in the calculation and it is common instead to assume that  $V_{pn}$  is of very short range. In this case, we can write

$$V_{pn} \phi_d(r_{pn}) \equiv D(r_{pn}) \approx D_0 \delta(r_{pn}) \quad 1.3$$

where  $\phi_d(r_{pn})$  is the spatial part of the deuteron internal wave function. Effective-range analysis results in the value





$$D_0^2 \approx 1.5 \times 10^4 \text{ MeV}^2 F^3 \quad 1.4$$

in order to get the correct asymptotic normalization of the deuteron wave function.

It is not necessary to make such a drastic approximation. It has been shown that the full finite-range calculations can be well approximated by the local energy approximation (Pe 64), and the calculations reported here, except those specified as zero-range calculations, make use of the local energy method.

The differential cross-section can be written (Sa 64)

$$\frac{d\sigma(\theta)}{d\Omega} = \frac{M_d M_p}{(2\pi\hbar^2)^2} \frac{k_p}{k_d} \frac{\sum |T^2|}{(2J+1)(2S+1)} \quad 1.5$$

where  $M_d$  and  $M_p$  are the reduced masses of the deuteron and proton, and  $k_d$  and  $k_p$  are their respective wave numbers.  $J$  is the spin of the target nucleus and  $S$  represents the deuteron spin.

The formal expression for the polarization of the emitted particle is considerably more complicated. Complete details are given in reference Sa 64.

Toosi and Ivash (To 68) list a number of effects that are neglected in most DWBA calculations including the present ones. Thus, compound nucleus contributions are not included in the calculations, however, estimates of the compound nucleus contribution have been made by means



of Hauser-Feshbach calculations and these results are reported in section 3.3. The calculations indicate that even at 5 MeV, compound nucleus contributions are quite small but not negligible.

The optical potential for the deuteron (equations 3.1 - 3.3) does not include tensor interactions but only a vector spin-orbit coupling interaction. The vector polarization and two of the three components of the tensor polarization have been measured for  $d-^{40}\text{Ca}$  elastic scattering at 22 MeV (Be 63, 63a). These data have been analyzed by Raynal (Ra 63) who found no evidence for the inclusion of a tensor term in the polarization in that case. This is by no means conclusive and the inclusion of a tensor term may be required eventually to explain all the data.

Other complications that have been neglected are the effects due to exchange stripping such as heavy particle stripping, and the knocking out of a target proton rather than the simple capture of the neutron from the deuteron. It is argued (Le 64) that these effects are not important because of the more complicated nuclear overlaps involved.

Although it was suggested in the previous section that the polarization of the deuteron does not have a large effect on the elastic scattering angular distribution, this does not necessarily imply that polarization effects are not important in stripping reactions. It is exactly this point that Butler makes in proposing his new stripping theory (Bu 67). This effect is also neglected in the present calculations.





The non-exact cancelling of the bracketed expression in equation 1.2 has already been mentioned. This approximation has been discussed by Lee (Le 64).

Johnson and Santos (Jo 67) have shown that neglecting the D-state admixture of the deuteron wave function can have a significant effect on the distributions for large angular momentum transfers, of which the  $^{40}\text{Ca}(d,p)^{41}\text{Ca}$  ground state reaction is a good example. Inclusion of the D-state introduces appreciable differences in the  $\ell = 3, j = \frac{5}{2}$  and  $\ell = 3, j = \frac{7}{2}$  distributions. It is likely that including the D-state into the calculations will also alter the polarization results.





## CHAPTER 2

### EXPERIMENTAL METHODS

#### 2.1 Elastic Scattering and (d,p) Stripping Distributions

The deuteron elastic scattering distributions were measured at incident deuteron energies of 5.0, 6.0 and 6.5 MeV using the deuteron beam from the University of Alberta Van de Graaff accelerator. The (d,p) reaction leading to the ground state of  $^{41}\text{Ca}$  was studied at 5.0 and 6.0 MeV and the reactions leading to the 1.95, 2.47 and 3.95 MeV states of  $^{41}\text{Ca}$  were studied at 5 MeV only. Angular distributions were measured in 5 degree steps from  $20^\circ$  to  $140^\circ$ .

The deuteron beam was collimated by a pair of tantalum slits  $1/16'' \times 3/16''$  and separated by  $16''$ , located immediately upstream from the scattering chamber. The scattering chamber was  $8''$  in diameter and was coupled by means of a  $0.010''$  stainless steel strap sliding over an 'O' ring seal to the 50 cm. magnetic spectrometer. The chamber contained a target holder capable of holding up to three targets and an air-cooled Faraday cup in which the beam was stopped. To prevent the loss of electrons from the cup, a suppressor ring was mounted on a teflon spacer  $3/8''$  from the cup and biased at  $-1500$  volts. Facilities were also available for mounting solid state detectors inside the chamber.



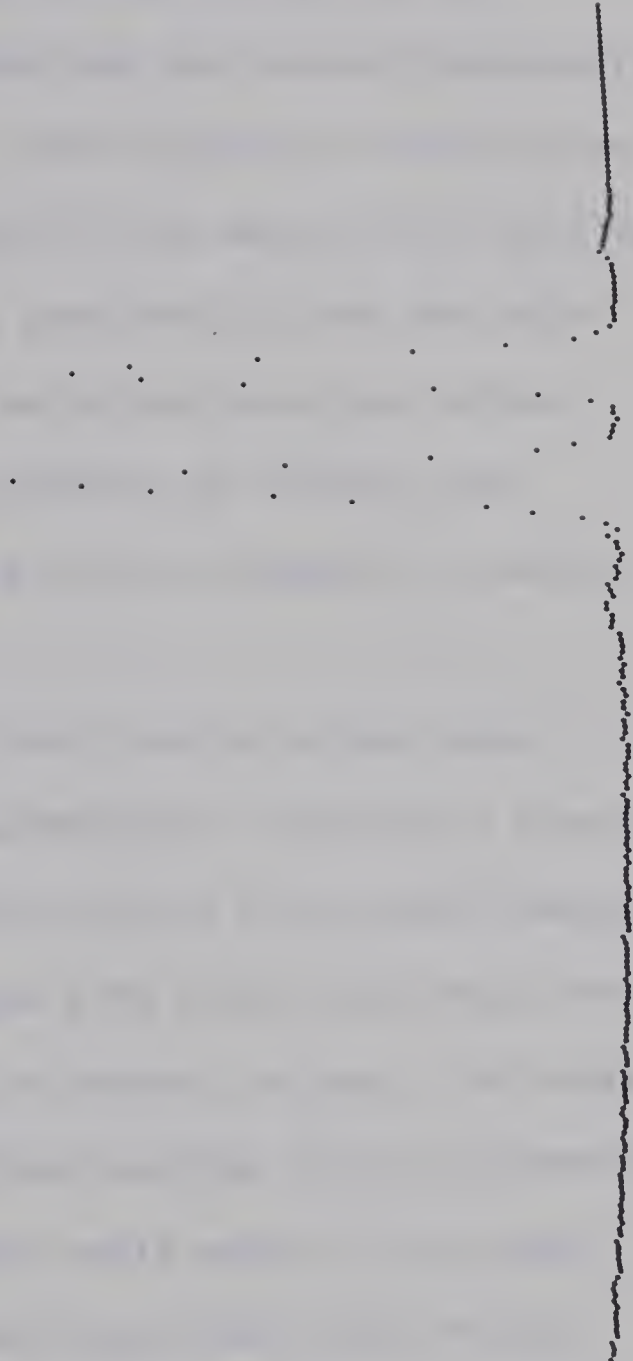
A surface barrier or lithium drifted silicon detector was located on the  $90^\circ$  ray and in the focal plane of the spectrometer and detected the particle group under investigation. In order to provide 'a picture' of the image and also to aid in centering the particle group on the detector, a four step energy degrader was placed directly in front of the detector. The first step contained no absorber and succeeding steps increasing thicknesses of thin copper or nickel foils. A photograph of a typical step wedge spectrum taken directly from this display screen of the computer is shown in fig. 2.1. A number of different step wedges were used during the course of the experiments depending on the energy and kind of particles being detected. The procedure was to adjust the magnet current until the particle group was centered on the middle two steps. Typically 90% of the counts were contained in the two central steps. By observing when the number of counts in the side steps become asymmetrical, it was possible to ascertain when particles from other reactions were beginning to enter the detector. This method, for instance, made it clear when protons from the  $^{12}\text{C}(\text{d},\text{p})^{13}\text{C}$  reaction began to interfere with the  $^{40}\text{Ca}(\text{d},\text{p})^{41}\text{Ca}^*$  3.95 reaction. The energy resolution of the magnet was measured to be approximately 12 keV/mm (24 keV/step) for 5 MeV deuterons and 10 MeV protons, which are roughly the energies of the particles involved in the experiments. Fig. 2.3 shows a diagram of the system with the polarimeter in place. For the measurements described in this section, the polarimeter was replaced by the detector-step wedge assembly and



Figure 2.1 A typical step wedge spectrum photographed from the computer display screen



ပုဒ်မိမိ၊ ပုဒ်မိမိ၊ ပုဒ်မိမိ၊ ပုဒ်မိမိ







the quadrupole lens was removed to enable measurements to be made at angles greater than  $120^\circ$ .

The data for a particular distribution were normalized to the same total charge as measured by the Faraday cup and current integrator. For the elastic scattering distributions, the statistical uncertainties at some back angles were between 2% and 3%, but for most of the distributions, the statistical uncertainties were considerably less than this. For the (d,p) distributions, the statistical errors were also always kept less than 3%. Checks on the reproducibility of the data were extremely satisfactory indicating the data could be repeated to within 2%.

Thin ( $\sim 20 \mu\text{gm}/\text{cm}^2$ ) calcium and calcium fluoride targets were prepared by standard vacuum evaporation techniques. The calcium fluoride targets were evaporated from a tantalum boat onto a thin formvar backing,<sup>†</sup> whereas the calcium targets were evaporated from a wire cone wound from 0.020" tungsten wire, onto a thin carbon on formvar backing. The target thicknesses were estimated from the observed counting rates, the measured absolute cross-sections and the approximate solid angle of the magnet ( $\sim 10^{-3}$  steradians). The calcium fluoride targets were used for the elastic scattering and (d,p) ground state distributions. For the (d,p) distributions leading to the excited states of  $^{41}\text{Ca}$ , calcium targets

---

<sup>†</sup> Formvar solution was prepared by dissolving 10 gms of Formvar 15/95E (Shawinigan Resins Corp., Springfield, Mass.) in 150 ml. of 1,2 Dichloroethane. A single drop of this solution will form a thin film when allowed to slide onto the surface of water.



were used because of the overlap of protons from these states with protons from levels in  $^{20}\text{F}$ .

Absolute cross-sections were found by measuring the elastic scattering of 2.5 and 3 MeV protons at  $30^\circ$  using the same target, and immediately afterwards measuring the 5 MeV deuteron elastic distribution. The scattering of 2.5 and 3 MeV protons at  $30^\circ$  from calcium is expected to be pure Rutherford scattering. This was substantiated by optical model calculations using average proton parameters (1.00 and 0.99 at 2.5 and 3 MeV, respectively). Fig. 2.2 shows a plot of the proton counting rate against Rutherford scattering cross-section. The absolute cross-section obtained in this way is believed to be accurate to better than  $\pm 10\%$ . All other distributions were then normalized using the 5 MeV elastic scattering absolute cross-section as a secondary standard. In practice after measuring any of the other distributions, without changing the target or removing the detector, the elastic scattering of 5 MeV deuterons was measured at  $50^\circ$ ,  $60^\circ$  and  $70^\circ$ . The average conversion factor between counting rate and cross-section was then obtained. This procedure was considerably simpler than changing over to protons and also changing step wedges at the end of each run. The calcium used in the targets was natural calcium which is 97%  $^{40}\text{Ca}$ . The scattering from the other isotopes of calcium ( $^{42}\text{Ca}$ ,  $^{44}\text{Ca}$ ) would not be resolved from the  $^{40}\text{Ca}$  scattering, whereas only protons from  $^{40}\text{Ca}$  would contribute to the (d,p) reactions, consequently a 3% correction was applied to the (d,p) cross-sections.



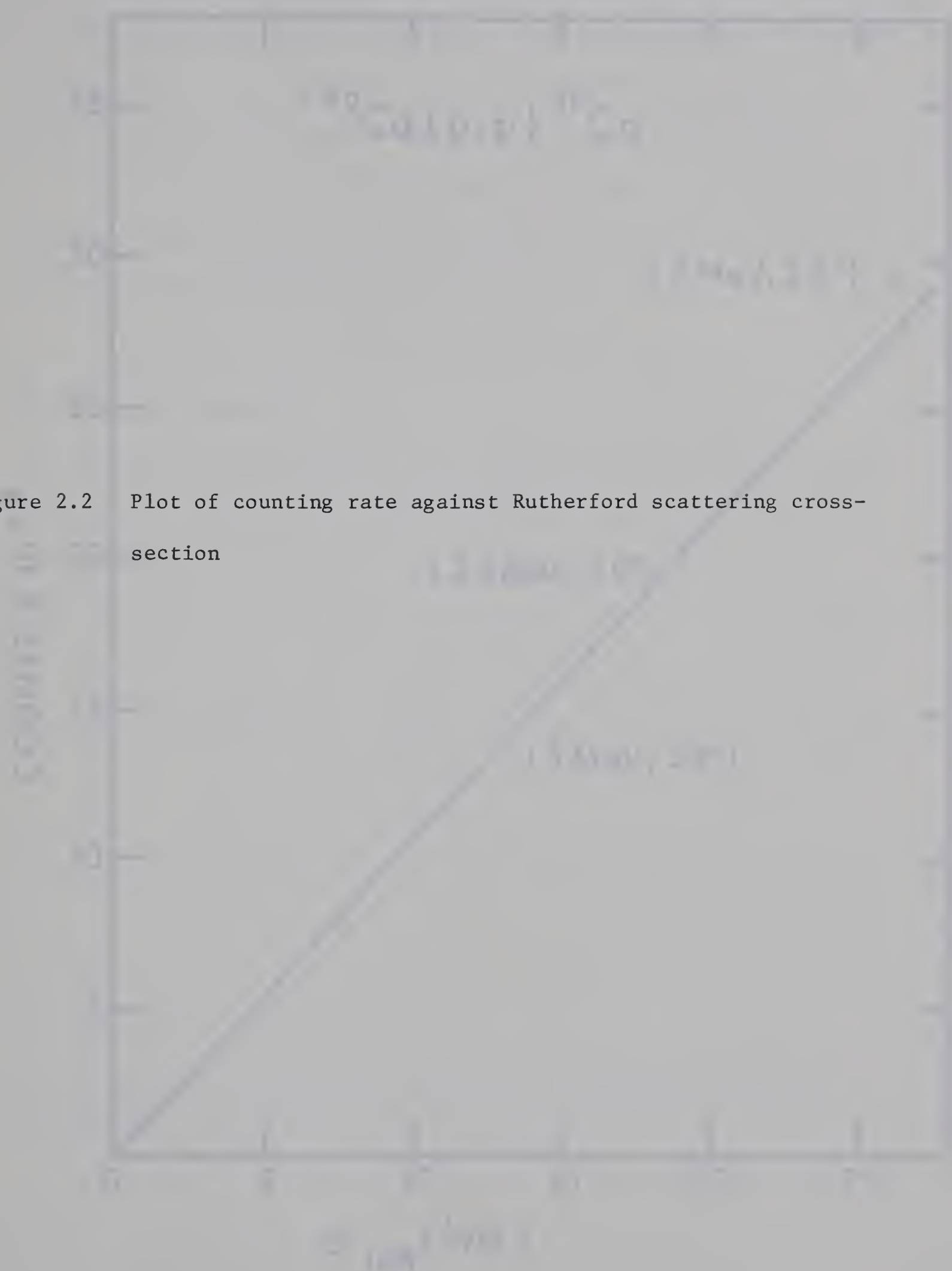
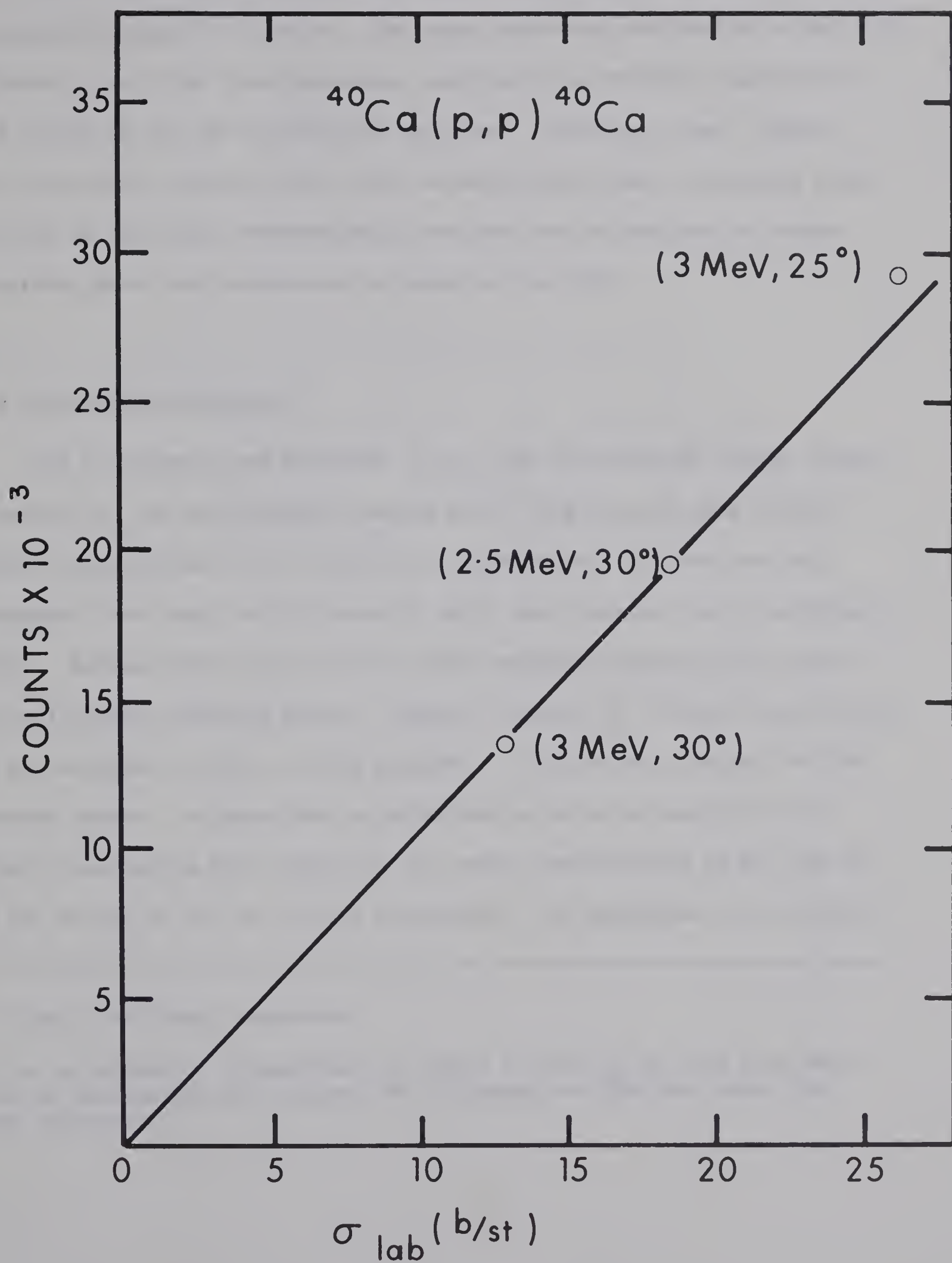


Figure 2.2 Plot of counting rate against Rutherford scattering cross-section









The electronics was extremely simple consisting of an Ortec<sup>†</sup> 108-410 preamplifier-amplifier system. The early data were analyzed by a TMC 1024 kicksorter, all the later data were analyzed by a TMC 1024 channel ADC and stored in the on-line SDS-920 computer. 'Converter busy' signals were available from the ADC so that accurate dead time corrections could be made to the data, nevertheless, data were not accumulated at rates requiring dead time corrections of greater than 10%.

## 2.2 The Proton Polarimeter<sup>\*</sup>

The polarimeter was designed to fit into the existing vacuum chamber connected to the spectromagnet vacuum box. This imposed some rather severe restrictions on the size of the polarimeter (maximum vertical dimension less than 2-1/2"), most of which were overcome quite satisfactorily. Helium would have been the ideal analyzer because of its large and well-known analyzing power. However, because of the size limitations, it was necessary to use a solid analyzer. In this case, carbon was the obvious choice. A great deal of polarization data is available for elastic scattering from carbon in the energy region below 10 MeV (Mo 65, Ba 66, Du 67, Ev 61, Ro 62) and furthermore, the magnitude of the polari-

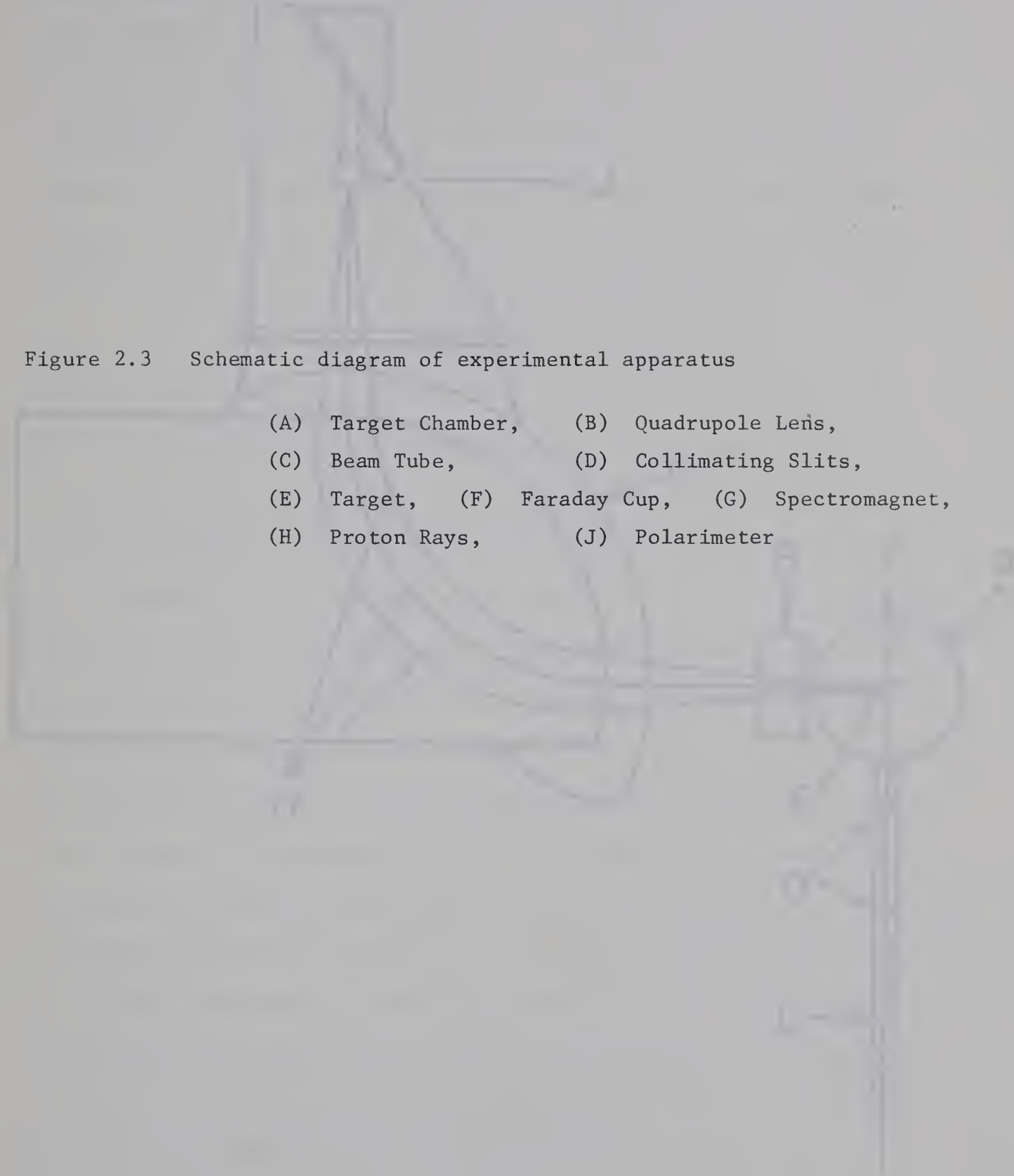
---

<sup>†</sup> Ortec, Oak Ridge, Tennessee.

<sup>\*</sup> The polarimeter is described in detail by Gurd et al. (Gu 68a, 68b). Most of the figures of this and the following section are taken from this reference.

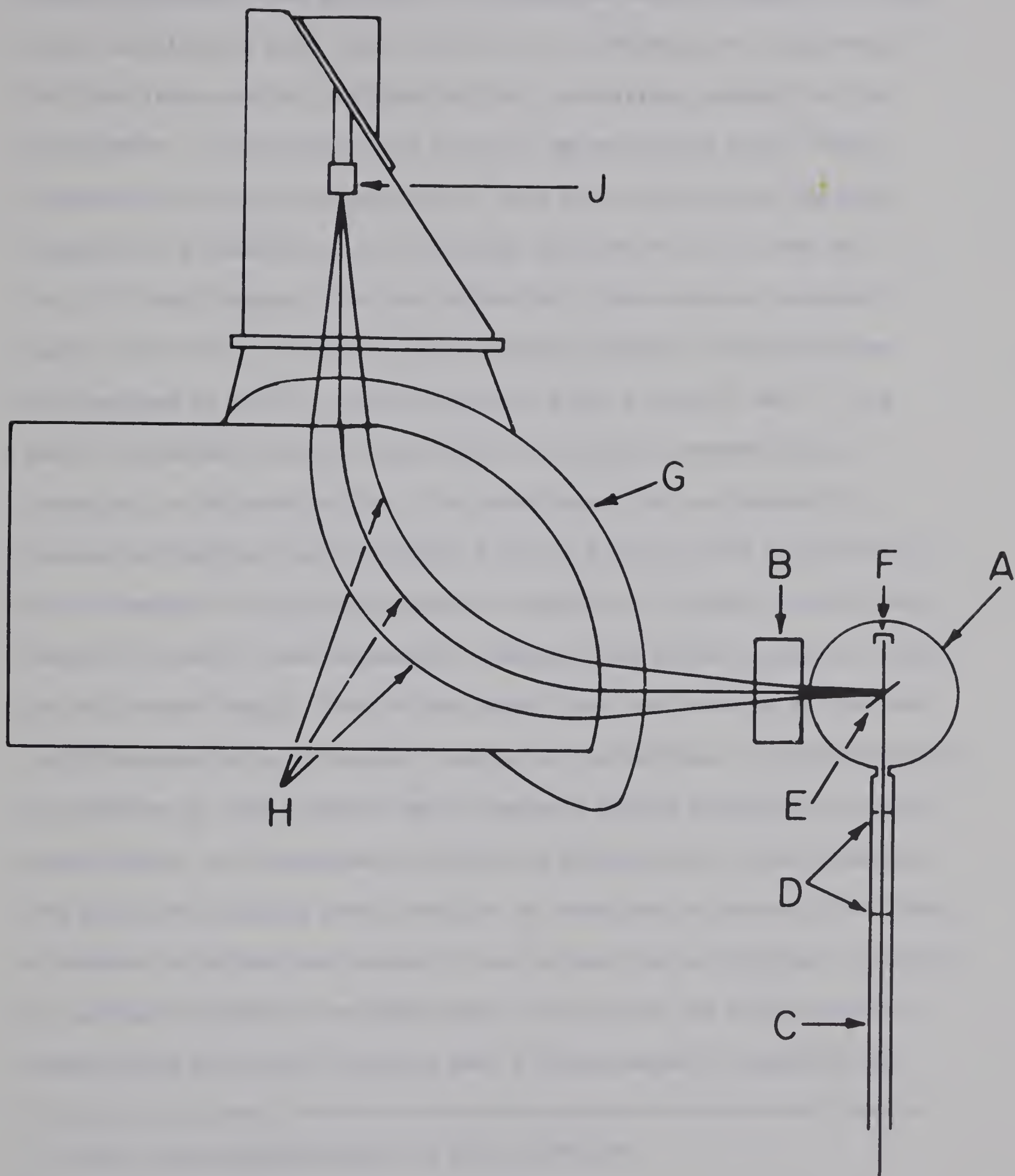


Figure 2.3 Schematic diagram of experimental apparatus

- 
- (A) Target Chamber, (B) Quadrupole Lens,  
(C) Beam Tube, (D) Collimating Slits,  
(E) Target, (F) Faraday Cup, (G) Spectromagnet,  
(H) Proton Rays, (J) Polarimeter









zation is greater than 80% at  $45^\circ$  for energies in the vicinity of 6 MeV. Crude calculations were then carried out to determine, by considering both the cross-section and polarization, the optimum geometry of the polarimeter. It was decided to use a  $17 \text{ mg/cm}^2$  carbon foil,<sup>†</sup> which represents an average energy loss of 1100 keV, and to place the side counters at a distance of  $3/4''$  from the foil and at  $45^\circ$  to the  $90^\circ$  ray. At this distance from the carbon foil, the counters subtended angles from  $37.5^\circ$  to  $52.5^\circ$  in the horizontal plane. The polarimeter was designed so that it could be rotated about a central axis. This made it possible to measure and cancel out certain asymmetries as described in the next section. The polarimeter was calibrated for protons of incident energy between 5.39 and 6.00 MeV (see section 2.4). As the energy of the protons from the reaction of interest were of the order of 11 MeV, it was necessary to degrade the proton energy to within the calibrated range. Part of the energy loss was taken up by the thin fully-depleted silicon detector located at the entrance to the polarimeter. The purpose of this detector was to impose a gating condition on the two side counters and consequently reduce the background in these counters. The effect of imposing this condition is described in section 2.3. Using a counter to degrade the energy of the protons has an advantage in itself. By setting a window on the  $dE/dx$  peak, the tail of the  $dE/dx$  spectrum, representing particles that have lost a large amount of energy in the

---

<sup>†</sup> Ultra Carbon Corporation, Bay City, Michigan.



dE/dx counter, can be gated out. A fourth "straight through" detector was located on the axis of the polarimeter and behind the carbon analyzer. The purpose of this detector was to aid in steering the beam into the polarimeter. A two step energy degrader was placed in front of this detector to give some rough position information. This detector was also used in verifying that the protons entered the polarimeter within the calibrated energy range as described in section 2.4. A photograph of the polarimeter and a schematic diagram of the body of the polarimeter are shown in figs. 2.4 and 2.5.

A block diagram of the simple electronics of the system is shown in fig. 2.6. The diagram indicates the system used for accumulating data, as opposed to the slightly different setup used in the preliminary measurements before a polarization run that were required in order to set the magnet current correctly. For the preliminary measurements, the dE/dx counter was used to gate both itself and the 'straight-through' counter, and both of these counters were fed into the computer. The magnet current was then varied until the counting rate in the straight-through counter was maximized. The purpose of gating the dE/dx counter on itself was to verify by observing the gated spectrum that only the correct portion of the dE/dx spectrum was being used to gate the other counters.

The delay in the second gating circuit on one of the side counters shown in fig. 2.6 is to determine the number of random counts being recorded in any one counter. This always turned out to be negligible with the standard gate length of 2  $\mu$ secs.





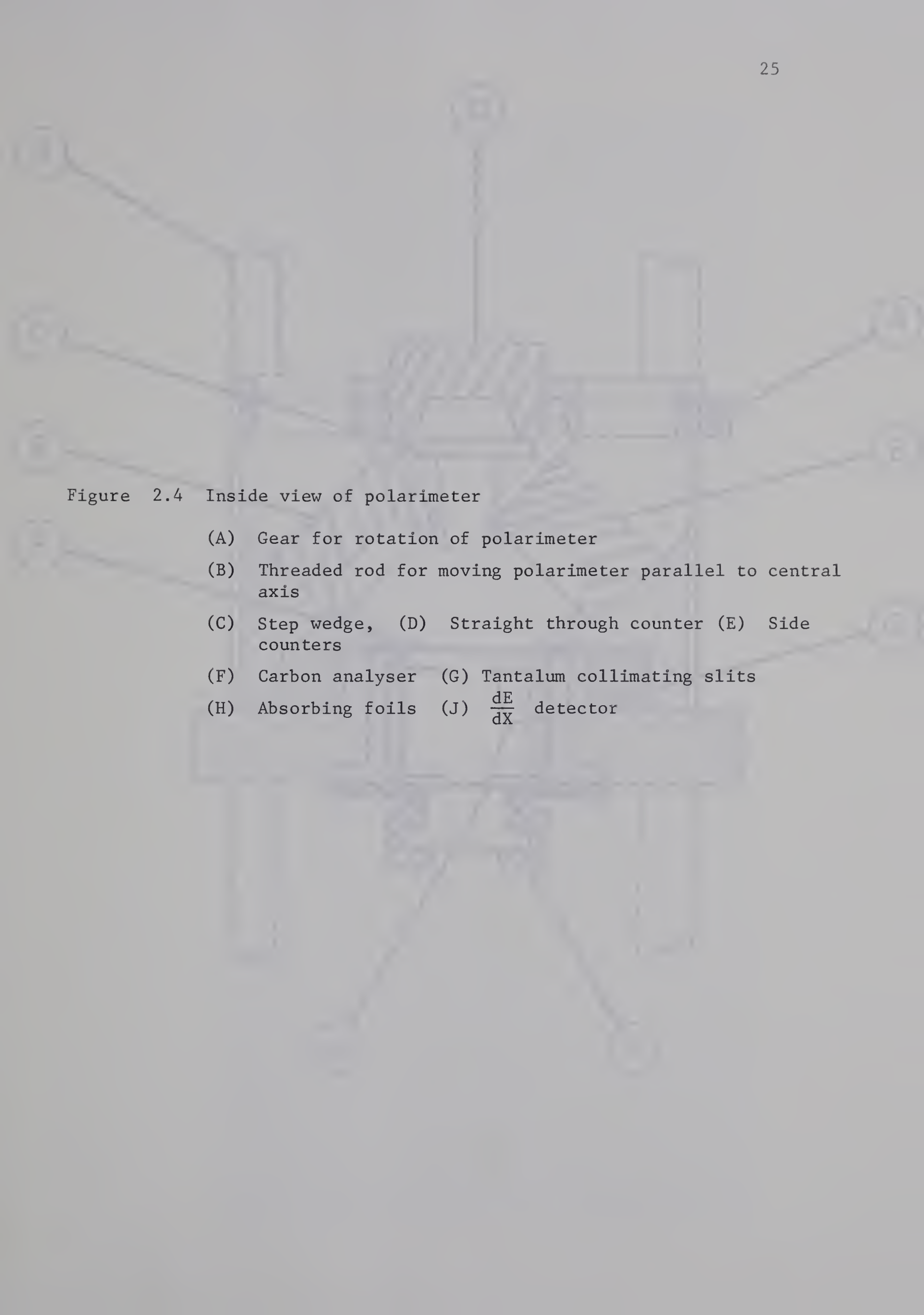


Figure 2.4 Inside view of polarimeter

- (A) Gear for rotation of polarimeter
- (B) Threaded rod for moving polarimeter parallel to central axis
- (C) Step wedge, (D) Straight through counter (E) Side counters
- (F) Carbon analyser (G) Tantalum collimating slits
- (H) Absorbing foils (J)  $\frac{dE}{dX}$  detector



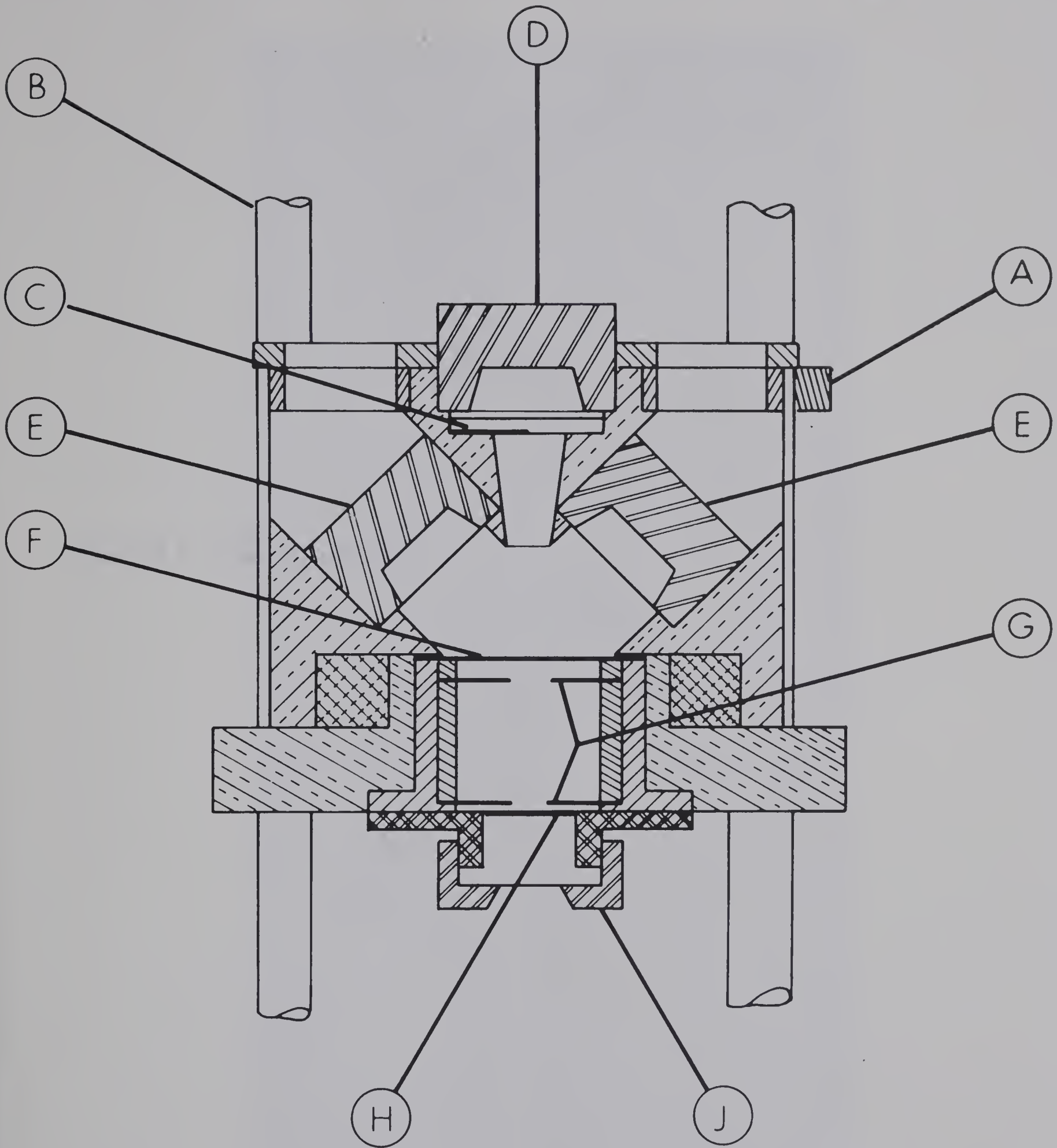






Figure 2.5 The polarimeter





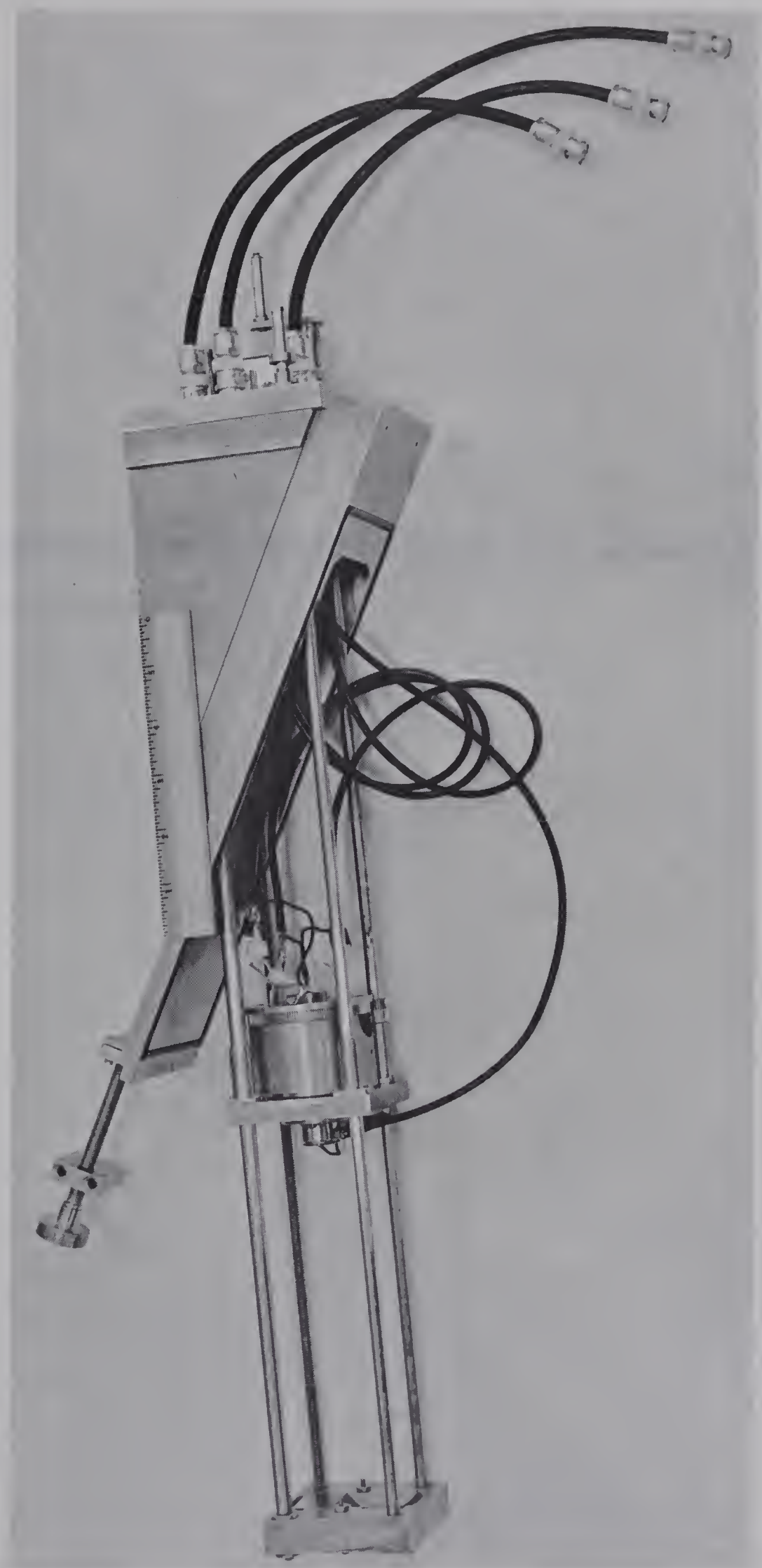
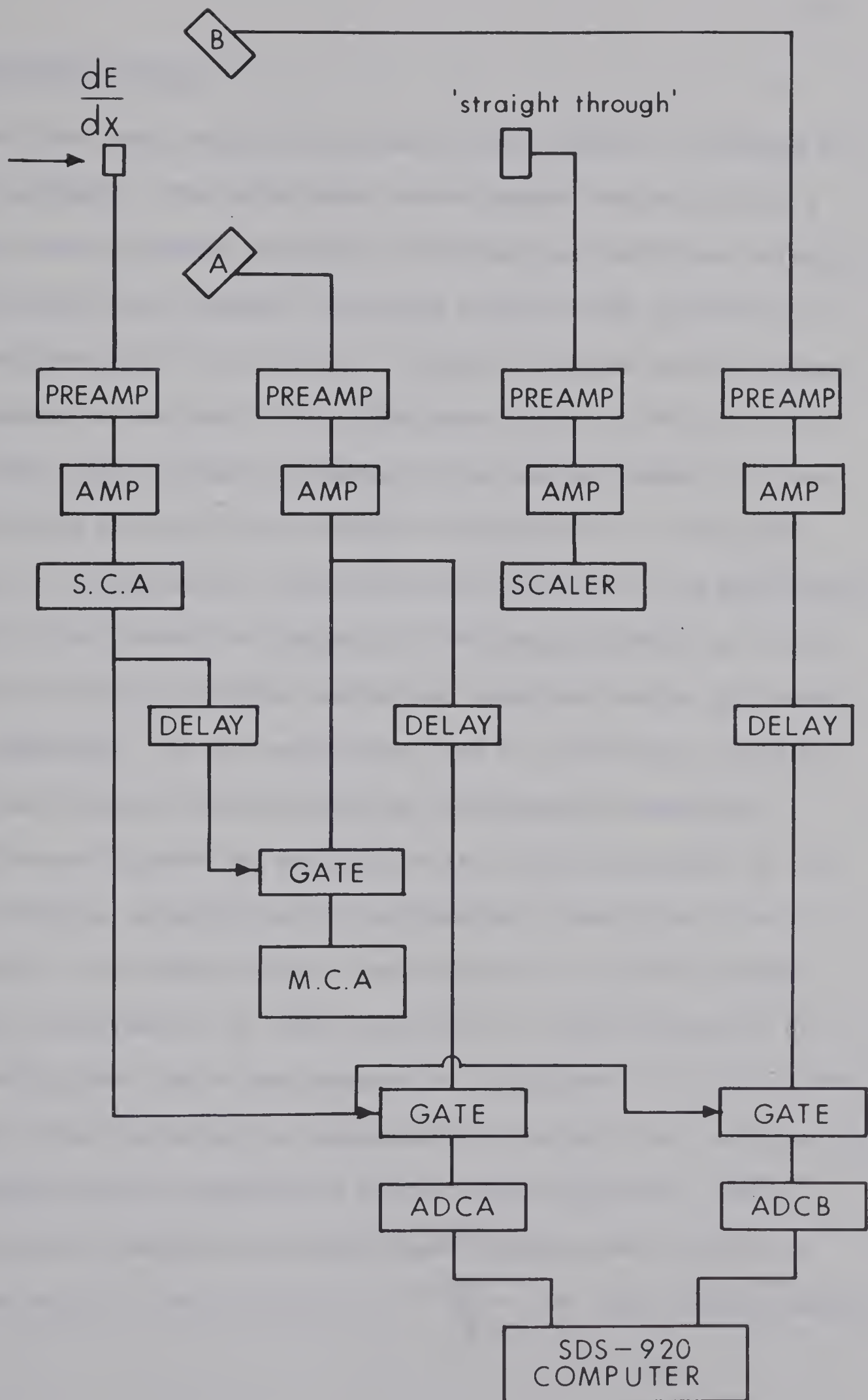






Figure 2.6 Schematic diagram of electronics used in conjunction with the polarimeter









### 2.3 Polarimeter Tests

The first tests with the polarimeter were checks to determine the optical alignment. The polarimeter vacuum chamber was mounted on a bench and the polarimeter installed. The analyzer, dE/dx and straight-through counters were removed, the dE/dx counter being replaced by a small collimator 1/8" in diameter. A transit was then used to compare the alignment of the axis of the polarimeter with the 90° ray of the magnet whose position had been marked on the vacuum chamber. It was found that the two lines were parallel to within 0.4°. It was also important to determine how reproducible the position of the polarimeter was when it was removed and replaced in the vacuum chamber as it was necessary to change the dE/dx counter and absorbers during the course of the experiment. It was established that the polarimeter could be removed and replaced without affecting the alignment measurably.

The vacuum chamber and polarimeter were then reconnected to the magnet and tests conducted on the instrumental asymmetries of the polarimeter. The carbon analyzer was replaced by a 0.001" tantalum foil, and the asymmetry for the scattering of 5.3 MeV protons at 45° from a thin carbon target was measured as a function of the magnet NMR frequency. The scattering was expected to be Coulomb, and consequently, the tantalum foil was expected to have no analyzing power. These assumptions were verified by optical model calculations in which it was found that for 6 MeV protons at 45°  $\frac{\sigma}{\sigma_R} = 1.00$  and the polarization



for an unpolarized incident beam was  $\sim 10^{-7}$ . Fig. 2.7 shows a plot of the results of the asymmetry test. The significant features are that the asymmetry was indeed zero when the counting rate in the straight-through counter was maximized and that the asymmetry was highly sensitive to the magnet current. The fact that the zero asymmetry condition coincided with the maximum counting rate indicated that there were no serious asymmetries in the construction of the polarimeter. As a further check on the instrumental asymmetries, each point was repeated with the polarimeter rotated by  $180^\circ$ . No significant differences were found between the asymmetries measured in the two modes. Nevertheless, all subsequent polarization measurements consisted of a determination of the asymmetry in the two orientations of the polarimeter.

The extreme sensitivity of the polarimeter to the magnetic field was at first highly disturbing. However, this turned out not to be a serious problem. The polarization measurements in the (d,p) reactions required thick targets with the result that due to the large energy spread of the protons, the image at the carbon analyzer was much broader. Furthermore, the cross-section for elastic scattering from carbon at  $45^\circ$  in the vicinity of 6 MeV varies less quickly as a function of angle than does the Rutherford cross-section. This effect also contributes to a reduced sensitivity under experimental conditions. Tests with a thick ( $\sim 400$  keV to 5 MeV deuterons) calcium target<sup>†</sup> and the carbon analyzer

---

<sup>†</sup> The 5 mgm/cm<sup>2</sup> rolled calcium targets were obtained from Oak Ridge.



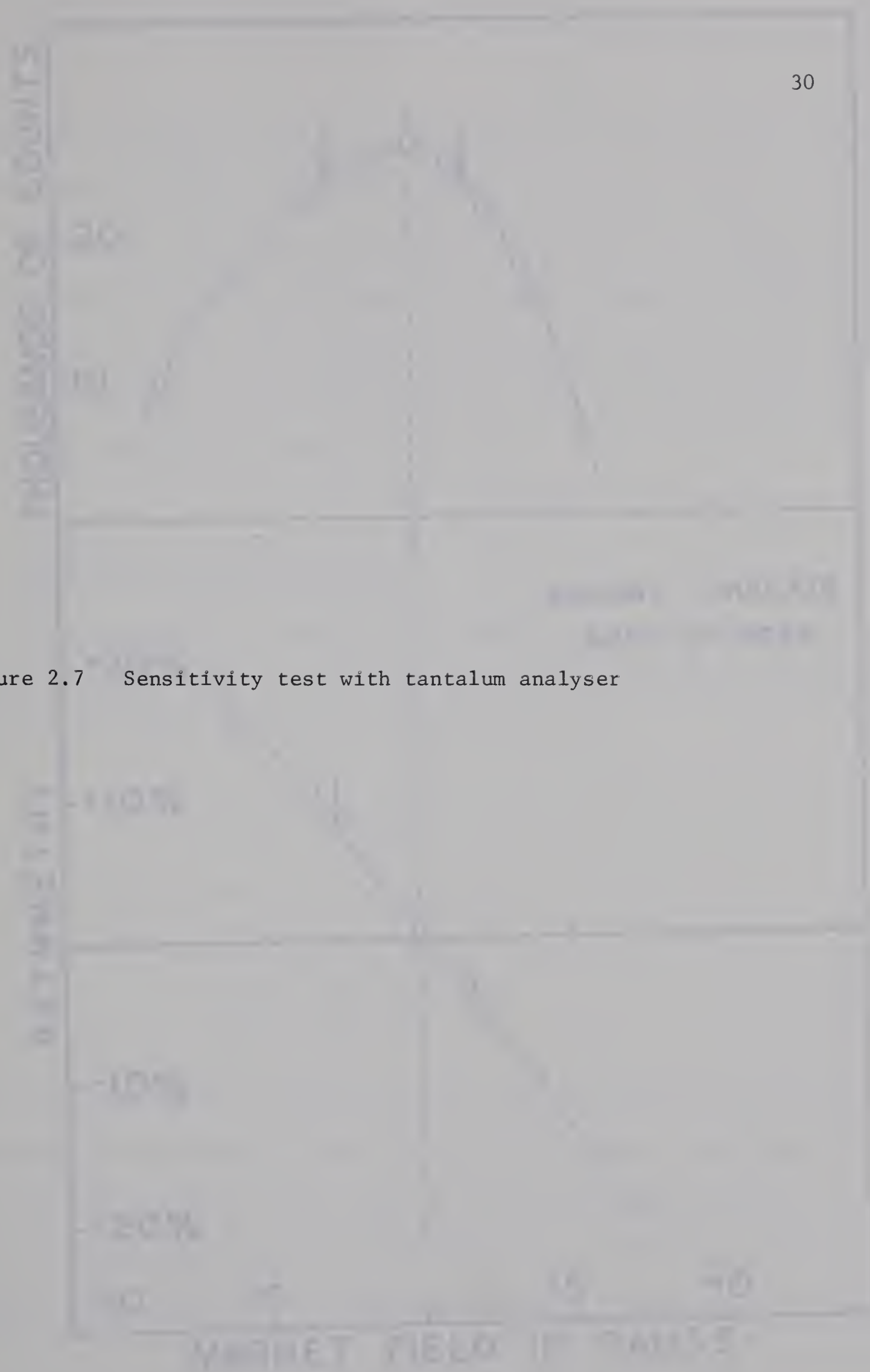
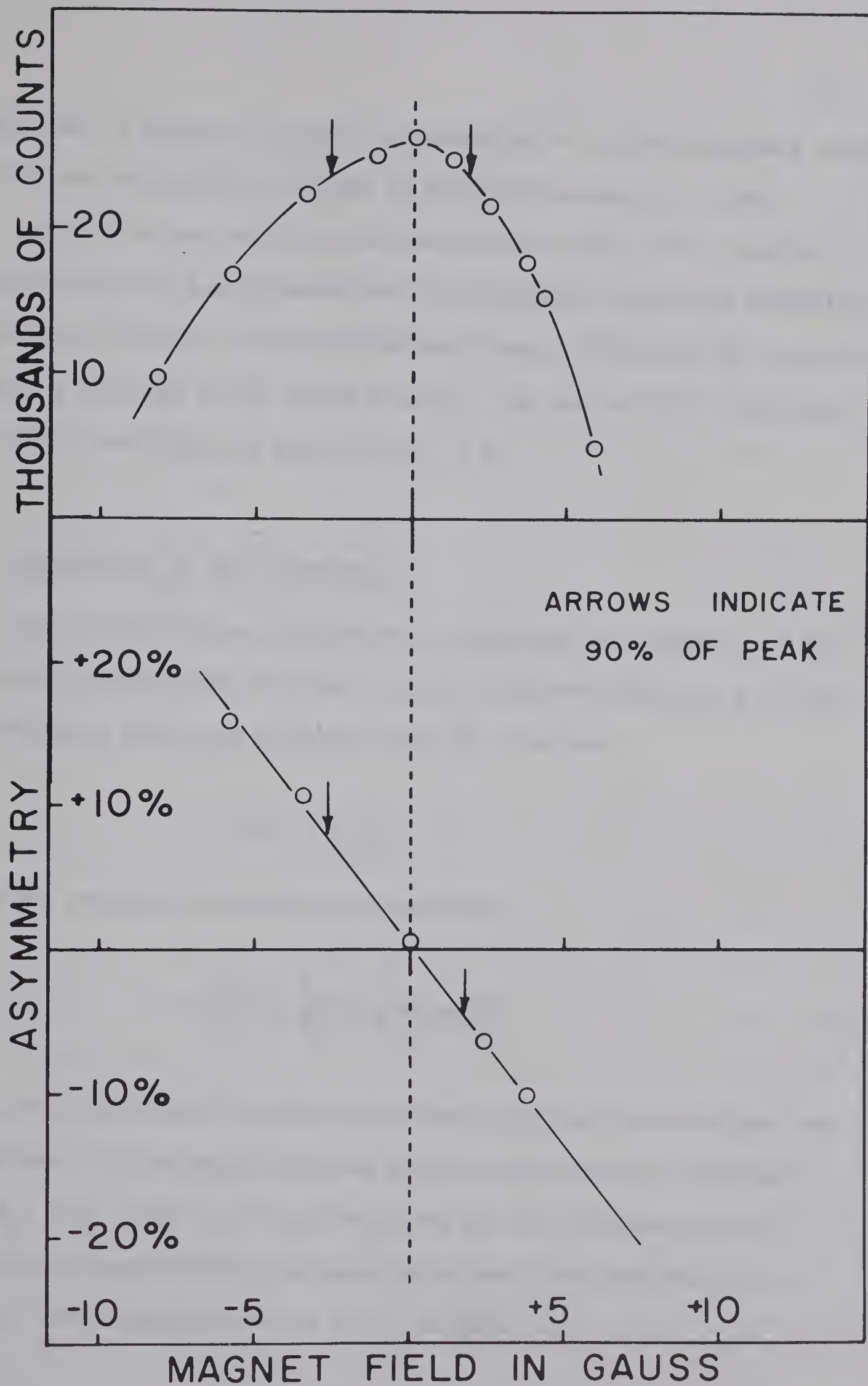


Figure 2.7 Sensitivity test with tantalum analyser









showed that a change in current corresponding to an NMR frequency change of 200 kcps resulted in a change in measured asymmetry of 3.6%.

During the long polarization measurements which often totalled 12 hours or more for both orientations, considerable background accumulated in the side counters. This problem was largely alleviated by the gating condition provided by the dE/dx counter. The spectra with and without the gating condition are shown in fig. 2.8.

#### 2.4 Calibration of the Polarimeter

The polarimeter was calibrated by measuring the asymmetry of the polarized protons from the elastic scattering from carbon at 6.18 MeV. The analyzing power was evaluated from the relation

$$P_2(E) = \frac{\epsilon}{P_1(\theta)} \quad 2.1$$

$\epsilon$  is the asymmetry defined by the equation

$$\epsilon = \frac{N_{L1} - N_{R1} + N_{L2} - N_{R2}}{N_{L1} + N_{R1} + N_{L2} + N_{R2}} \quad 2.2$$

where the subscripts L,R refer to the left and right counters and the subscripts 1,2 distinguish between the two orientations. Provided  $N_1 = N_{L1} + N_{R1}$  and  $N_2 = N_{L2} + N_{R2}$  are not too different, errors due to one counter having a greater efficiency than the other will cancel. The statistical error in  $\epsilon$  is given by



$$\Delta\epsilon = \frac{2(N_{L1} + N_{R2})^{\frac{1}{2}} (N_{L2} + N_{R1})^{\frac{1}{2}}}{(N_{L1} + N_{R2} + N_{L2} + N_{R1})^{3/2}} \quad 2.3$$

The values of  $P_1(\theta)$  were taken from the results of Moss and Haeberli (Mo 65). All signs are in accordance with the Basel convention, i.e. if  $\vec{k}_a$  is the momentum of the incident particle, and  $\vec{k}_b$  is the momentum of the emitted particle, the magnitude of the polarization is positive if the polarization vector  $\vec{P}$  is in the direction  $\vec{k}_a \times \vec{k}_b$ .

No dE/dx counter could be used for the calibration measurements. This did not create a serious problem, however, since at the relatively high counting rates and correspondingly short time of these runs background was quite small. Fig. 2.9 shows a plot of the combined data from a calibration run in the two orientations.

The high sensitivity of the polarimeter to the magnet current with thin targets discussed in the previous section did present a problem. The procedure adopted was to line up the beam with the tantalum scatterer in place, replace it with the carbon analyzer, measure the asymmetry in both orientations, then replace the carbon analyzer with the tantalum scatterer to check that the asymmetry was still zero, and then repeat this whole procedure again. The procedure was carried out at  $45^\circ$  and turned out to be perfectly satisfactory, the two values of the asymmetry being  $54.5\% \pm 3\%$  and  $54.1\% \pm 3\%$ . Another indication of the reproducibility of the results was that the difference in the asymmetries measured in the two orientations in both cases was less than 1%. As a further check of the





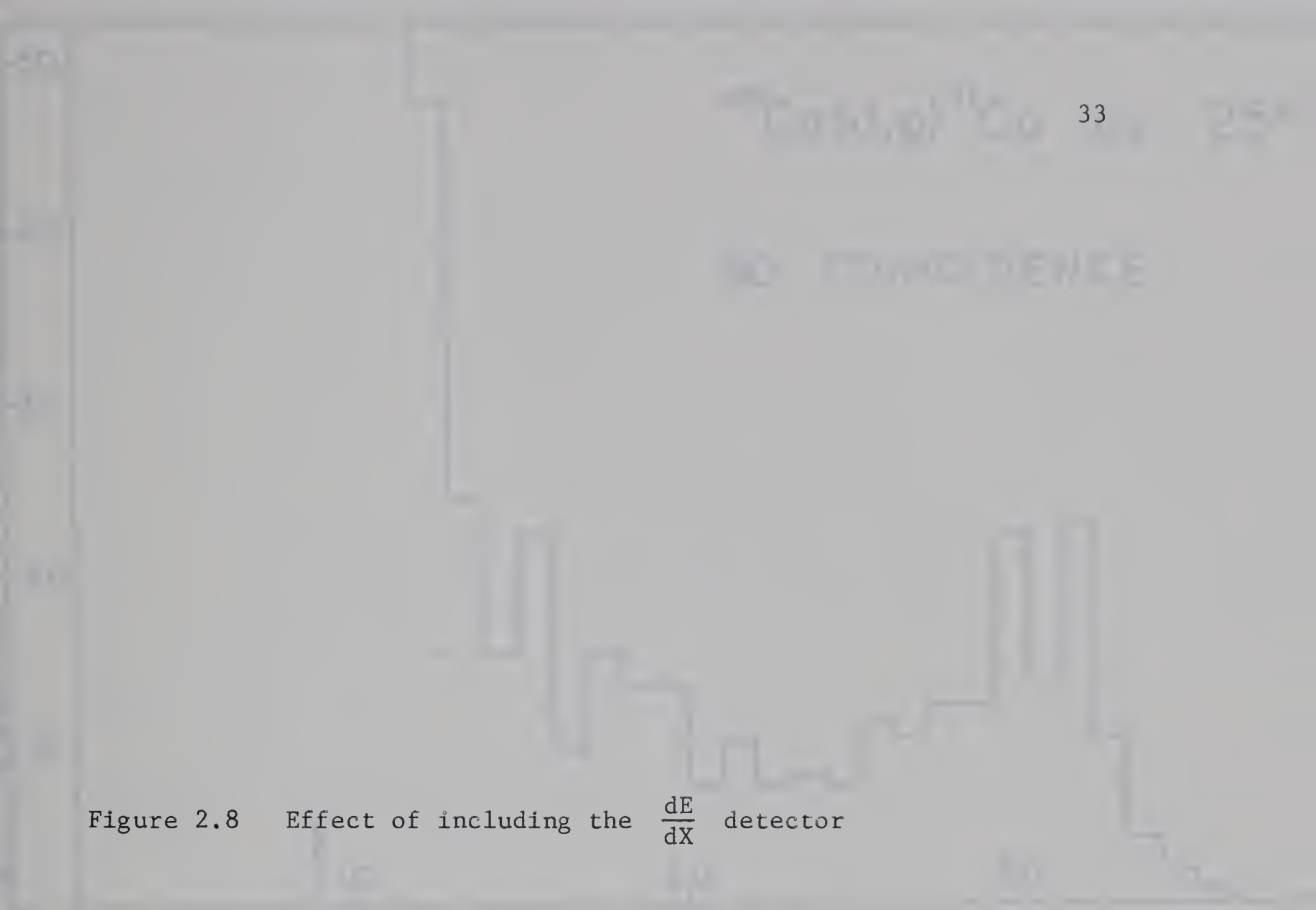
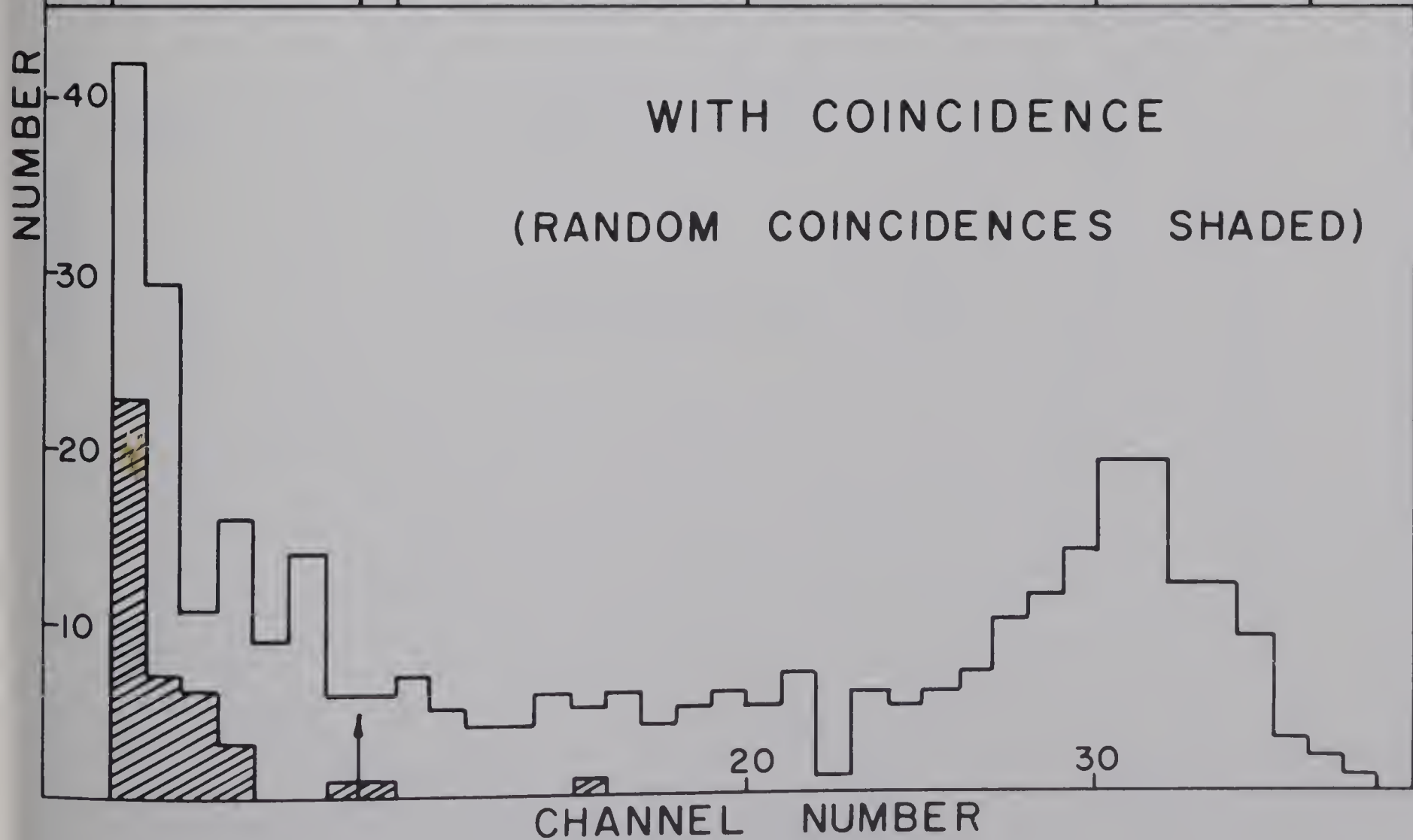
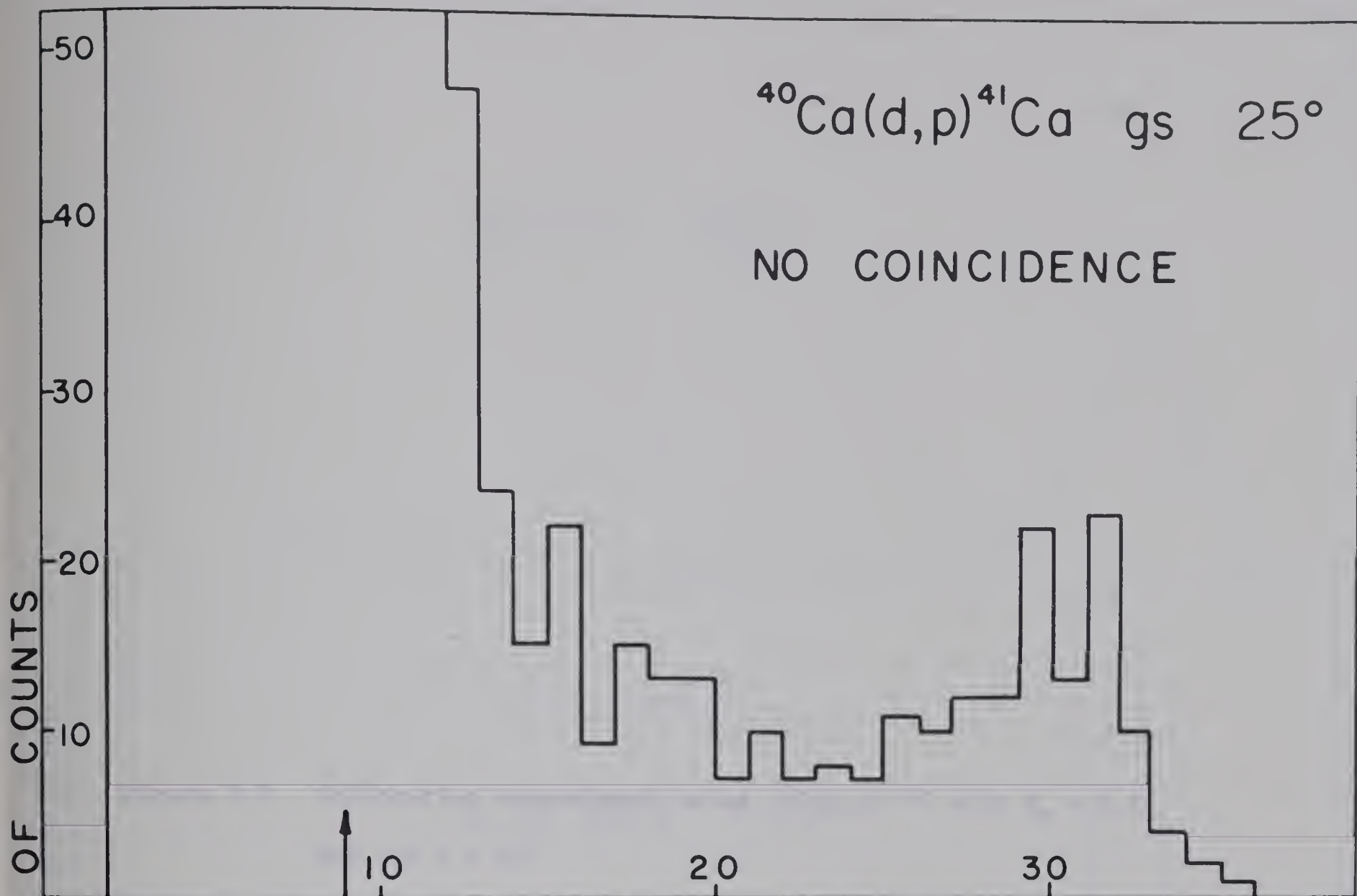


Figure 2.8 Effect of including the  $\frac{dE}{dX}$  detector











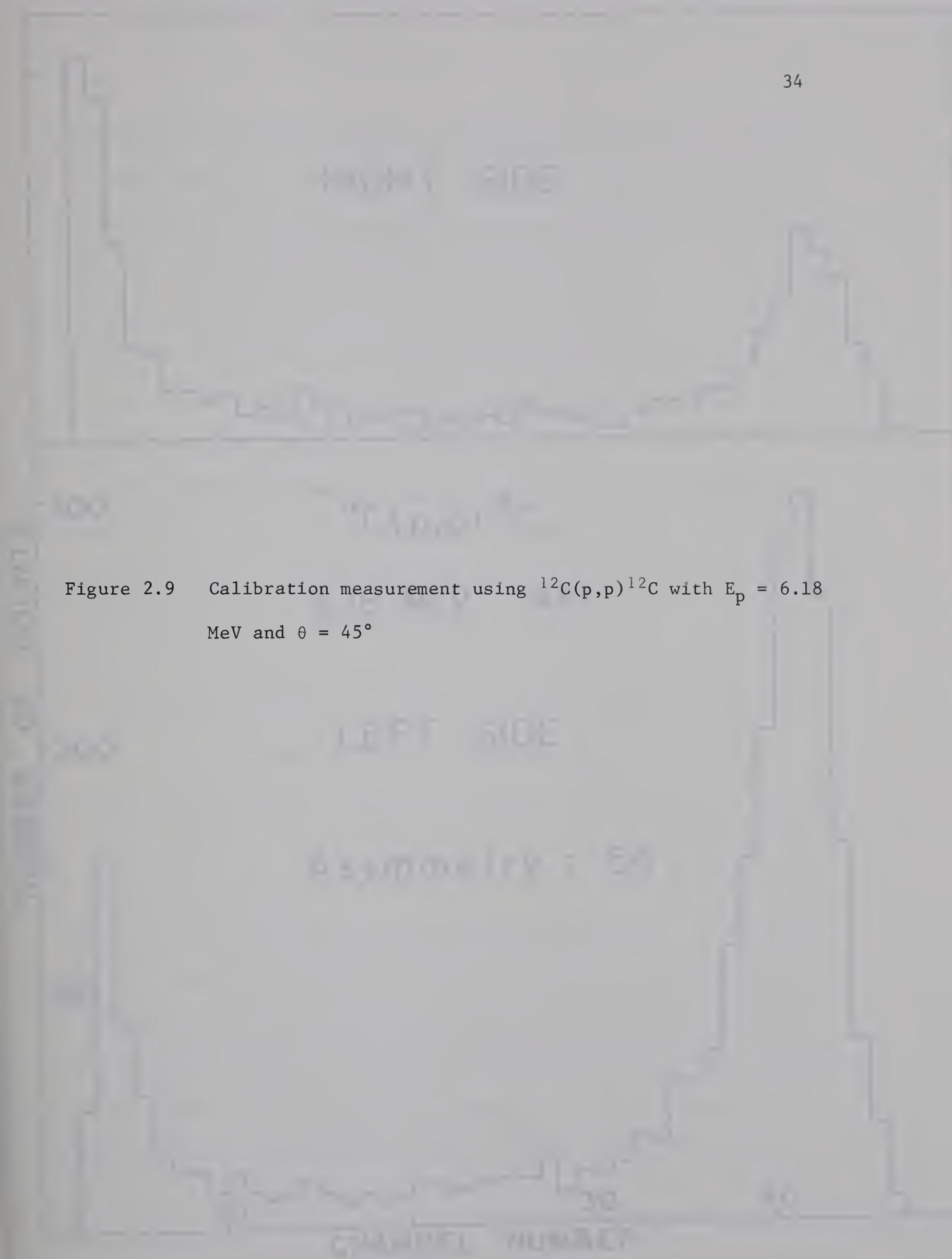


Figure 2.9 Calibration measurement using  $^{12}\text{C}(\text{p},\text{p})^{12}\text{C}$  with  $E_p = 6.18$  MeV and  $\theta = 45^\circ$



RIGHT SIDE

$^{12}\text{C}(p,p)^{12}\text{C}$

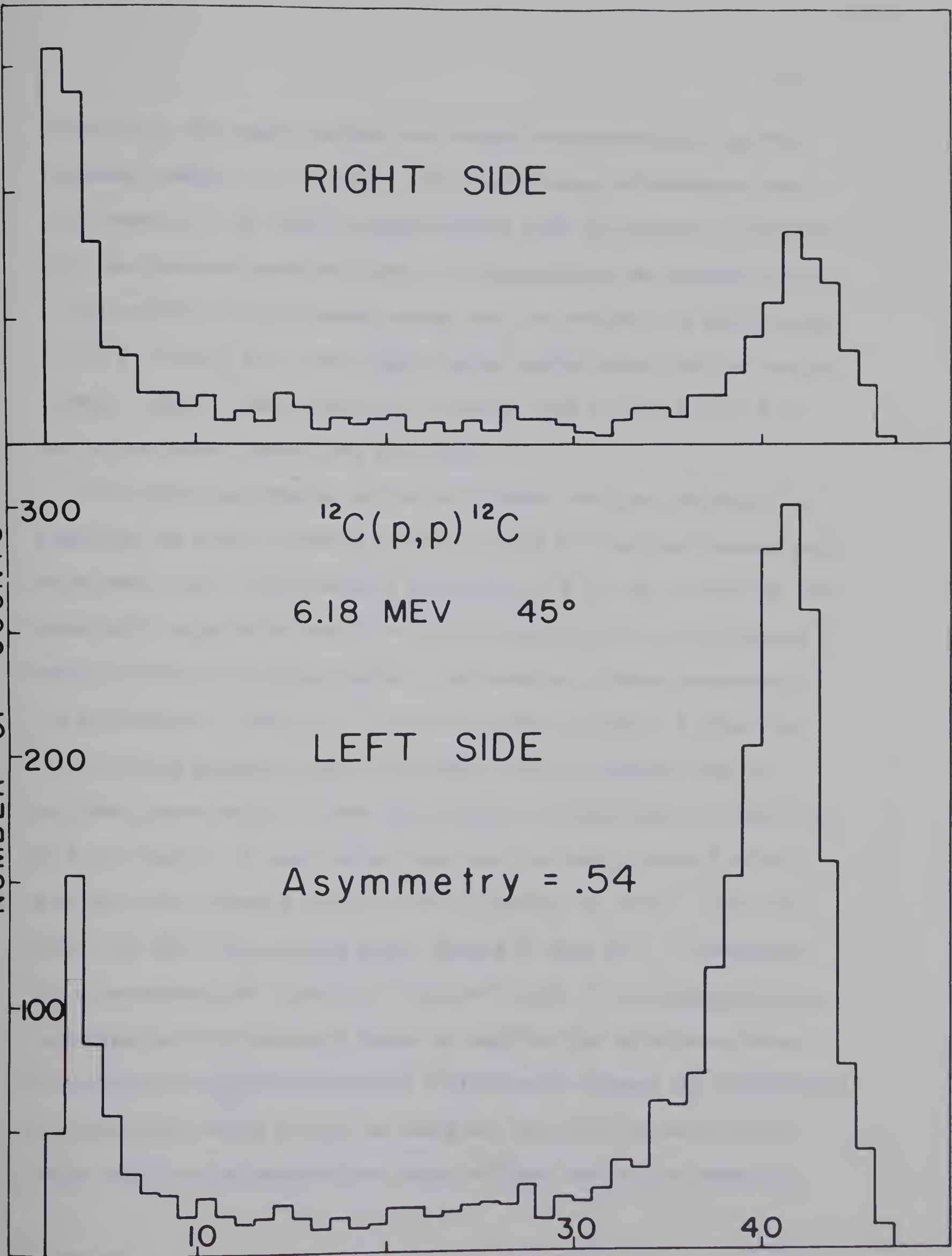
6.18 MEV  $45^\circ$

LEFT SIDE

Asymmetry = .54

NUMBER OF COUNTS

CHANNEL NUMBER







sensitivity, the magnet current was changed corresponding to an NMR frequency change of  $\pm 10$  kcps. The extreme change in asymmetry over this range was 7.5% which is approximately half the measured sensitivity with the tantalum second scatterer. This procedure was carried out at  $45^\circ$  where the scattered proton energy was 5.87 MeV and the polarization  $P_1(45) = -0.81 \pm 0.02$ , this figure being interpolated from the results of Moss. Hence, from equation 2.1, we find that  $P_2(5.87 \text{ MeV}) = 0.67$ , with an estimated uncertainty of  $\pm 0.03$ .

The energy sensitivity of the polarimeter was then determined by repeating the above procedure at  $80^\circ$ ,  $65^\circ$  and  $35^\circ$ , but only taking each measurement once. Unfortunately the errors in  $P_1(\theta)$  at  $60^\circ$  and  $80^\circ$  are relatively large which results in quite large errors in the analyzing power at the corresponding angles. The results of these measurements are summarized in table 2.1. The last column of table 2.1 gives the values of the analyzing power calculated from the geometry and the published phase shifts. These calculations are described in detail by Gurd (Gu 68a,b). It does appear that over the energy range 5.65 to 6.00 MeV, the analyzing power is fairly constant at about  $-0.67$  and below 5.65 MeV the analyzing power appears to drop off. In comparing the experimental and calculated values of  $P_2(E)$ , it is perhaps not too surprising that the measured value is less than the calculated value. This argument would then introduce a discrepancy between the experimental and calculated values at the low energies, but it is in exactly this region that the calculations are least reliable due to the anomaly in



Table 2.1 Measured and calculated values of the polarimeter analyzing power

$\theta_{\text{lab}}$	$\theta_{\text{cm}}$	$E_p(\text{out})$	$P_1(\theta)$	$\epsilon$	$P_2(E)$	$P_2(\text{Predicted})$
35	37.8	6.00	$-0.78 \pm 0.03$	$+0.52 \pm 0.03$	$-0.68 \pm 0.05$	$-0.77$
45	48.4	5.87	$-0.81 \pm 0.02$	$+0.54 \pm 0.02$	$-0.67 \pm 0.03$	$-0.74$
60	64.2	5.68	$-0.36 \pm 0.03$	$+0.24 \pm 0.02$	$-0.67 \pm 0.08$	$-0.67$
80	84.7	5.39	$+0.92 \pm 0.13$	$-0.62 \pm 0.04$	$-0.61 \pm 0.09$	$-0.60$



the polarization at about  $E_p = 5.6$  MeV (Mo 65).

To aid in determining whether the protons were entering the polarimeter within the calibrated range, a pulser peak was superimposed on each of the two peaks in the straight-through counter for the  $45^\circ$  calibration point and the corresponding settings noted. Before a polarization run was taken, the position of the straight-through counter peaks were compared with the position of the pulser peaks. In this way, it was possible to verify simply that the protons were, in fact, entering the polarimeter within the correct energy range.





## CHAPTER 3

### RESULTS AND ANALYSIS

#### 3.1 Yield Curves

The optical model can only be expected to describe the elastic scattering angular distributions if the corresponding yield curves vary smoothly as a function of energy. To investigate this point, an elastic scattering yield curve was measured from 4.70 to 6.54 MeV in 20 keV steps at laboratory scattering angle of  $90^\circ$ . The results of these measurements are shown in fig. 3.1. As can be seen from the figure, the yield is quite smooth, the statistical uncertainties being of the order of 2%. Consequently, we can hope to find optical model parameters that vary smoothly as a function of energy.

Similar curves are shown in the same figure for the (d,p) and (d,n) reactions leading to the ground states of  $^{41}\text{Ca}$  and  $^{41}\text{Sc}$ , respectively. The fluctuations are more serious here, being up to 15% in the (d,p) case and a little less for the (d,n) reaction. This will introduce some uncertainty when the experimental distributions are compared with DWBA predictions, particularly in the extraction of spectroscopic factors. A short yield curve (4.8 - 5.2 MeV) was also measured in 20 keV steps for the protons leaving  $^{41}\text{Ca}$  in the 1.95 MeV state. In this case, fluctuations of up to 10% were observed.





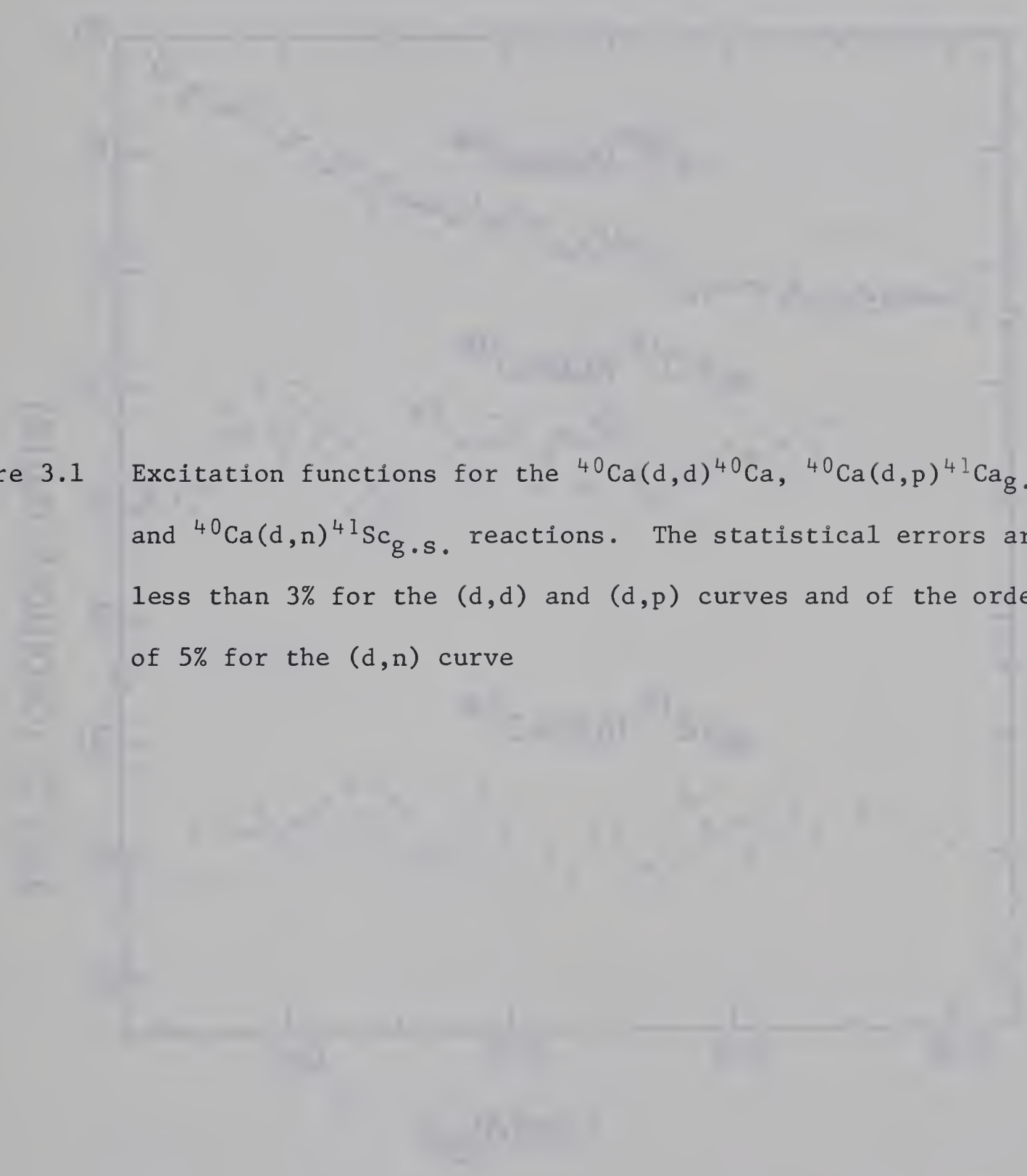
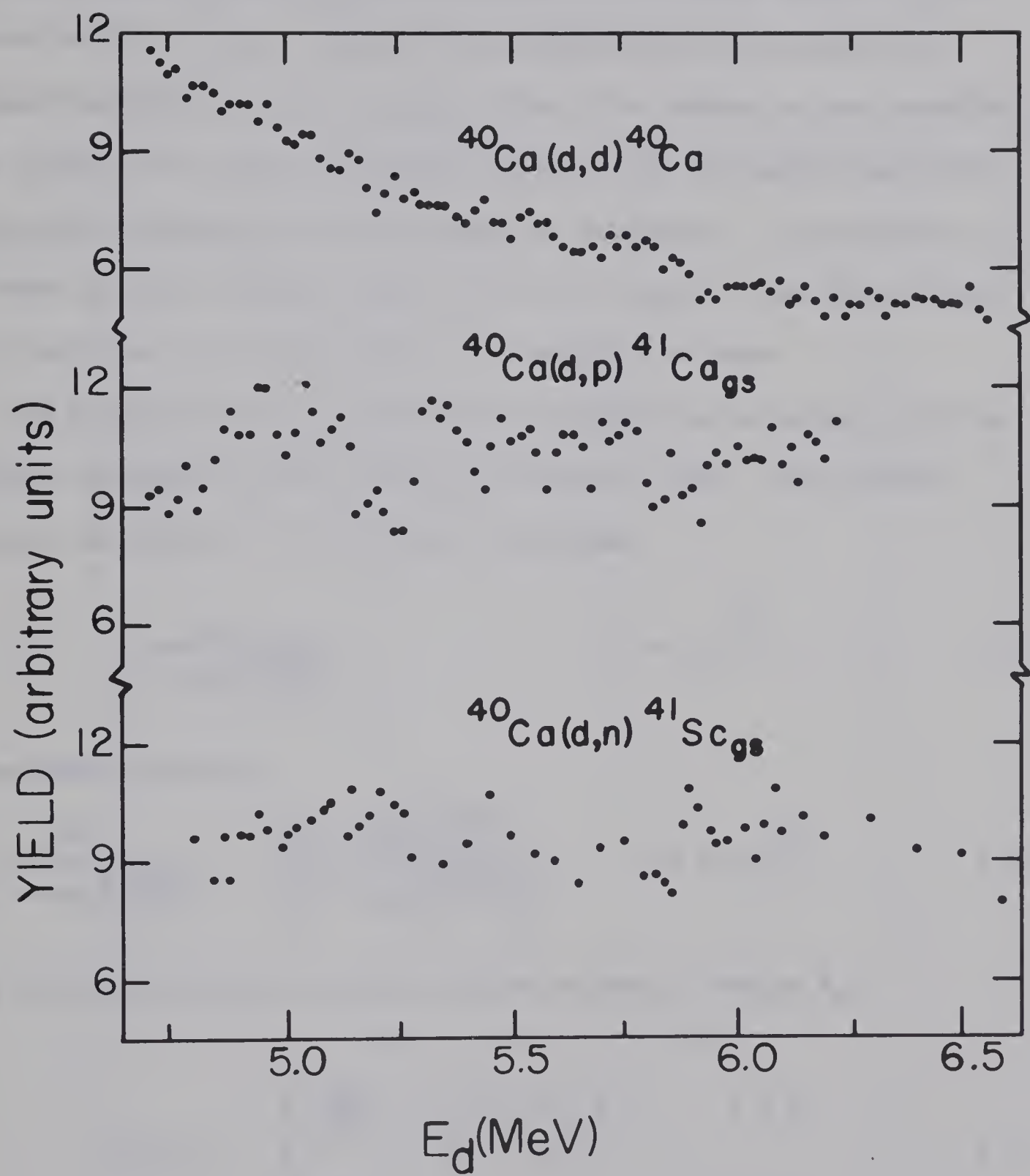


Figure 3.1 Excitation functions for the  $^{40}\text{Ca}(d,d)^{40}\text{Ca}$ ,  $^{40}\text{Ca}(d,p)^{41}\text{Ca}_{\text{g.s.}}$ , and  $^{40}\text{Ca}(d,n)^{41}\text{Sc}_{\text{g.s.}}$  reactions. The statistical errors are less than 3% for the (d,d) and (d,p) curves and of the order of 5% for the (d,n) curve







### 3.2 Elastic Scattering

The elastic scattering distributions are given in table 3.1 and plotted in fig. 3.2 as a ratio of the Rutherford cross-section for incident energies of 5.0, 6.0 and 6.5 MeV. The shapes of the distributions exhibit the usual oscillatory pattern with the maxima and minima becoming more pronounced as the energy is increased. In particular, at 45° there is only a slight inflection in the shape of the distribution at 5.0 MeV, but at 6.5 MeV, there is a definite minimum.

The distributions were fitted by an optical model program with an automatic parameter search written by Perey (Pe 63a). The optical potential is given by a real central potential,

$$\frac{-V}{1 + \exp\left(\frac{r-R}{a}\right)} \quad R = r_0 A^{\frac{1}{3}}, \quad 3.1$$

an imaginary potential,

$$\frac{W_S}{1 + \exp\left(\frac{r-R'}{a'}\right)} + \frac{4W_D \exp\left(\frac{r-R'}{a'}\right)}{\left[1 + \exp\left(\frac{r-R'}{a'}\right)\right]^2} \quad R' = r_0' A^{\frac{1}{3}}, \quad 3.2$$

and a Coulomb potential due to a charged sphere of radius  $R_C$ ,

$$U_C(r) = \begin{cases} \frac{Ze^2}{2R_C} \cdot \left(3 - \frac{r^2}{R_C^2}\right) & r < R_C \\ \frac{Ze^2}{r} & r \geq R_C \end{cases} \quad 3.3$$





Table 3.1

Differential cross sections for the elastic scattering  
of deuterons from calcium

c.m. angle (degrees)	c.m. differential cross sections (mb/sr)		
	$E_d = 5.0$ MeV	6.0 MeV	6.5 MeV
21.0	23300	—	—
26.2	8040	5420	4890
31.4	3770	2520	2180
36.7	2020	1320	1040
41.9	1130	700	552
47.0	708	440	342
52.2	459	294	237
57.4	309	207	169
62.5	217	143	123
67.6	150	102	86.2
72.7	107	70.4	59.1
77.8	77.2	48.0	39.4
82.9	55.9	34.2	28.4
87.9	41.6	25.7	22.3
92.9	33.1	21.5	19.6
97.9	27.6	20.8	19.1
102.9	25.5	20.8	19.5
107.8	24.5	20.6	19.5
112.7	23.3	20.5	18.1
117.6	22.8	19.2	16.3
122.5	21.1	17.9	14.3
127.4	19.8	15.9	11.8
132.2	18.1	13.8	9.55
137.0	16.1	11.2	7.65
141.9	14.1	9.49	6.30



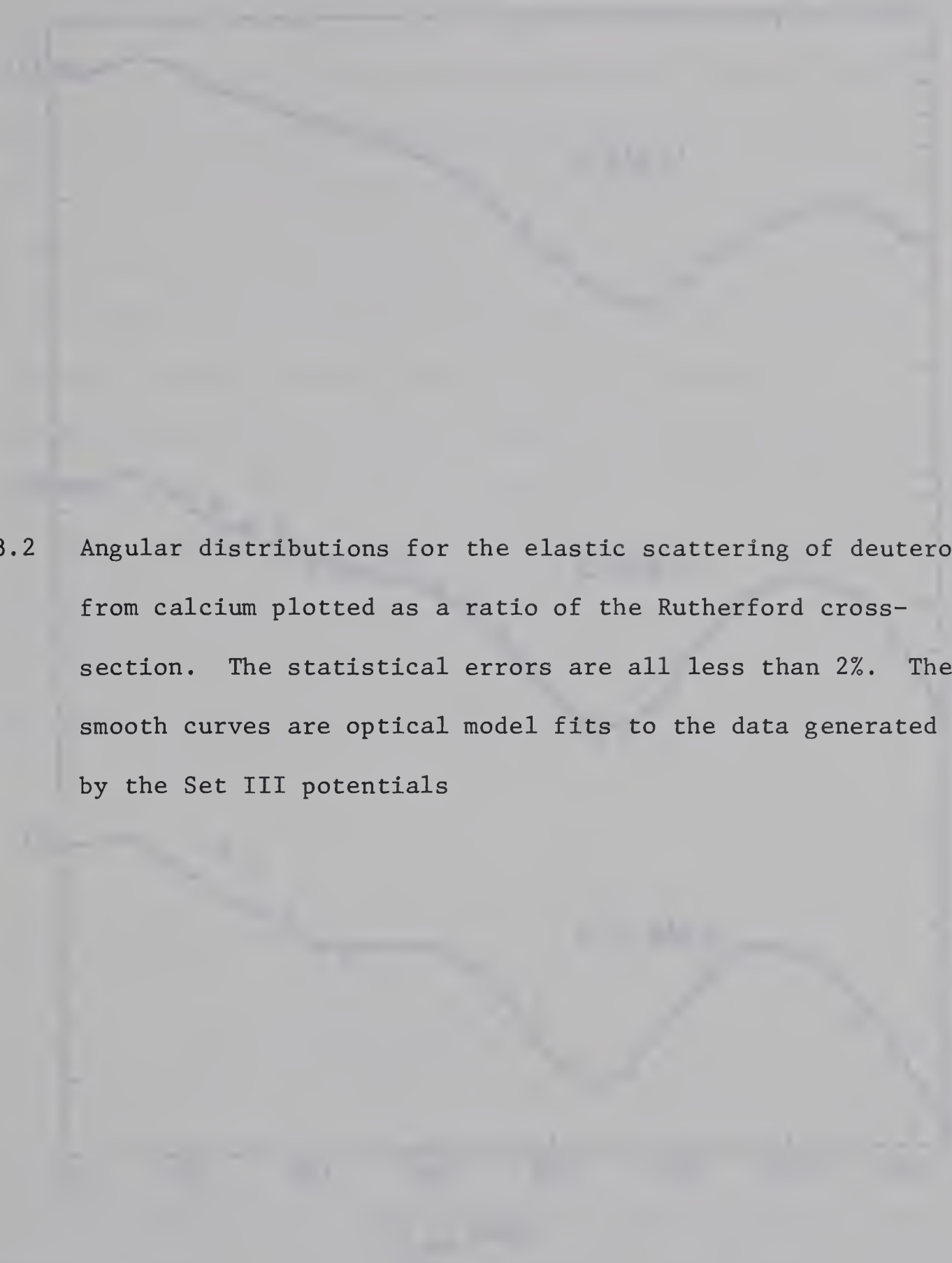
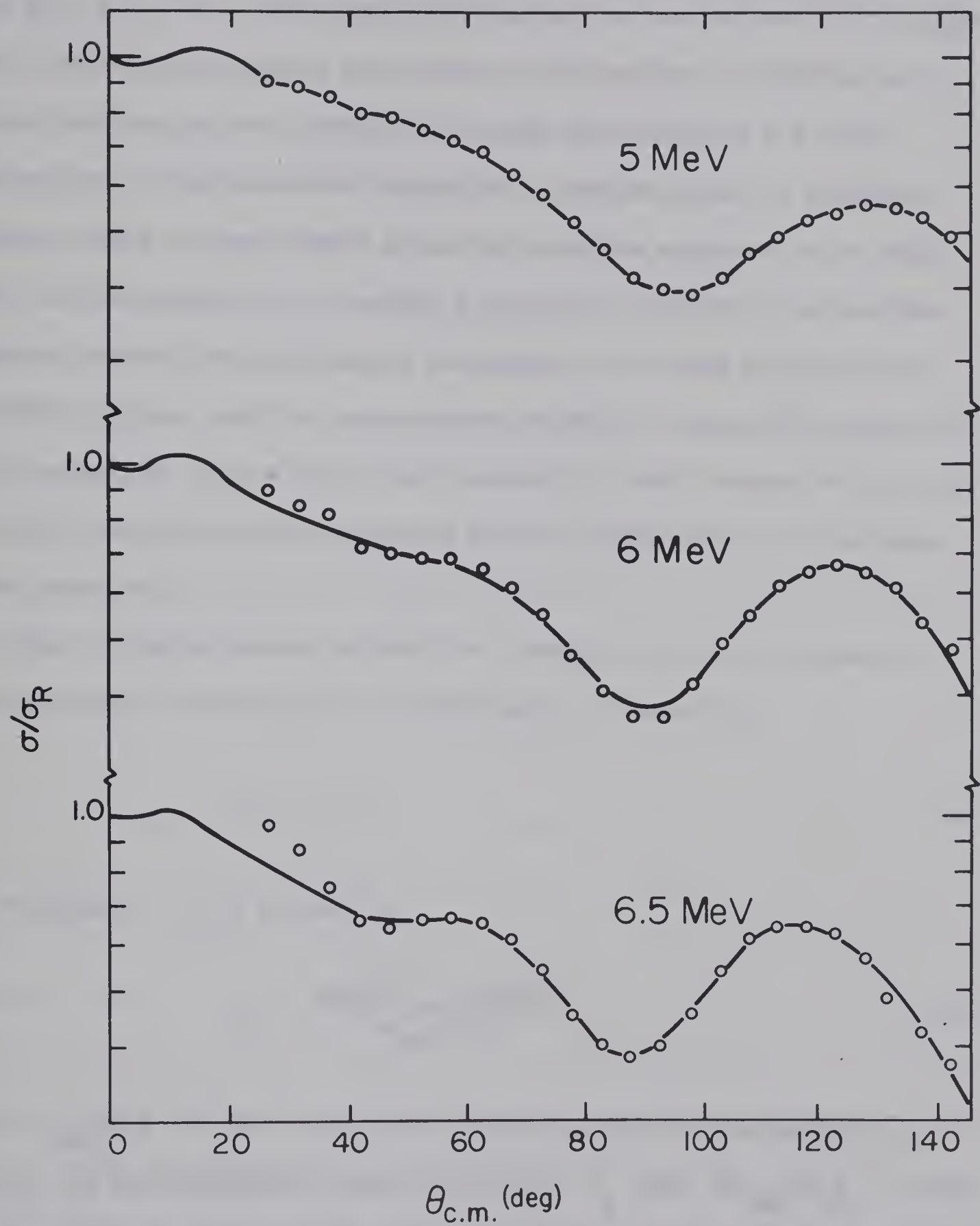


Figure 3.2 Angular distributions for the elastic scattering of deuterons from calcium plotted as a ratio of the Rutherford cross-section. The statistical errors are all less than 2%. The smooth curves are optical model fits to the data generated by the Set III potentials







with  $R_c = 1.3 A^{\frac{1}{3}}$  F. There was no provision for the inclusion of a spin-orbit potential for spin-1 particles in this program. This was not a severe handicap as the elastic scattering distributions are quite insensitive to the spin-orbit potential. Looking ahead to the DWBA analysis where the spin-orbit potential might be expected to be important, the procedure was to include a spin-orbit potential in the DWBA code and compare the new elastic scattering, which was calculated by the DWBA program, with the calculations without a spin-orbit potential. Where necessary, it was found that generally a small change in  $W_D$  could be made to approximately compensate for the introduction of the spin-orbit potential.

The fitting procedure allowed any combination of the parameters in the optical potential to be varied until the quantity

$$\chi^2 = \sum_i \chi_i^2 \quad 3.4$$

was minimized.  $\chi_i$  is defined by

$$\chi_i = \frac{\sigma_{\text{exp}}(\theta_i) - \sigma_{\text{th}}(\theta_i)}{\Delta\sigma_{\text{exp}}(\theta_i)} \quad 3.5$$

where  $\sigma_{\text{exp}}(\theta_i)$  is the experimental cross-section at the angle  $\theta_i$ ,  $\sigma_{\text{th}}(\theta_i)$  is the calculated cross-section at  $\theta_i$  and  $\Delta\sigma_{\text{exp}}(\theta_i)$  is the experimental uncertainty in  $\sigma_{\text{exp}}(\theta_i)$ . Although, as was stated earlier, a realistic estimate of  $\Delta\sigma$  would be 5%, due to some early over-optimism,





the data cards were all punched up with  $\Delta\sigma$  set equal to 3%. This is of no great consequence as it is only the relative values of  $\chi^2$  that are important, which are of course unchanged.

Nearly all the searches described here are with  $W_s = 0$  in equation 3.2, that is with only surface absorption of the deuteron. It has been found (Ha 64) that equivalent fits can be found with either volume or surface absorption and so in order to provide continuity with higher energy studies, we have chosen to concentrate on potentials with no volume absorption.

First attempts were to fit the distributions with a potential in which the real and imaginary shape parameters were constrained to be the same. That is

$$r_0 = r_0' \quad a = a' . \quad 3.6$$

The starting parameters were arbitrarily chosen to be  $r_0 = r_0' = 1.3$  F,  $a = a' = 0.6$  F and  $W_D = 10.0$  MeV. Initially  $V$  was not free, but kept fixed during a particular search while the other three parameters were allowed to vary.  $V$  was gridded from 30 to 170 MeV in 10 MeV steps. The plots of  $\chi^2$ ,  $r_0$ ,  $a$  and  $W_D$  against  $V$  for the three incident energies are shown in figs. 3.3 - 3.5. The same type of analysis was also carried out on the 7 MeV data of Bassel et al. (Ba 64) and is shown in fig. 3.6. In the evaluation of  $\chi^2$  in this case, the values of  $\Delta\sigma$  are those assigned by Bassel and consequently the values of  $\chi^2$  that are found here for their 7 MeV data may be compared with the values quoted by Bassel. The



solid circles indicate searches over  $V$ ,  $r_0$ ,  $a$  and  $W_D$  starting from parameters corresponding to the minima in  $\chi^2$ . The curves all exhibit four distinct minima at real well depths of about 45, 80, 120 and 180 MeV. Between these minima,  $r_0$  varies so as to keep  $Vr_0^2$  constant and  $a$  and  $W_D$  are more or less constant. This behaviour cannot be considered a true  $Vr^2$  ambiguity though, since in most cases, the minima in  $\chi^2$  are very sharp. The parameters corresponding to the potentials for which  $\chi^2$  has a minimum are denoted as the Set I parameters and are given in table 3.2. The fits generated by these parameters are very good, the  $\chi^2$  at 6.5 MeV being slightly less than that for the set ultimately settled on (Set III), while at 5 and 6 MeV, the  $\chi^2$  is higher than that for the Set III parameters. The Set I parameters were then used in DWBA calculations of the (d,p) and (d,n) angular distributions. Although equally good fits were obtained with these parameters as with any of the other sets of parameters found (see fig. 3.13), these parameters were rejected for the following reason. One expects the deuteron parameters to vary fairly smoothly as a function of energy. Bassel found in the higher energy study that neither volume nor surface absorption potentials could give good fits to the experiment with a potential that had the same radius for the real and imaginary parts. This was verified by the results of our search on their 7 MeV data shown in fig. 3.6 where it can be seen that the minimum value of  $\chi^2$  is 140 compared to Bassel's value of 25. Consequently the next step was to release the constraints of equations





Figure 3.3 Diagram indicating the results of optical model searches for the 5 MeV elastic scattering in which the real and imaginary shape parameters were constrained to be the same. The open circles indicate searches over  $W_D$ ,  $r$ , and  $a$ ; the solid circles are the results of searches over  $V$ ,  $r$ ,  $a$  and  $W_D$





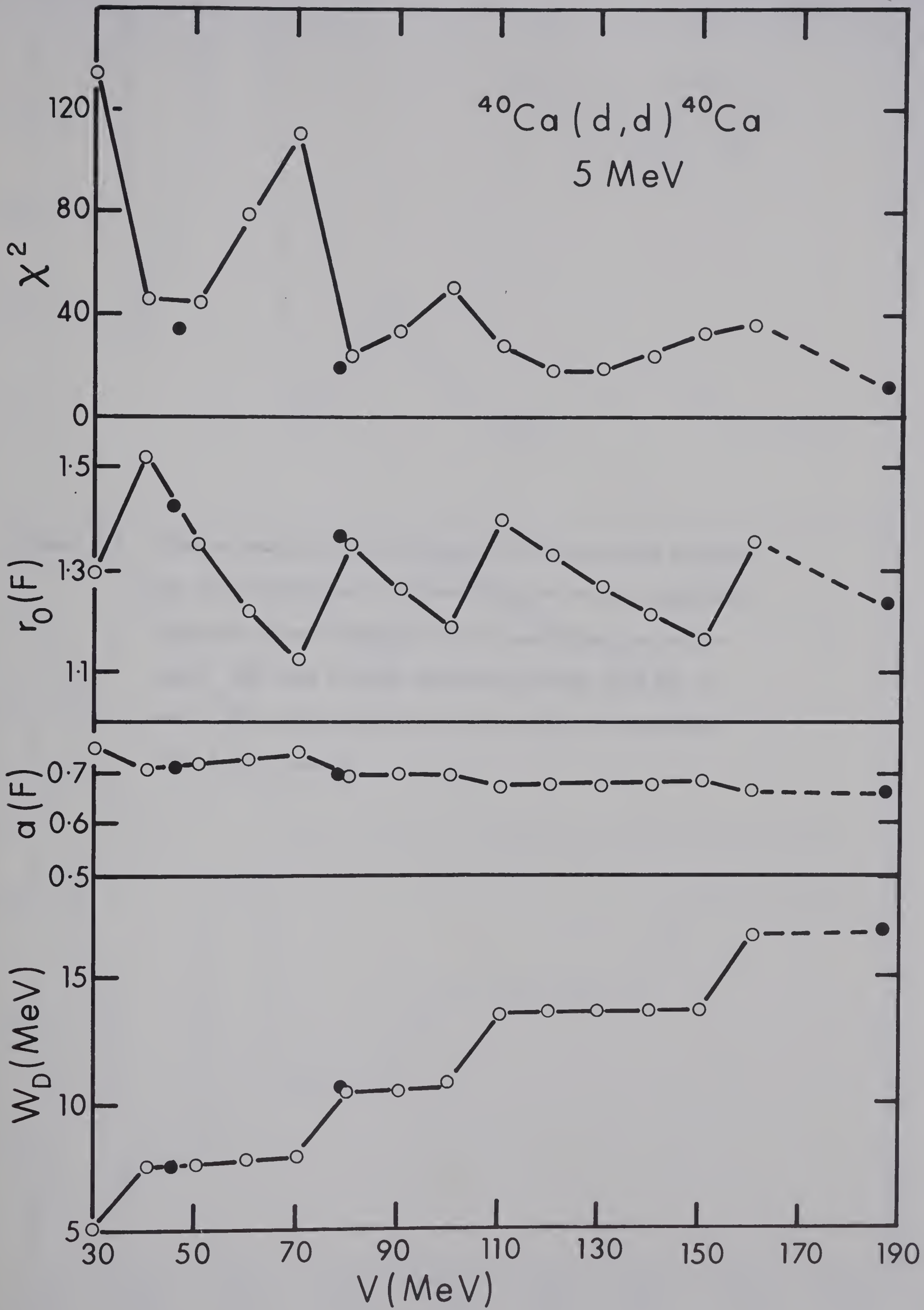




Figure 3.4 Diagram indicating the results of optical model searches for the 6 MeV elastic scattering in which the real and imaginary shape parameters were constrained to be the same. The open circles indicate searches over  $W_D$ ,  $r$ , and  $a$ ; the solid circles are the results of searches over  $V$ ,  $r$ ,  $a$  and  $W_D$



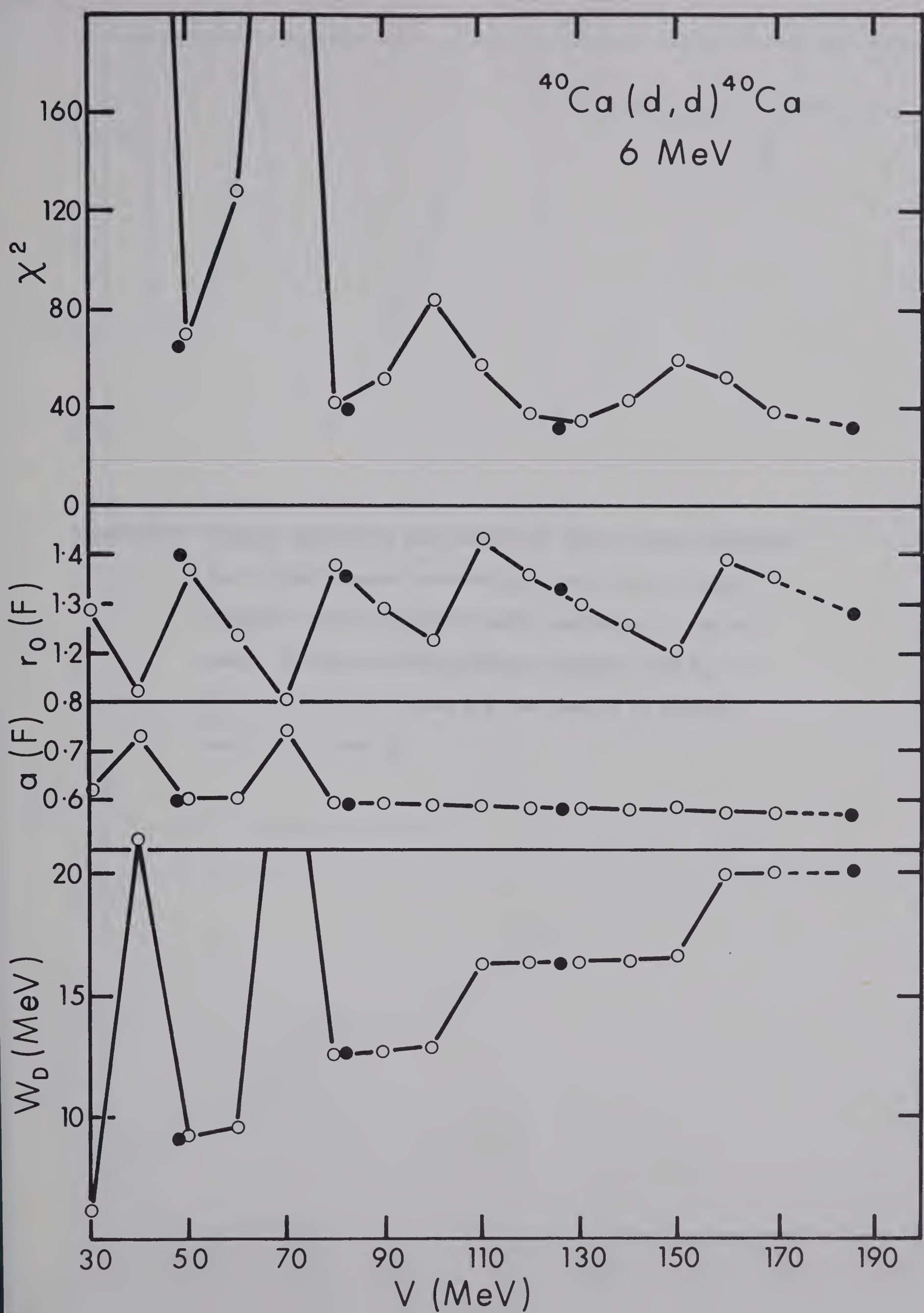






Figure 3.5 Diagram indicating the results of optical model searches for 6.5 MeV elastic scattering in which the real and imaginary shape parameters were constrained to be the same. The open circles indicate searches over  $W_D$ ,  $r$ , and  $a$ ; the solid circles are the results of searches over  $V$ ,  $r$ ,  $a$  and  $W_D$





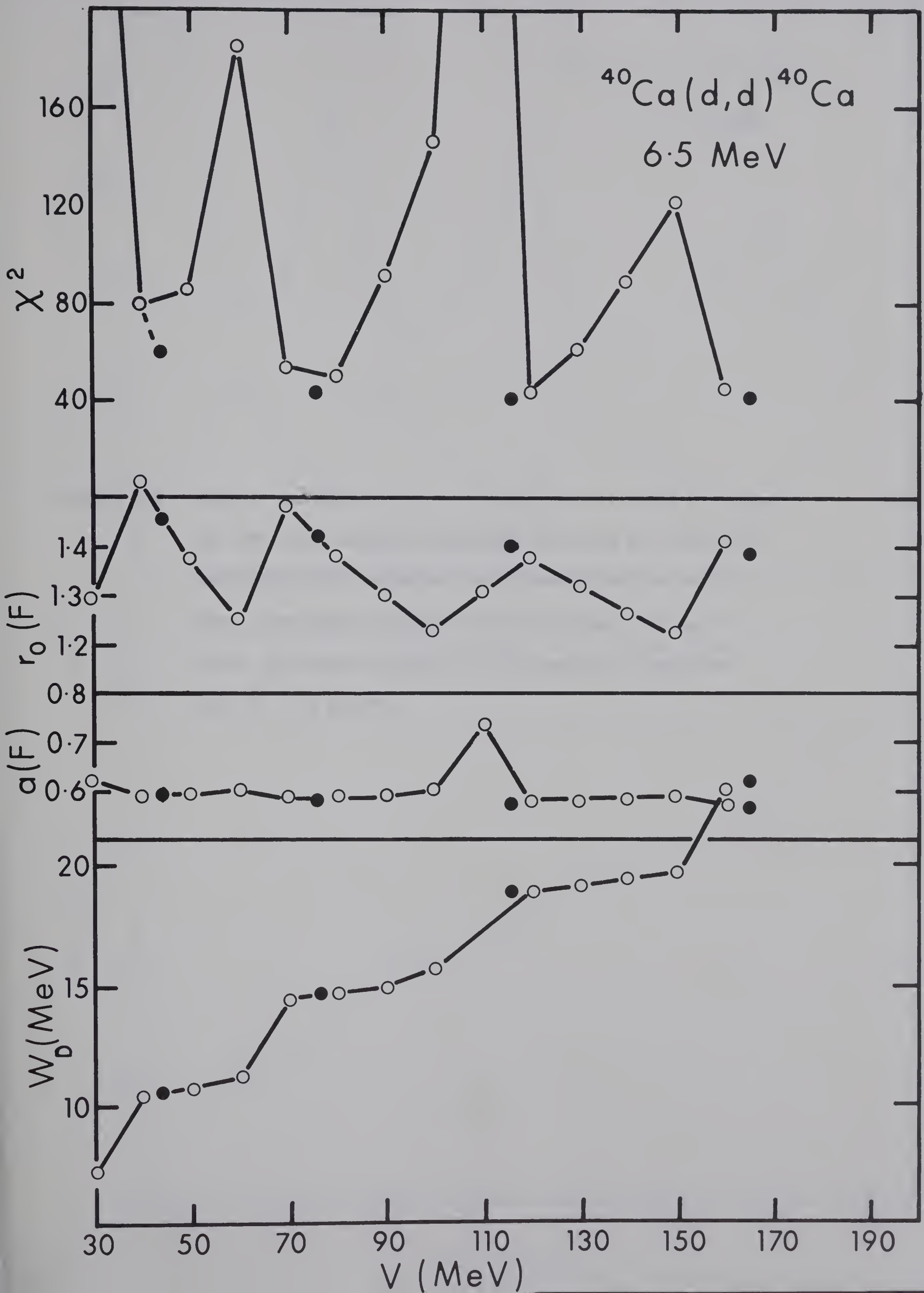




Figure 3.6 Diagram indicating the results of optical model searches for the 7 MeV elastic scattering in which the real and imaginary shape parameters were constrained to be the same. The open circles indicate searches over  $W_D$ ,  $r$ , and  $a$ ; the solid circles are the results of searches over  $V$ ,  $r$ ,  $a$  and  $W_D$



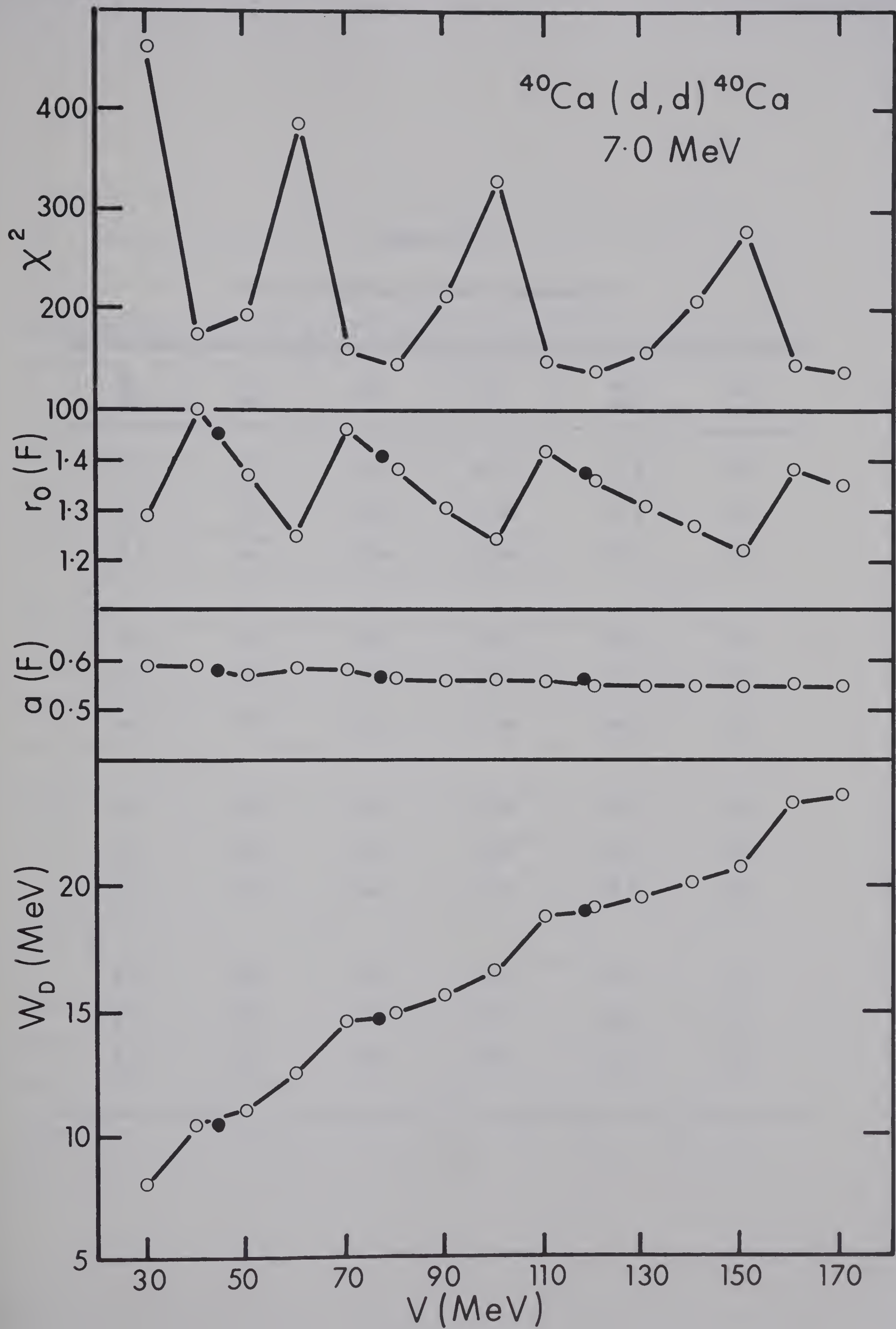






Table 3,2

## Set I Deuteron potential parameters

$E_d$ MeV	V MeV	$r_0$ F	a F	$W_D$ MeV	$\chi^2$
5.0	46	1.42	0.71	7.6	32
6.0	48	1.40	0.60	9.2	66
6.5	44	1.46	0.59	10.6	60
5.0	78	1.37	0.70	10.6	21
6.0	82	1.36	0.59	12.7	40
6.5	76	1.42	0.58	14.6	43
5.0	125	1.30	0.68	13.6	19
6.0	126	1.33	0.58	16.3	33
6.5	116	1.40	0.57	18.8	40
5.0	186	1.24	0.67	17.0	12
6.0	186	1.28	0.57	20.0	31
6.5	165	1.38	0.56	23.2	41



3.6 on  $r_0'$  and  $a'$ . A series of searches were carried out using the Set I parameters of table 3.2 as starting values and allowing all of the parameters except  $V$  to vary independently,  $V$  being held fixed at its starting value. The resultant parameters, referred to as the Set II parameters, are given in table 3.3. The success of these parameters in subsequent DWBA calculations is discussed in the next section. The conclusions drawn from these considerations were that the Set II parameters are also unsatisfactory and they also did not fit in with the trend of the parameters found in the higher energy study.

A third set of searches was then undertaken with  $V$  somewhat arbitrarily fixed at 110 MeV, and the other parameters being allowed to vary. The starting values of the other parameters were this time the Set II parameters except for  $r_0$  which was started at 1.10 F. The final values are indicated in table 3.4. It can be seen by comparing tables 3.4 and 3.3 that the fits are not improved, in fact, the  $\chi^2$  is in all cases slightly worse for Set III. No improvement resulted when  $V$  was allowed to vary also, using the Set III parameters as starting values, therefore,  $V$  was kept at the value of 110 MeV. The theoretical fits in fig. 3.3 correspond to the Set III parameters. Fig. 3.7 shows a plot of the best fit parameters from the 7 to 12 MeV study of Bassel and the Set III parameters of this work. The parameters follow fairly smooth trends. There are some obvious deviations such as the large value of  $V$  and small value of  $r_0$  for the 7 MeV fit, and the high value of  $W_D$  together with a low value of  $a'$  for the 8 MeV data.



Table 3.3

## Set II Deuteron potential parameters

$E_d$ MeV	$V_0$ MeV	$r_0$ fm	$a$ fm	$W_D$ MeV	$r_0'$ fm	$a'$ fm	$\chi^2$
5.0	78	1.31	0.87	20.2	1.76	0.32	3.2
6.0	82	1.31	0.76	19.6	1.66	0.34	16.4
6.5	76	1.39	0.67	17.5	1.60	0.44	39.1
5.0	125	1.24	0.83	22.1	1.75	0.32	3.2
6.0	126	1.28	0.72	23.1	1.66	0.32	16.8
6.5	116	1.37	0.63	21.1	1.58	0.43	38.5
5.0	186	1.24	0.67	16.9	1.21	0.69	13.6
6.0	186	1.24	0.69	24.7	1.65	0.33	18.2
6.5	165	1.36	0.60	24.9	1.57	0.42	38.9





Table 3.4

## Set III Deuteron potential parameters

$E_d$ MeV	$V_0$ MeV	$r_0$ fm	$a$ fm	$W_D$ MeV	$r_0'$ fm	$a'$ fm	$\chi^2$
5.0	110	1.03	0.92	9.8	1.64	0.53	3.9
6.0	110	1.06	0.81	9.9	1.57	0.55	21.6
6.0 <sup>a</sup>	110	1.00	0.98	11.6	1.72	0.52	10.3
6.5	110	1.08	0.71	7.4	1.56	0.74	46.0
6.5 <sup>a</sup>	110	1.02	0.91	10.2	1.68	0.61	10.2
5.0 <sup>b</sup>	110	1.05	0.87	4.6	2.02	0.43	4.4
6.0 <sup>b</sup>	110	1.09	0.73	4.6	1.97	0.50	25.7
6.5 <sup>b</sup>	110	1.10	0.66	4.0	2.15	0.51	45.4

a Data renormalized by a factor of 0.9

b Volume absorption potential





These deviations probably reflect ambiguities of the  $Vr^2$  and  $Wa'$  kind in the optical model and are not significant.

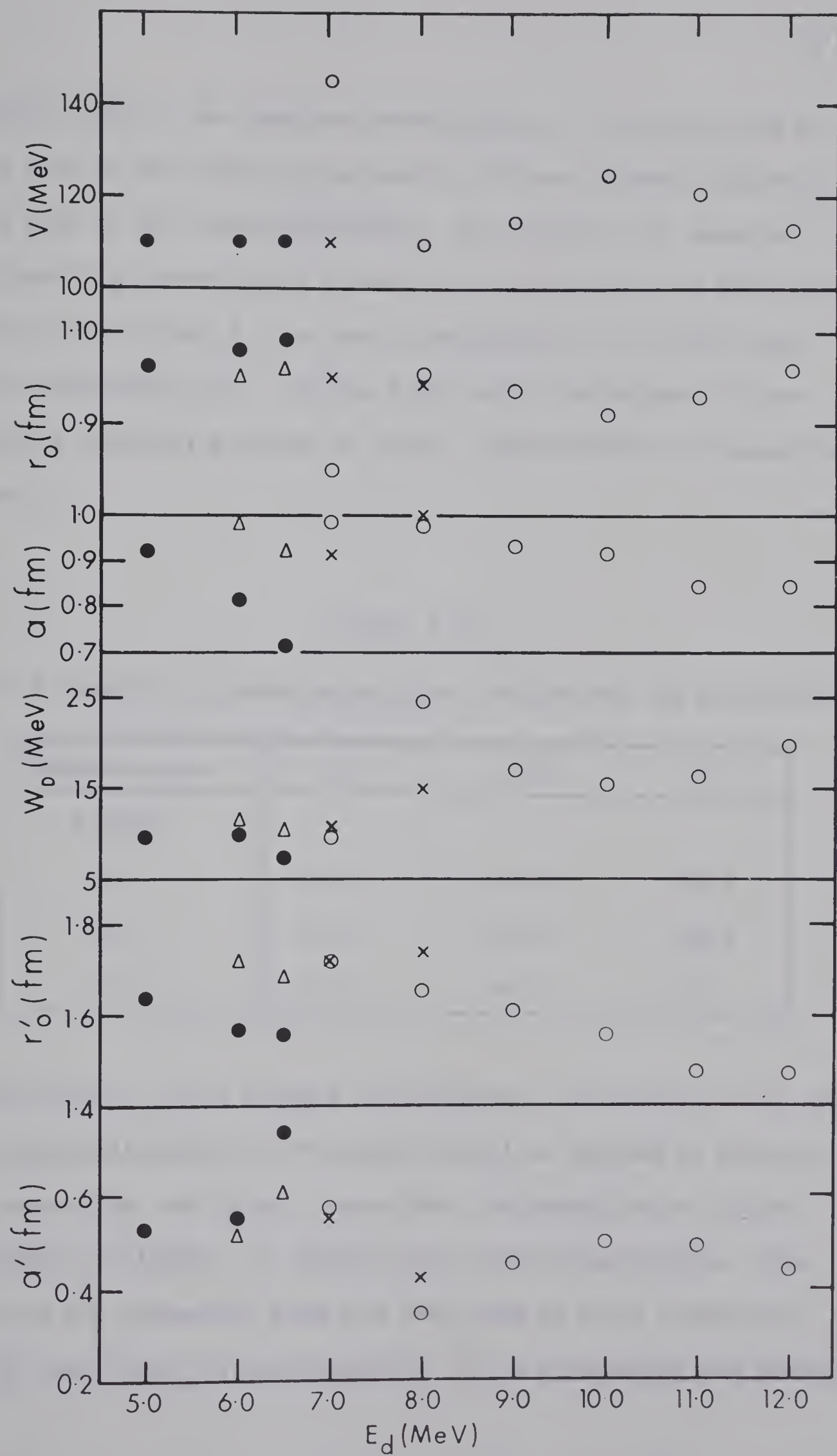
To verify this assumption, optical model searches were carried out on the 7 MeV and 8 MeV data. Initially  $V$  was fixed at 110 MeV for the 7 MeV data instead of the value of 145 MeV found by Bassel. A good fit was found with  $\chi^2$  going from 25 to 52, but  $r_0$  dropped to 0.64 F which is far off the average trend of  $r_0$ . A second search was attempted with  $V$  fixed at 110 MeV and  $r_0$  at 1.00 F. A fit then resulted with a  $\chi^2$  of 51 and parameters denoted by crosses in fig. 3.7 that agreed well with the overall trend. A similar effect was found for the 8 MeV data. In this case, it was necessary to fix  $V$  and  $W$  at 109.4 MeV and 15.0 MeV, respectively. In this case, the  $\chi^2$  went from an optimum value of 90.1 to 146. The corresponding parameters are again indicated by crosses in fig. 3.7.

Although the gross fluctuations in the energy dependence have been rather forcibly removed, the trends are not as smooth as one would hope for. The values of  $a$  are on the low side as are the values of  $r_0'$ . When the comparison between the optical model fits and the experimental data is looked at more closely, it is apparent that the agreement at the forward angles is not as good as might be expected, the data being consistently higher than the theoretical curves. This could be an indication of an error in absolute normalization of the cross-sections. To investigate this point a little farther, the data at all three energies were renormalized by factors 0.9 and 1.1, that being the estimated range



Figure 3.7 Plot of the 'best Z' parameters of Bassel (Ba 64) and the Set III parameters as a function of deuteron energy. The crosses indicate searches over the 7 and 8 MeV data in which constraints have been imposed, as described in the text. The triangles correspond to searches over the 6 and 6.5 MeV data renormalized by a factor of 0.9









in possible error of the absolute normalization. At both 6.5 and 6.0 MeV, the fits to the data renormalized by 0.9 were markedly improved over the fits to the unnormalized data. The new fits are shown in fig. 3.8 and the corresponding parameters are also given in table 3.4. The fits to the 6.0 and 6.5 MeV data normalized by 1.1 on the other hand were especially poor. For the 5 MeV data, the optimum fit was found with a normalizing factor of unity. These results are summarized in table 3.5.

Table 3.5

$\chi^2$  as a function of normalizing factor for the Set III parameters

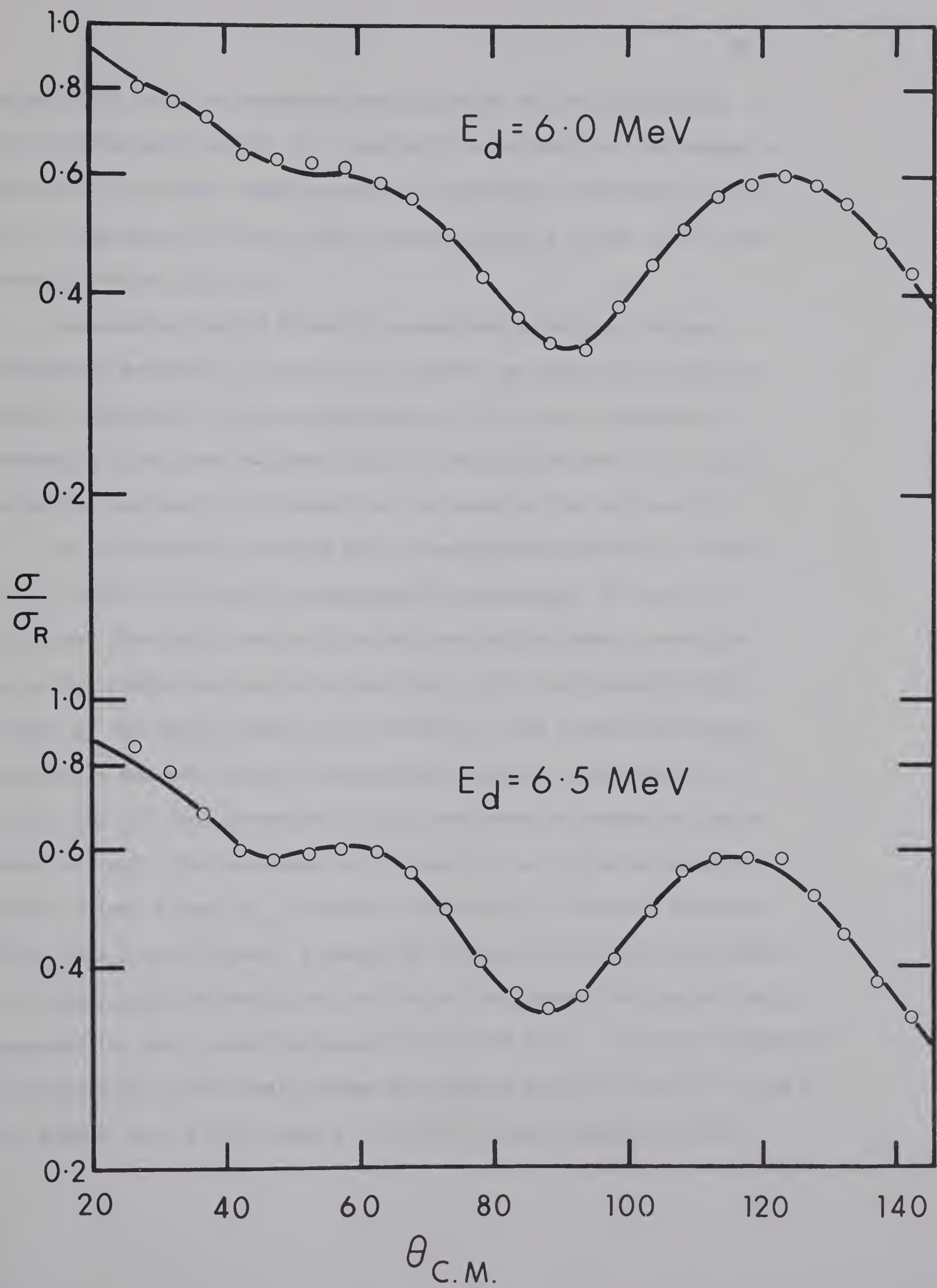
Normalization	0.9	1.0	1.1
$E_d$ (MeV)			
5.0	20.5	3.9	26.9
6.0	10.3	21.6	58.5
6.5	10.2	46.0	134

Unfortunately, as is pointed out by Dickens and Perey (Di 65), due to the oversimplification of the optical model as applied to deuteron elastic scattering, one cannot assume that the normalization factor corresponding to minimum  $\chi^2$  defines the correct distribution. The variation in the parameters does give some idea of their uncertainty due to the uncertainty in normalization. It is interesting and perhaps



Figure 3.8 Optical model fits to the 6 and 6.5 MeV elastic scattering distributions renormalized by a factor of 0.9







significant that the parameters most affected are the diffuseness  $a$  and the imaginary radius  $r_0'$ , precisely the parameters that seemed to lie below the higher energy trend. The parameters resulting from the fit to the data at 6 and 6.5 MeV renormalized by a factor of 0.9 are also plotted in fig. 3.7.

Included in table 3.4 are the parameters found for a volume absorption potential. As mentioned earlier, no stress was placed on volume absorption in this investigation, but it was of interest to determine if and how the DWBA calculations differed when this type of potential was used. This aspect is discussed in the next section.

Up to this point, we have been concerned about finding the best fit to each of the elastic scattering distributions. As has been discussed previously, one would expect the optical model parameters to either remain constant or at most vary slowly and smoothly with energy if the optical model is to be valid. Very acceptable average parameters had been found to describe the elastic scattering from 7 to 12 MeV (Ba 64) and, therefore, efforts were made to extend the range down to 5 MeV. The procedure was to hold  $r_0$ ,  $a$ ,  $r_0'$  and  $a'$  constant and to allow  $V$  and  $W_D$  to vary to minimize  $\chi^2$  for each distribution from 5 to 14.3 MeV. A number of different starting combinations of these parameters were tried and the set was chosen that subjectively provided the best overall agreement to all the data. The shape parameters corresponding to this best average set denoted as Set IV are  $r_0 = 1.00$  F,  $a = 0.88$  F,  $r_0' = 1.55$  F and  $a' = 0.50$  F. These parameters differ





slightly from the Z2 parameters of Bassel (Ba 64) who found that  $r_0 = 1.00$  F,  $a = 0.90$  F,  $r_0' = 1.55$  F and  $a' = 0.47$  F gave the best overall agreement to the higher energy data. The Set IV parameters gave equally good fits as the Z2 parameters to the higher energy data and considerable improvement to the 5, 6 and 6.5 MeV experiments. The Set IV parameters, together with the  $\chi^2$ , corresponding to both the Set IV and Z2 parameters are given in table 3.6. The parameters for the 14.3 MeV data of Hjorth et al. (Hj 65) are also given in table 3.6. From this table, it can be seen that the real well depth  $V$  varies fairly smoothly decreasing with increasing energy from 118.4 MeV down to about 112 MeV. The imaginary well depth on the other hand, fluctuates rather more. Except for the 5 MeV value, it is equal to  $16.9 \pm 1.7$  MeV. The lower value at 5 MeV is not too surprising as it is to be expected that as the energy decreases in this region, the absorption will also decrease. The investigation in the higher energy region indicated a tendency for  $r_0'$  to decrease with increasing energy, the smoothest dependence of  $V$  and  $W_D$  being found when  $r_0'$  was represented by  $r_0' = (1.98 - 0.04E)$  F. Accordingly, a similar variation was incorporated in the Set IV parameters, but with unsatisfactory results. There was little if any improvement to the higher energy distributions and extremely poor agreement to the lower energy distributions with the higher absorption radius.

In all of this analysis, the tacit assumption has been made that the compound elastic contribution is small compared to the observed elastic



Table 3.6

Set IV Deuteron potential parameters<sup>a)</sup>

$E_d$ MeV	$V$ MeV	$r_0$ F	$a$ F	$W_D$ MeV	$r_0'$ F	$a'$ F	$\chi^2$ Set IV	$\chi^2$ Z2
5.0	118.4	1.00	0.88	10.6	1.55	0.50	19	71
6.0	116.1			15.9			294	410
6.5	116.7			18.3			266	365
7.0	115.0			17.2			161	198
8.0	112.1			18.6			385	342
9.0	112.8			18.1			290	280
10.0	112.6			16.1			313	320
11.0	111.9			15.3			221	243
12.0	112.3			15.2			465	479
14.3	115.0			14.6			1037	976

a) Note that  $\chi^2$  at 5.0, 6.0 and 6.5 MeV cannot be compared to values at higher energies owing to the different definitions of  $\chi^2$ .





scattering. This assumption was verified by Hauser-Feshbach calculations performed by Davison (Da 68). These calculations are approximate because of the necessity of describing the higher states of  $^{42}\text{Sc}$ ,  $^{41}\text{Sc}$  and  $^{41}\text{Ca}$  by level density formulae. Some degree of confidence can be had in the results of the calculations in as much as they reproduce well the measured cross-sections of reactions that are expected to proceed only by the compound nucleus process. Fig. 3.9 shows plots of the results of the calculations for the three energies considered here. In all cases, it can be seen that the calculated compound nucleus contributions are negligible compared to the observed elastic cross-sections, being about 1% at the furthest back angles. Due to the uncertainty in the calculated cross-sections, the compound nucleus contribution at the back angles were not subtracted from the observed cross-sections.

### 3.3 Stripping Distributions

The cross-sections for the five (d,p) distributions measured are given in table 3.7 and the distributions are plotted in figs. 3.10 - 3.12. The distributions each have a well-defined stripping peak indicating that the reactions are to a large extent direct. The peak at  $40^\circ$  for the ground state distributions is characteristic of an  $\ell = 3$  transfer, and the peaks at  $20^\circ$  for the other reactions are characteristic of  $\ell = 1$  distributions. It was not possible to measure the cross-section for the 3.95 MeV state between  $55^\circ$  and  $70^\circ$  because







Figure 3.9 Hauser-Feshbach calculations of the contributions of compound elastic scattering to the observed elastic scattering



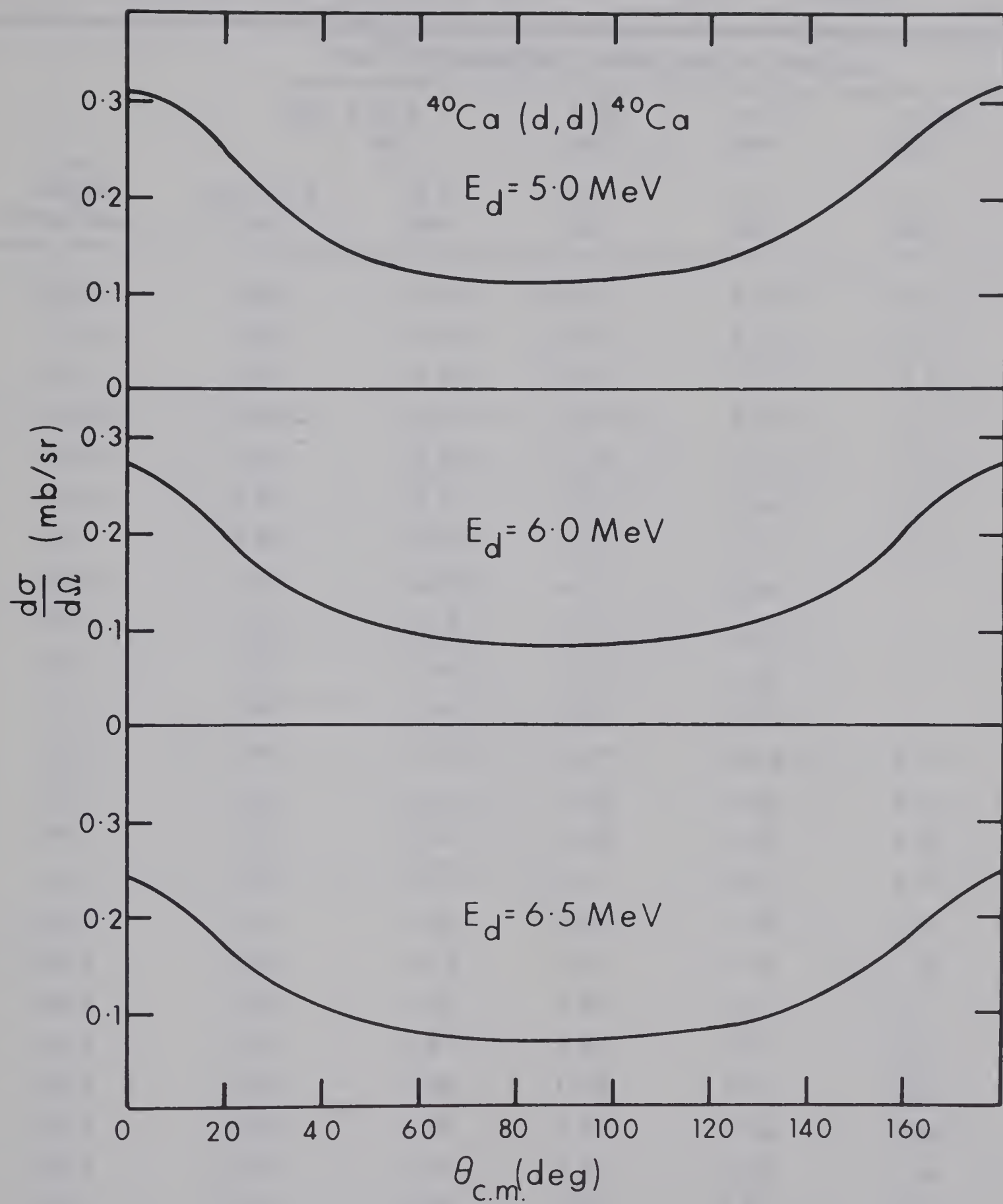




Table 3.7

Differential cross sections for the  $^{40}\text{Ca}(\text{d},\text{p})^{41}\text{Ca}$  reaction

c.m. differential cross section (mb/sr)					
c.m. angle (degrees)	$E_{\text{xn}} = 0.0$				
	$E_{\text{d}} = 5.0$	6.0	5.0	5.0	5.0
	MeV	MeV	MeV	MeV	MeV
20.5	2.40	2.30	10.3	4.25	6.24
25.6	2.55	2.51	10.6	4.10	6.64
30.7	2.81	3.02	9.22	3.64	5.92
35.9	3.02	3.64	7.11	2.57	5.27
41.0	3.15	3.83	4.70	1.98	3.92
46.0	3.00	3.87	3.83	1.58	3.77
51.1	2.69	3.50	3.81	1.42	4.11
56.2	2.42	2.90	4.52	1.59	--
61.3	2.16	2.38	5.20	1.85	--
66.3	1.87	1.94	5.20	2.00	--
71.4	1.80	1.61	5.59	2.11	--
76.4	1.68	1.50	4.94	2.16	4.39
81.5	1.69	1.56	4.29	1.99	3.76
86.5	1.81	1.58	3.48	1.85	3.30
91.5	1.88	1.76	3.11	1.61	2.76
96.5	1.94	1.82	2.38	1.39	2.17
101.5	2.02	1.78	2.16	1.26	1.86
106.4	1.98	1.76	1.98	1.10	1.73
111.4	1.92	1.63	1.86	0.97	1.55
116.3	1.82	1.48	1.78	0.99	1.42
121.3	1.68	1.30	2.00	0.96	1.60
126.2	1.52	1.19	2.16	0.90	1.76
131.1	1.45	1.06	2.31	0.97	2.02
136.0	1.27	0.90	2.19	0.91	2.21
141.0	1.26	0.83	2.33	0.94	2.38



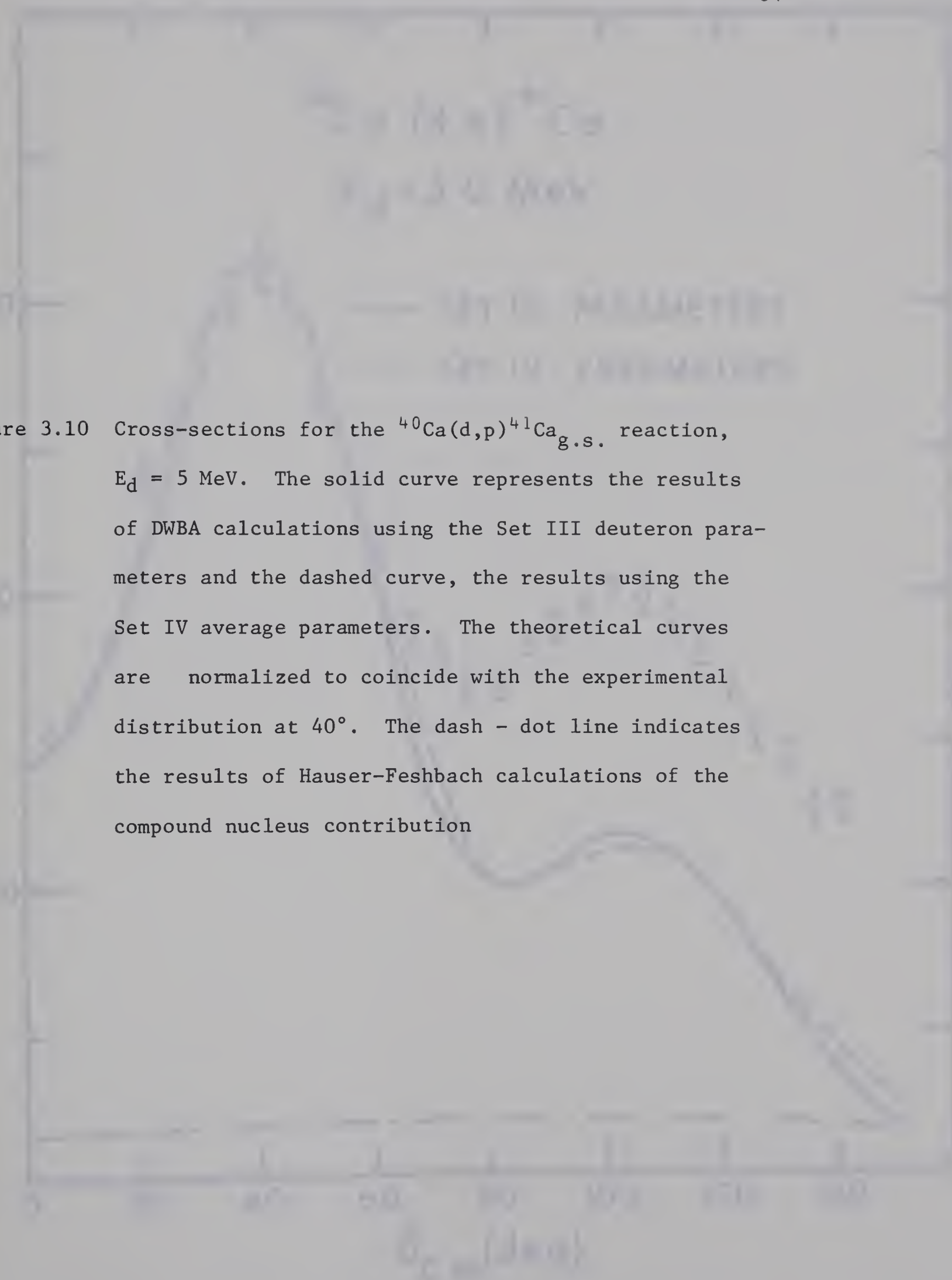


Figure 3.10 Cross-sections for the  $^{40}\text{Ca}(d,p)^{41}\text{Ca}_{\text{g.s.}}$  reaction,  $E_d = 5$  MeV. The solid curve represents the results of DWBA calculations using the Set III deuteron parameters and the dashed curve, the results using the Set IV average parameters. The theoretical curves are normalized to coincide with the experimental distribution at  $40^\circ$ . The dash - dot line indicates the results of Hauser-Feshbach calculations of the compound nucleus contribution





$^{40}\text{Ca} (d,p) ^{41}\text{Ca}$

$E_d = 5.0 \text{ MeV}$

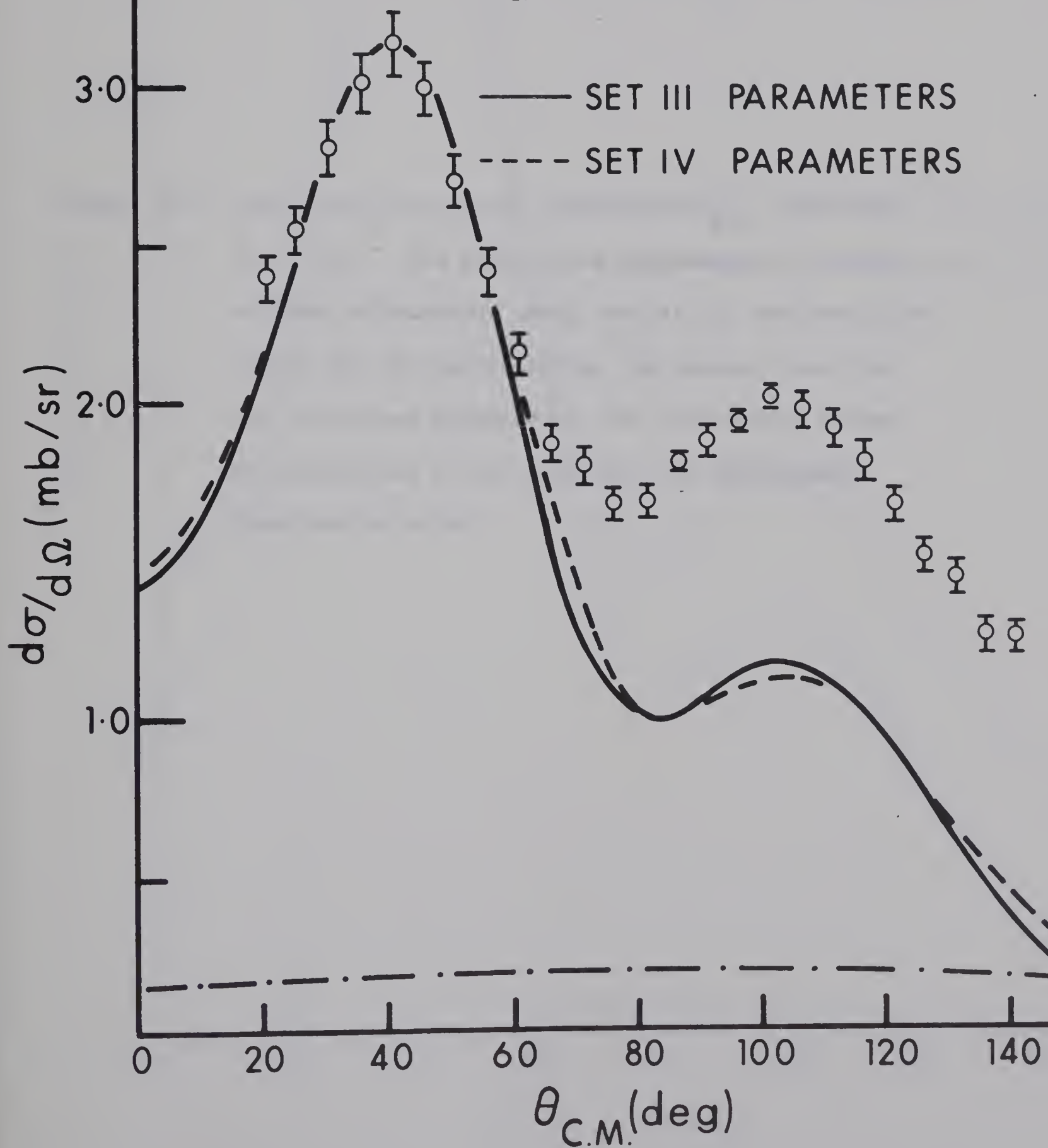




Figure 3.11 Cross-sections for the  $^{40}\text{Ca}(d,p)^{41}\text{Ca}_{g.s.}$  reaction,  $E_d = 6$  MeV. The solid curve represents the results of DWBA calculations using the Set III deuteron parameters and the dashed curve, the results using the Set IV average parameters. The theoretical curves are normalized to coincide with the experimental distribution at  $40^\circ$



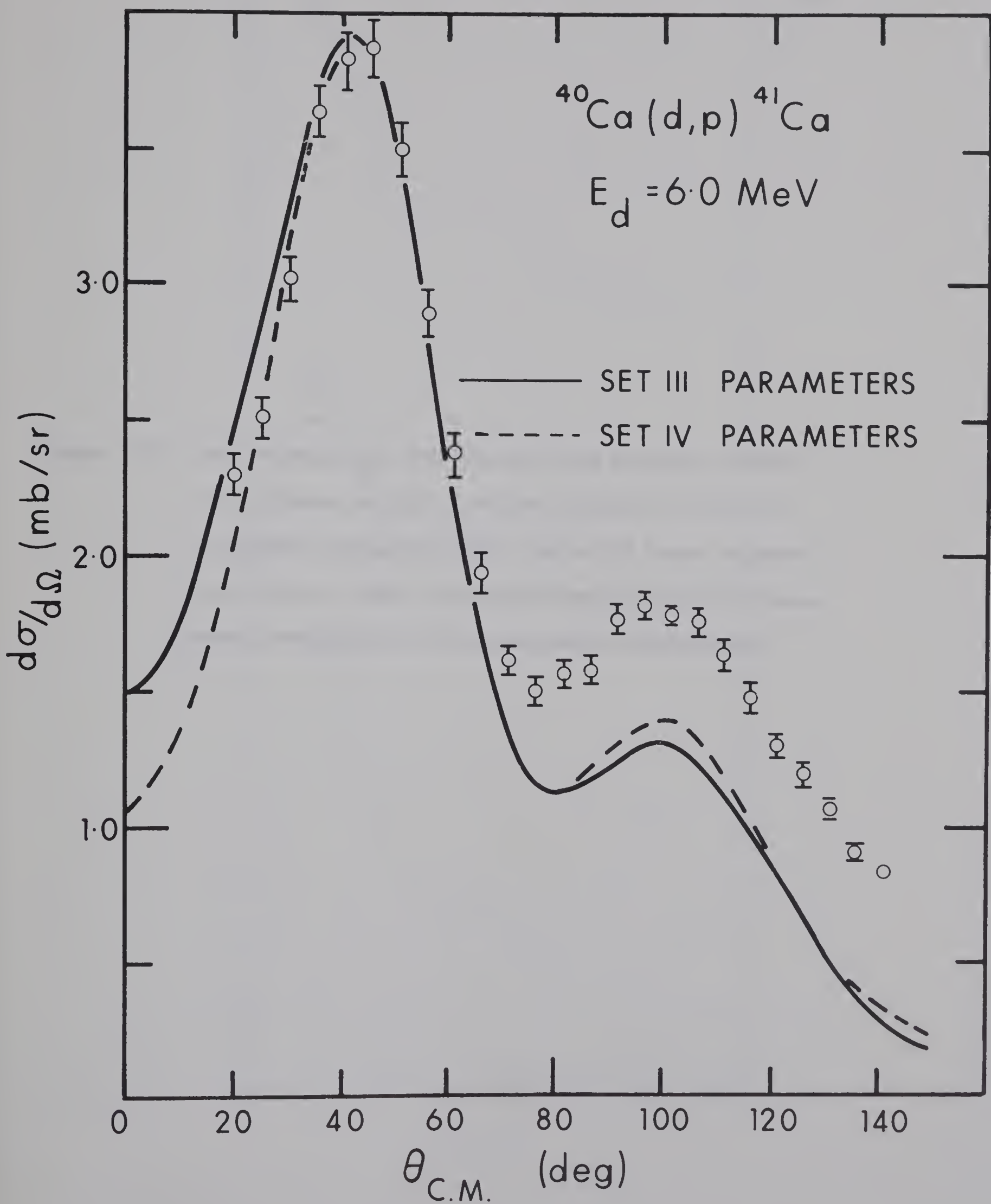
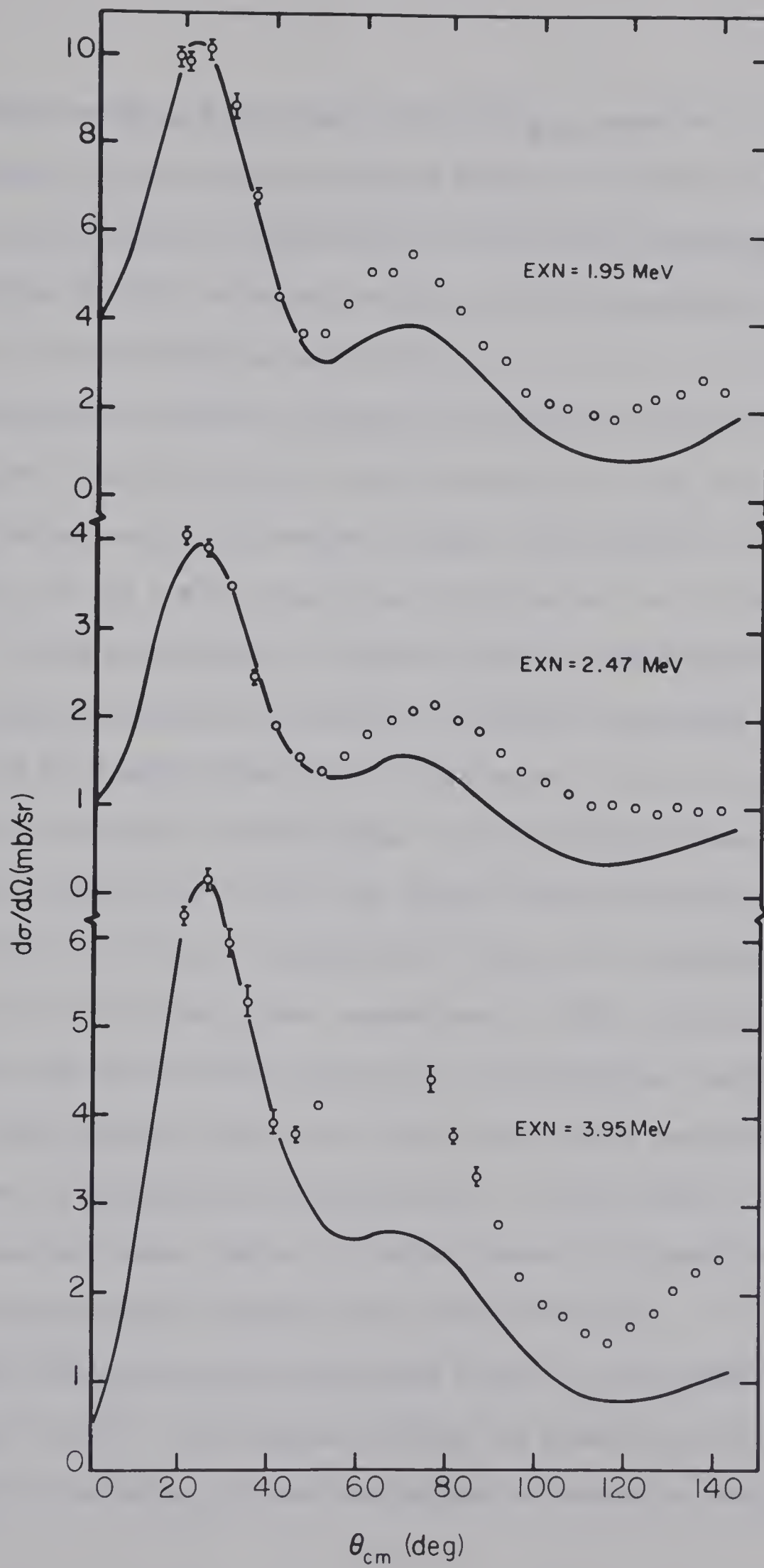






Figure 3.12 Cross-sections for the  $^{40}\text{Ca}(d,p)^{41}\text{Ca}$  reaction leading to the states at 1.95, 2.47 and 3.95 MeV in  $^{41}\text{Ca}$  for an incident energy of 5 MeV. The solid lines represent the results of DWBA calculations using the Set III parameters normalized to the experimental distributions.







of the intense background from the  $^{12}\text{C}(\text{d},\text{p})^{13}\text{C}_{\text{g.s.}}$  reaction. Also the 1.95 MeV state was not resolved from the state at 2.01 MeV in  $^{41}\text{Ca}$ . However, the 2.01 state is approximately 1/50 of the intensity of the 1.95 MeV state (Bo 57), and consequently, it is not expected to alter the shape of the distribution appreciably.

To estimate the compound nucleus contributions to these reactions, Hauser-Feshbach calculations were again carried out using the same programs referred to in the previous section. The results of these calculations for the 5 MeV ground state distribution are included in fig. 3.9. At the back angles, it appears that the contributions to the stripping distribution are of the order of 12% for the ground state at 5 MeV and 10% at 6 MeV, 7% for the 1.95 MeV state, 13% for the state at 2.47 MeV and 4% for the 3.95 MeV state. At the stripping peak, these values drop to about 5% for the 5 MeV ground state distribution and less than 4% for the other distributions. Due to the uncertainty in the accuracy of the calculations, comparisons of DWBA calculations with the data are made only for the uncorrected distributions, and the spectroscopic factors quoted also do not take into account compound nucleus contributions to the measured distributions. In this sense, the spectroscopic factors are upper limits; of course, other considerations would affect the spectroscopic factors in the other direction.

The DWBA calculations were performed using the code DWUCK written by P.D. Kunz (Ku 67). The program includes the possibility of spin-orbit terms in the potentials and the options of volume or surface





absorption (or both), zero or finite range calculations, and the inclusion of a nonlocality in the three potentials.

The deuteron potentials used were those described in the previous section that were found to fit the elastic scattering, except that various spin-orbit potentials were included in the calculations as described below. The spin-orbit potential was of the form

$$\left(\frac{\hbar}{m\pi c}\right)^2 (V_S + iW_S) \frac{\mathbf{L} \cdot \mathbf{g}}{r} \frac{d}{dr} \{1 + \exp[(r-r_0 A^{\frac{1}{3}})/a]\}^{-1}$$

Calculations were carried out in both the zero and finite range approximations, and whilst most calculations were performed with local potentials, nonlocalities were introduced in a few cases.

The captured neutron was assumed to be bound in a Woods-Saxon well. The predicted absolute cross-sections are quite sensitive to the radius of the well, increasing with increasing radius, and consequently, calculations were carried out with radii  $r_{0n} = 1.20 A^{\frac{1}{3}}$  and  $1.25 A^{\frac{1}{3}}$ . The diffuseness  $a_n$  was set equal to 0.65 F. A spin-orbit potential of 25 times the Thomas term was also included in the potential. The program adjusted the well depth to reproduce the correct binding energy of the state being considered. Table 3.8 lists the well depths found to give the required last particle separation energy for the four levels studied and for both radii.

Most of the calculations were carried out using the proton potential of Buck (Bu 63), namely  $V_p = (52.6 - 0.28 E) \text{ MeV}$ ,  $W_p = 10.6 \text{ MeV}$ ,  $R_p =$



Table 3.8

Neutron well depths in  $^{41}\text{Ca}$  in MeV

Excitation (MeV)	0.0	1.95	2.47	3.95
radius (F)				
1.20	56.1	58.6	57.6	59.3
1.25	52.8	55.1	54.2	55.3

$R_p' = 1.25 A^{\frac{1}{3}} F$ ,  $a_p = 0.65 F$  and  $a_p' = 0.47 F$ . The spin-orbit potential had the same shape parameters as the real potential with  $V_s = 8$  MeV. To test the sensitivity to the proton potential, some calculations were repeated using the average proton potential of Perey (Pe 63a) in which  $V_p = [53.3 - 0.55 E + 0.4Z/A^{\frac{1}{3}} + 27(N-Z)/A]$  MeV,  $W_p = 11.5$  MeV,  $V_s = 8.5$  MeV and the other parameters being unchanged. This latter potential is similar to the potential found to best fit the elastic scattering of protons from  $^{40}\text{Ar}$  in the energy range from 8 to 14 MeV (Le 64).

Calculations were also carried out to compare the predictions for some sets of parameters with the (d,n) distributions of Grandy (Gr 67, 68) and the neutron polarization distribution of Gedcke (Ge 67, 68). In this case, the captured proton radius was  $1.25 A^{\frac{1}{3}} F$  and the diffuseness  $0.65 F$ . The neutron parameters were those of Perey and Buck (Pe 63) with  $V_n = 46.4$  MeV,  $W_n = 9.6$  MeV,  $R_n = R_n' = 1.27 A^{\frac{1}{3}} F$ ,  $a = 0.66 F$  and  $a' = 0.47 F$ .





The radius of the spin orbit potential was slightly smaller than the real potential radius  $R_s = 1.25 A^{\frac{1}{3}} F$ ,  $a_s = 0.66 F$  and  $V_s = 7.2 \text{ MeV}$ .

The program included the provision of cutting off the contributions to the stripping from the interior of the nucleus. It was found by Lee et al., however, (Le 64), that if such a radial cut-off was included in the calculations, it was impossible to get a consistent set of spectroscopic factors for the ground, 1.95 and 2.47 MeV states. In accordance with these findings, no radial cut-off was included in the present calculations.

### Set I Parameters

As mentioned earlier, the first potentials investigated were those in which the real and imaginary shape parameters were constrained to the same, ie. the Set I parameters. The results of the calculations for the (d,p) and (d,n) ground state reactions are compared with the experimental distributions in figs. 3.13 and 3.14. The potentials with  $V \sim 80 \text{ MeV}$  were taken as representative of the various members of the Set I potentials. The proton potential was that of Buck and the captured neutron potential radius was 1.25 F. The deuteron spin-orbit potential was set equal to zero for the calculations. The theoretical distributions for the (d,p) reactions are normalized to the experimental value of  $40^\circ$  and for the (d,n) reaction at  $0^\circ$ . This will be true for all the later calculations also.



The agreement between the calculations and experiment is quite good for the (d,n) case and not quite as good for the (d,p) distributions. The agreement at 6 MeV is considerably improved for the (d,p) reaction over that at 5 MeV. We also see that the spectroscopic factors found for the ground state of  $^{41}\text{Ca}$  are reasonable, although perhaps a little lower than might be expected (0.87 and 0.80 at 5 and 6 MeV), but quite consistent with the 7 - 12 MeV values. The spectroscopic factors for the ground state of  $^{41}\text{Sc}$ , on the other hand, are not satisfactory. They exhibit a large variation with energy,  $S = 1.14, 0.91$  and  $0.81$  at 5, 6 and 6.5 MeV, respectively, and the value of 1.14 is sufficiently greater than unity, that it cannot be easily explained away in terms of experimental errors. The spectroscopic factors for the various potential sets are summarized in table 3.9 and 3.10.

The main reason for not investigating this parameter set in more detail was, as mentioned earlier, that potentials of this form were unable to fit the higher energy elastic scattering data. Apart from this, it was hoped that better agreement to the 5 MeV (d,p) distributions might be obtained with a different potential, and also we would expect more consistent spectroscopic factors.

### Set II Parameters

The results of the Set II calculations, obtained by relaxing the constraints  $r_0 = r_0'$ , and  $a = a'$  in the optical model fits, are also





shown in figs. 3.13 and 3.14. The particular calculations shown are again those for which  $V \sim 80$  MeV, with the same nucleon parameters as in the Set I calculations. Fair agreement is obtained here also for the (d,p) case and again we find that the agreement at 6 MeV is better than at 5 MeV. The spectroscopic factors are 1.03 at 5 MeV and 0.88 at 6 MeV. This would imply a variation of about 15% which would be rather surprising. The equivalent calculations for the (d,n) distributions produced confusing results. As can be seen from fig. 3.14, only the fit at 6.5 MeV is shown. This is because it was found to be impossible to get answers from the code DWUCK from the calculations at the two lower energies. Calculations with other codes produced extremely poor fits to the data at 5 and 6 MeV. The fact that the agreement to the (d,n) distribution is quite good at 6.5 MeV, but is very poor (or uncalculable using DWUCK) at 5 and 6 MeV is highly suspicious and probably indicates that the calculations are not to be trusted, rather than that the particular potential is unable to describe the deuteron wave function for the (d,n) reaction in a specific energy region. Whichever of these two alternatives is true, the potential is not useful until the exact cause of the discrepancy is determined. Nevertheless, at 6.5 MeV, the agreement is quite good and the value of 0.83 for the spectroscopic factors is reasonable.



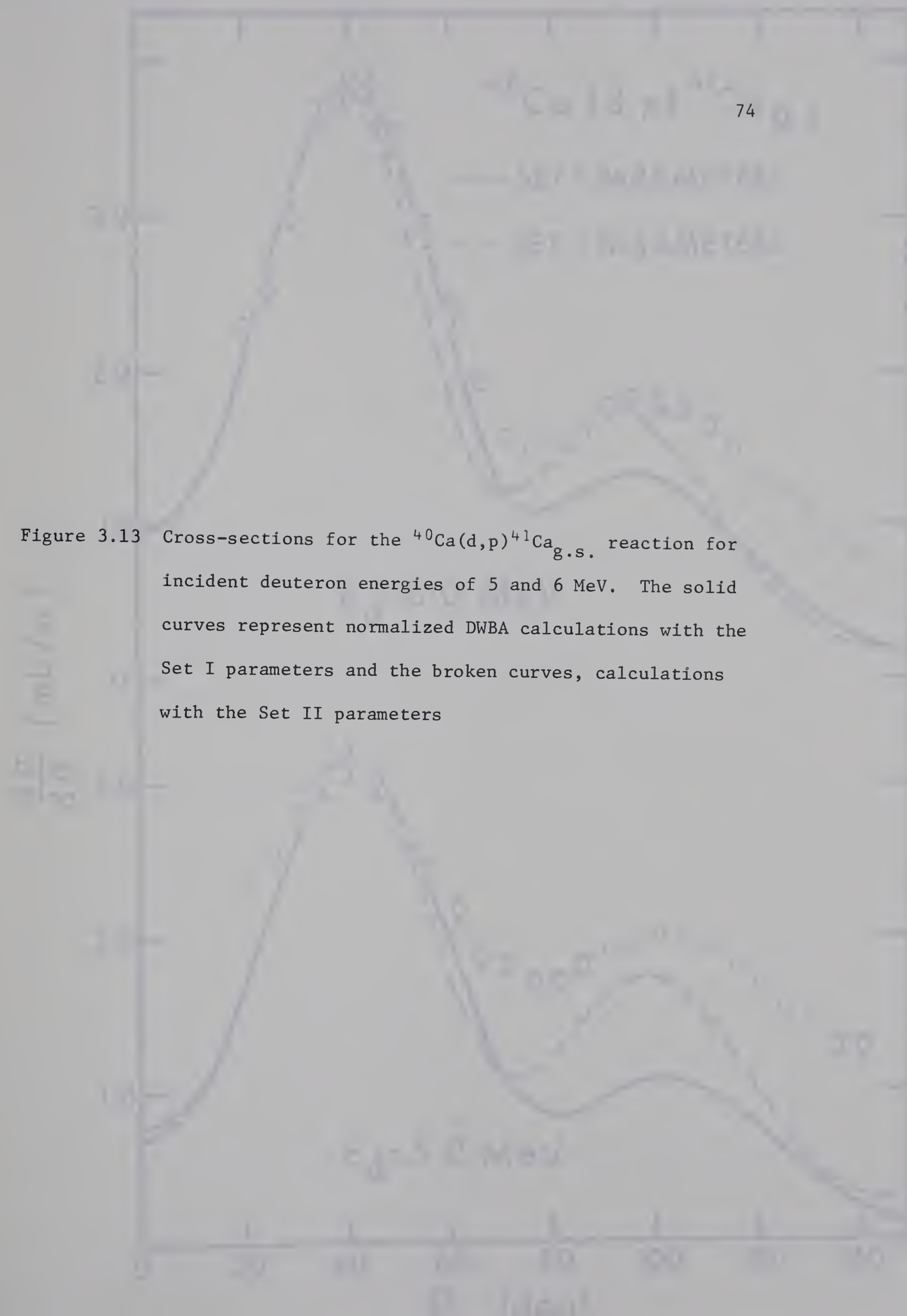
### Set III Parameters

The attempt to find a set of parameters that would fit smoothly with the higher energy parameters resulted in the Set III parameters described in section 3.2. The comparison between the calculated and experimental distributions for the (d,p) and (d,n) reactions leading to the ground states are shown in figs. 3.10, 3.11 and 3.15. Results of calculations leading to the excited states of  $^{41}\text{Ca}$  are shown in fig. 3.12. These plots are for calculations in which a spin-orbit potential of 5 MeV was included for the deuteron, the proton parameters of Buck were used and the captured particle radius was 1.25 F. The shape of the stripping distributions are, however, insensitive to the deuteron spin-orbit potential and, therefore, these fits may be compared directly with the previous ones that contained no spin-orbit terms. The agreement to the (d,p) ground state distributions are only fair, however the agreement with the excited state distributions is better. The back angles are consistently underestimated by the calculations and again it is apparent that for the ground state the fit at 6 MeV is better than at 5 MeV. This may be an indication of greater compound nucleus contributions at 5 MeV than at 6 MeV although this would imply a much larger compound nucleus contribution than that found from the Hauser-Feshbach calculations. It can also be seen that the fit to the forward side of the stripping peak is improved with this set of parameters compared to that of Sets I and II. The spectroscopic factors for the ground state reactions are given in table 3.9 for the case in which the spin-orbit



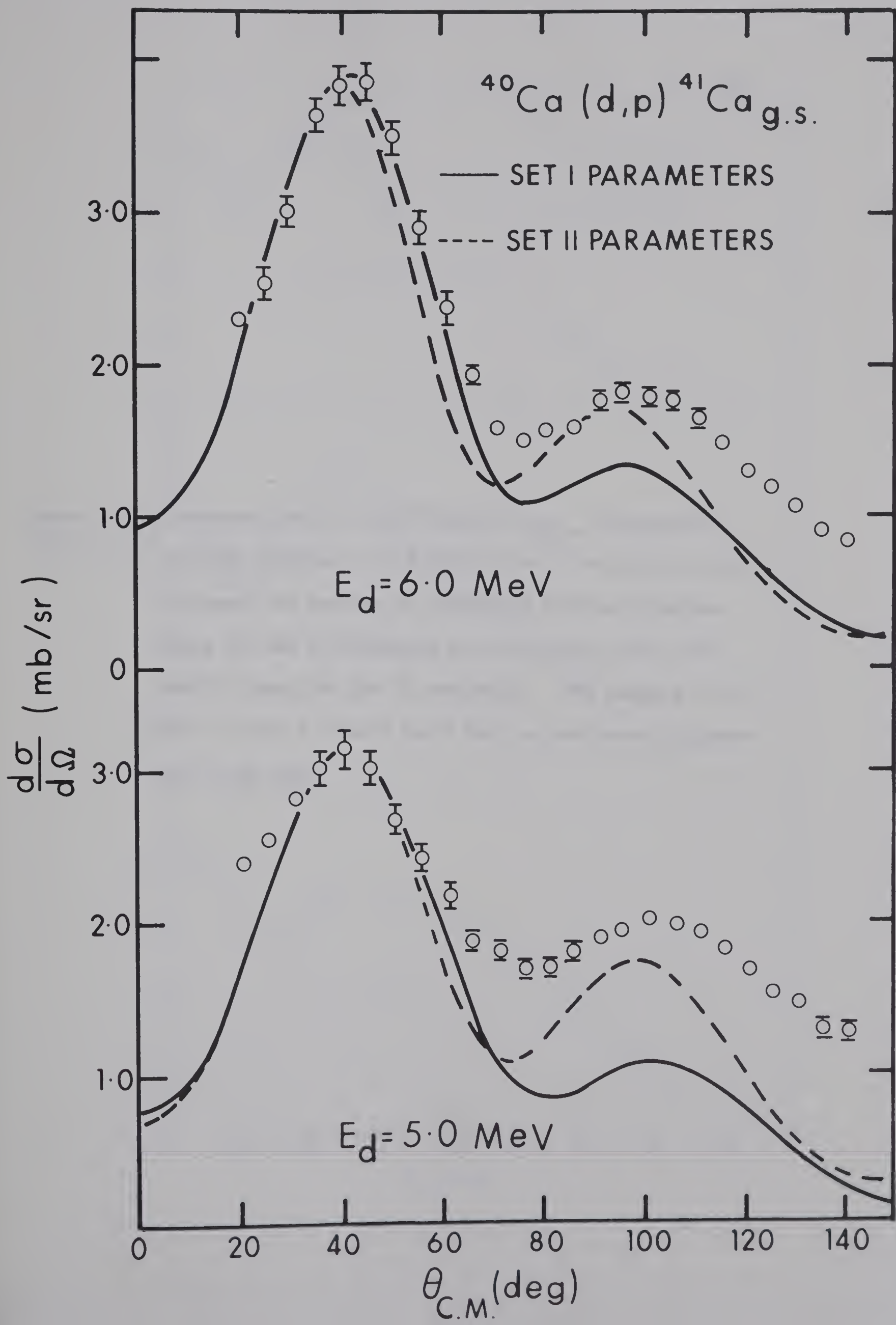


Figure 3.13 Cross-sections for the  $^{40}\text{Ca}(d,p)^{41}\text{Ca}_{\text{g.s.}}$  reaction for incident deuteron energies of 5 and 6 MeV. The solid curves represent normalized DWBA calculations with the Set I parameters and the broken curves, calculations with the Set II parameters











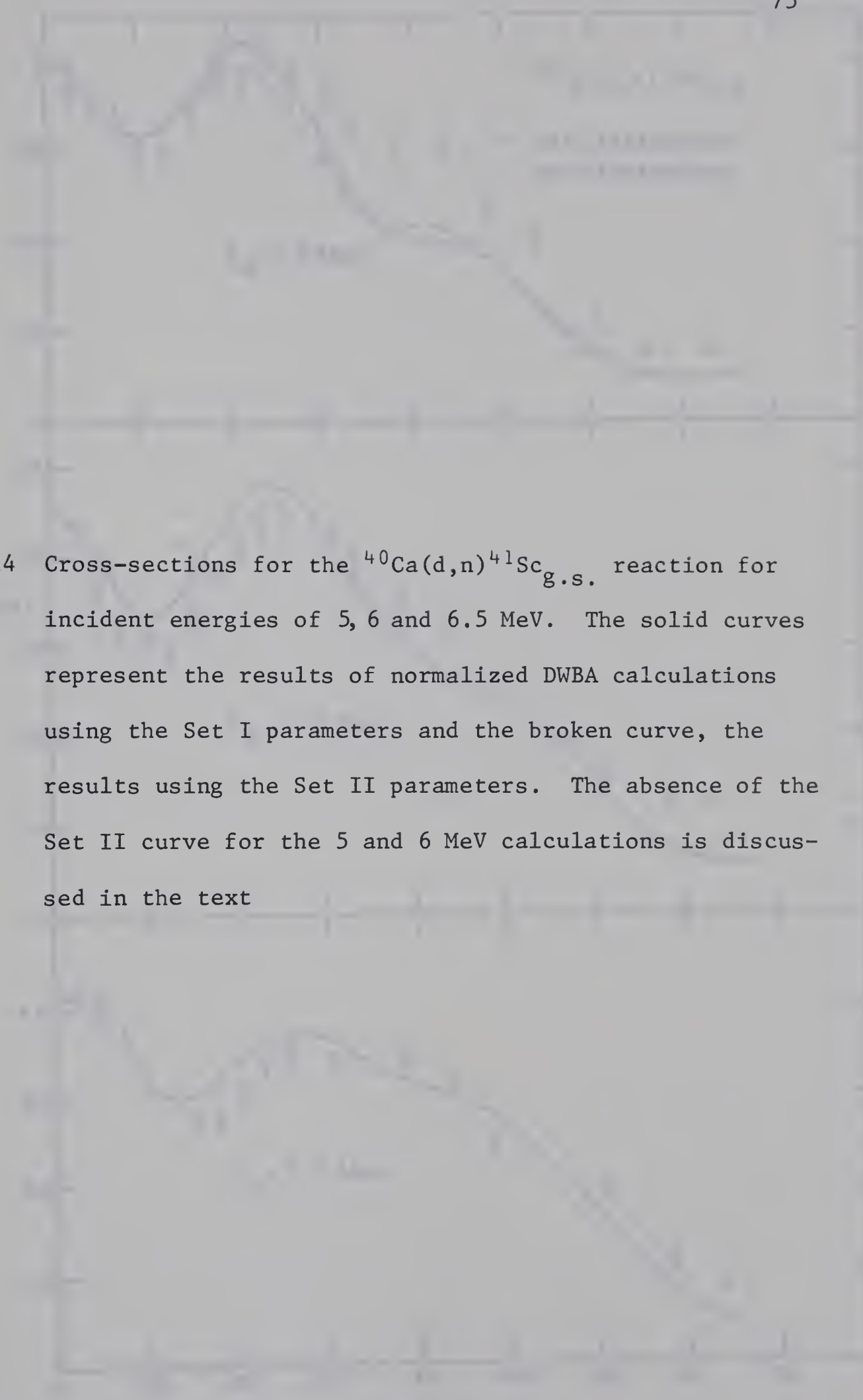


Figure 3.14 Cross-sections for the  $^{40}\text{Ca}(d,n)^{41}\text{Sc}_{g.s.}$  reaction for incident energies of 5, 6 and 6.5 MeV. The solid curves represent the results of normalized DWBA calculations using the Set I parameters and the broken curve, the results using the Set II parameters. The absence of the Set II curve for the 5 and 6 MeV calculations is discussed in the text



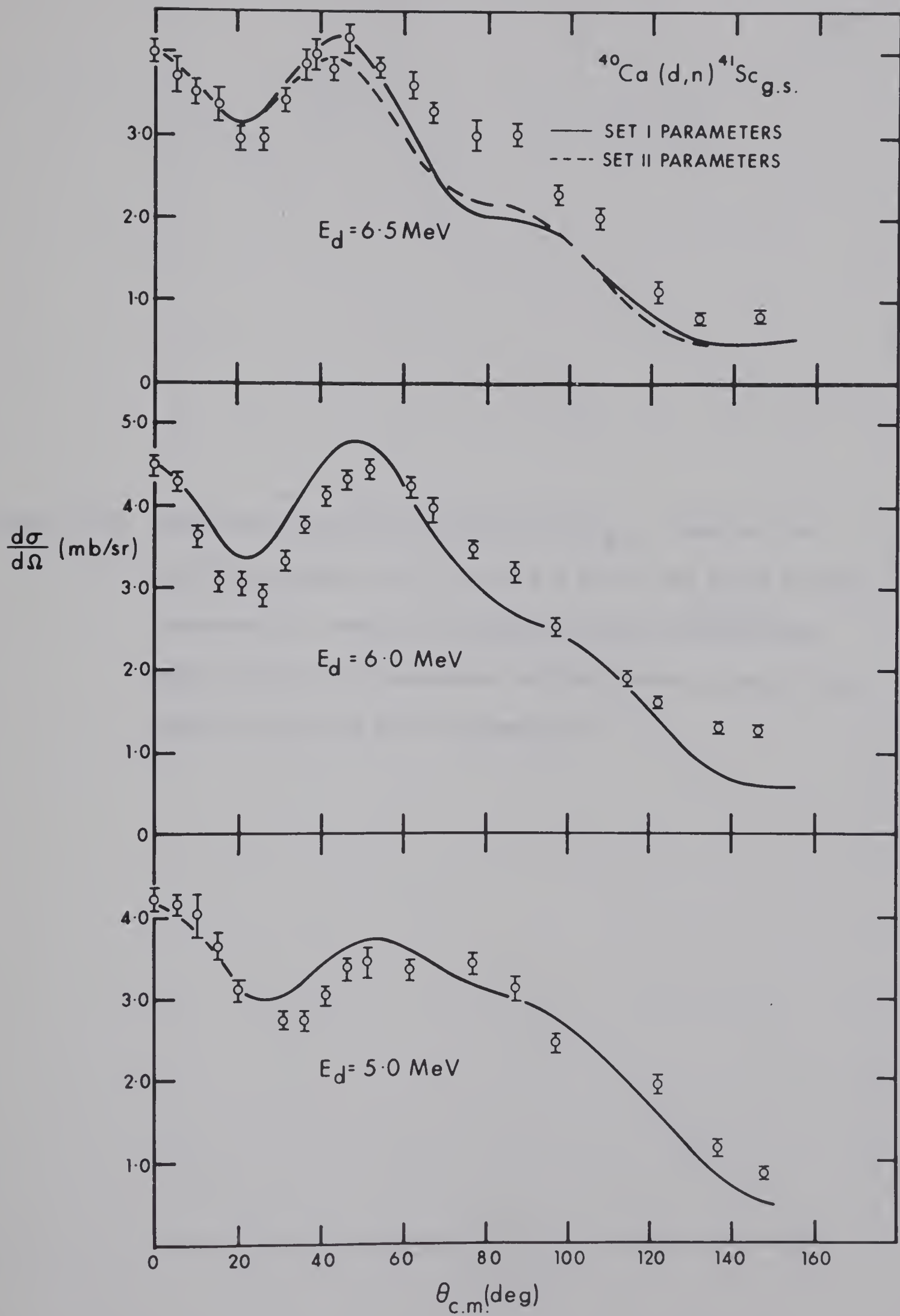


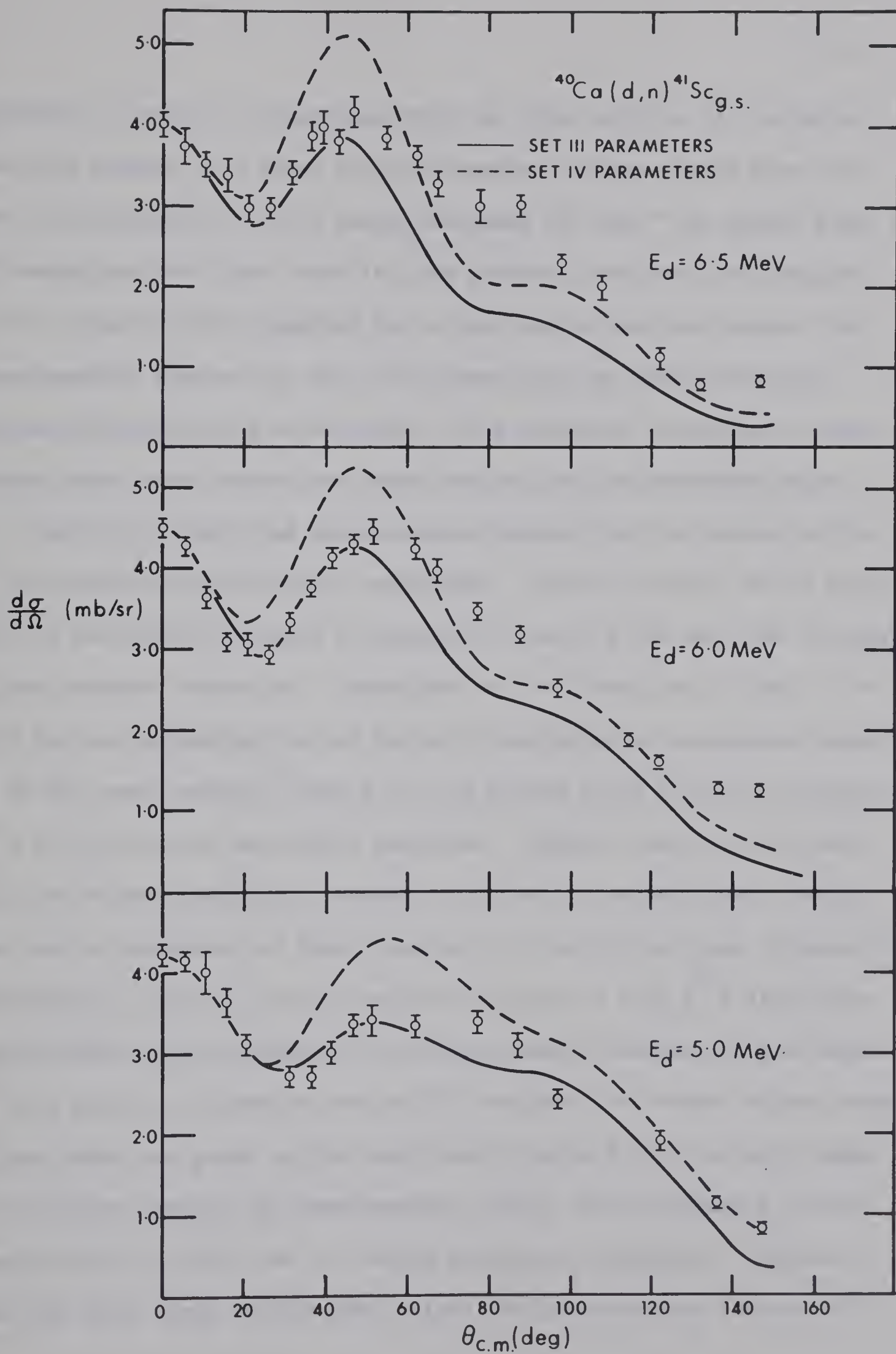




Figure 3.15 Cross-sections for the  $^{40}\text{Ca}(\text{d},\text{n})^{41}\text{Sc}_{\text{g.s.}}$  reaction for incident energies of 5, 6 and 6.5 MeV. The solid curves represent the results of normalized DWBA calculations using the Set III parameters and the broken curves, the results using the Set IV parameters









potential is zero for comparison with the other entries in the table. The most notable fact about the spectroscopic factors found from the Set III parameters is their marked decrease for the  $^{41}\text{Ca}$  ground state in comparison with that found for the previous sets and also compared to the value of unity expected for a good single particle state. The spectroscopic factors for the  $^{41}\text{Sc}$  ground state on the other hand, are not affected quite as seriously. The situation is improved considerably when other factors are taken into account as described below.

Table 3.10 lists the spectroscopic factors for the states in  $^{41}\text{Ca}$  as calculated under different conditions. All the entries in the table are for potentials in which a spin-orbit term of 5 MeV has been included in the deuteron potential. Comparison of the first line of table 3.10 with the corresponding line of table 3.9 indicates an increase of about 4% in the spectroscopic factors for the ground state with the inclusion of a 5 MeV deuteron spin-orbit potential. Similar results were found when the volume absorption potential was used in calculations. Using the proton parameters of Perey results in a further increase of about 5%. Reducing the captured neutron potential radius to  $1.20 A^{\frac{1}{3}} \text{ F}$  introduces a relatively large increase in the spectroscopic factors and the values at this point are close to, but still less than the average higher energy values which are given in the last line of table 3.10. The zero range calculations lowered the spectroscopic factor for the ground  $f_{\frac{7}{2}}$  state considerably but left the  $p$  states relatively unaltered. The fact that the zero range calculations affect the spectroscopic factors of



Table 3.9

Comparison of spectroscopic factors for the various parameter sets found to fit the elastic scattering. The particular deuteron parameters used are explained in the text. No deuteron spin-orbit potential is included in these results. The proton potential is that of Buck and does include the spin-orbit term. The captured particle potential radius is 1.25 F.

	$^{41}\text{Ca}_{\text{g.s.}}$		$^{41}\text{Sc}_{\text{g.s.}}$		
Set	5.0 MeV	6.0 MeV	5.0 MeV	6.0 MeV	6.5 MeV
I	0.87	0.80	1.14	0.93	0.81
II	1.03	0.88	-	-	0.83
III	0.62	0.69	0.79	0.82	0.83





Table 3.10

Spectroscopic factors for the states in  $^{41}\text{Ca}$  indicated,  
using the Set III and Set IV deuteron parameters and a deuteron  
spin-orbit potential of 5 MeV.

Excitation (MeV)	0.0		1.95	2.47	1.95 + 2.47	3.95
Deuteron Energy	5.0	6.0	5.0	5.0	5.0	5.0
A	0.64	0.72	0.53	0.19	0.72	0.48
B	0.67	0.76	0.54	0.21	0.75	0.48
C	0.77	0.87	0.61	0.22	0.83	0.52
D	0.55	0.65	0.53	0.20	0.73	0.49
E	0.65	0.74	0.45	0.16	0.51	0.40
F	0.74	1.11	0.66	0.24	0.90	0.49
G	0.86 $\pm$ .07		0.72 $\pm$ .12	0.32 $\pm$ .04	1.03 $\pm$ .15	0.78 $\pm$ .04

- A. Buck's proton parameters
- B. Perey's proton parameters
- C. Perey's proton parameters  $r_{0n} = 1.20$  F
- D. Buck's proton parameters Zero Range
- E. Buck's proton parameters Finite Range and non-local potentials
- F. Perey's proton parameters  $r_{0n} = 1.20$  F. Deuteron Set IV
- G. 7 - 12 MeV average spectroscopic factors



different states by different amounts implies that there may be considerable uncertainties even in relative spectroscopic factors extracted from zero range calculations. Calculations were also carried out, in which the wave functions were corrected in the local energy approximation (Pe 64) for the nonlocality of the potentials. The correction factor is given by the relation  $\phi_{NL} = [1 - \frac{1}{2} U(r) \cdot (\frac{M\beta^2}{\hbar^2})^{-\frac{1}{2}}] \phi_2$ . The nonlocality ranges were 0.54 F for the deuterons and 0.85 F for the nucleon potentials. The introduction of nonlocality into the calculations has little effect on the ground state but does reduce the spectroscopic factors for the excited state considerably. The next entry in table 3.10 gives the results for calculations with the average potential, Set IV. For these calculations, the proton potential of Perey was used and the neutron radius was  $1.20 A^{\frac{1}{3}} F$ . The spectroscopic factors are highest for this combination of potentials except for the ground state at 5 MeV and the 3.98 MeV state which are slightly reduced compared to the best fit values. Even for this set, the spectroscopic factors tend to be lower than the values found from the 7 - 12 MeV study. The large spread in values between the 5 and 6 MeV values is also rather disturbing. It is interesting that the spectroscopic factors found in the study of Hjorth et al. (Hj 65) are closer to the values found here. Whether there is any significance in this or not is speculation. There are a number of reasons why the spectroscopic factors may be in error. We know from the yield curves that the cross-section has fairly large fluctuations as a function of energy which certainly contribute to the uncertainty in the spectroscopic





factors. Apart from that there is the basic uncertainty in the determination of the absolute cross-section which is estimated at  $\pm 10\%$ . It is also possible that theoretical cross-sections calculated in this way become less reliable in the vicinity of the Coulomb barrier. Rawitscher (Ra 68b) obtained excellent agreement to the sum of the experimental cross-sections for the 2p states over the whole range from 5 - 11 MeV from a coupled channels calculation, which would seem to imply that the experimental cross-sections are not too seriously in error. On the other hand, the calculations of Rawitscher do not reproduce the elastic scattering distribution at 5 MeV, so the situation is not at all clear.

One final result from the extracted spectroscopic factors that can be compared with theory is the ratio of the single particle strength for the 1.95 MeV state to the 2.47 MeV state. The experimental value found here is 2.8 compared to the value of 2.9 from the three particle - two hole calculations of Gerace and Green (Ge 67a) and the 7 - 12 MeV experimental value of 2.3.

Little has been said about the shapes of the distributions for the different calculations because it was found that for the (d,p) distributions, they were quite insensitive to the changes discussed above. As an example, the results of the DWBA calculations corresponding to the entry A (solid line) and entry F (broken line) of table 3.10 are also plotted in figs. 3.10 - 3.11. Only minor differences in the shapes of the distributions occur and this is typical of all the potentials in table 3.10.





The average Set IV potential produced much larger deviations for the (d,n) calculations (see fig. 3.15) than was found in the (d,p) case. The agreement is consistently worse in the forward angle region with the Set IV parameters compared to the Set III parameters. On this basis, it appears that it is preferable to use in the DWBA calculations, the parameters that best fit the elastic scattering - a rather surprising result.

### 3.4 Polarization Distributions

The polarization distribution leading to the ground state of  $^{41}\text{Ca}$  are given in table 3.11 and are plotted in fig. 3.16. The error bars indicate statistical errors only and do not take into account the uncertainty in the analyzing power of the polarimeter. For comparison, the corresponding (d,n) distribution (Ge 67, 68) is also shown in the same figure. Ideally, these two distributions would have been measured at the same energy. Because of the low Q value for the (d,n) reaction, it was necessary to run at as high an energy as possible, whereas for the (d,p) experiments, it was necessary to compromise high energy with the requirement of stable accelerator operation for considerable periods of time. (A large portion of the data were taken in seven days of continuous operation). The data follow the trend of the higher energy results at 5.8, 10.0, 10.9 and 14.3 MeV (Ku 68, Be 64, Ka 65, Hj 65) in that the polarization tends to be small and negative in the forward direction, with evidence of a negative peak in the vicinity of  $100^\circ$ , although at 5 MeV the peak seems to be less



Table 3.11

 $^{40}\text{Ca}(\text{d},\text{p})^{41}\text{Ca}_{\text{g.s.}}$  polarization  $E_{\text{d}} = 5 \text{ MeV}$ 

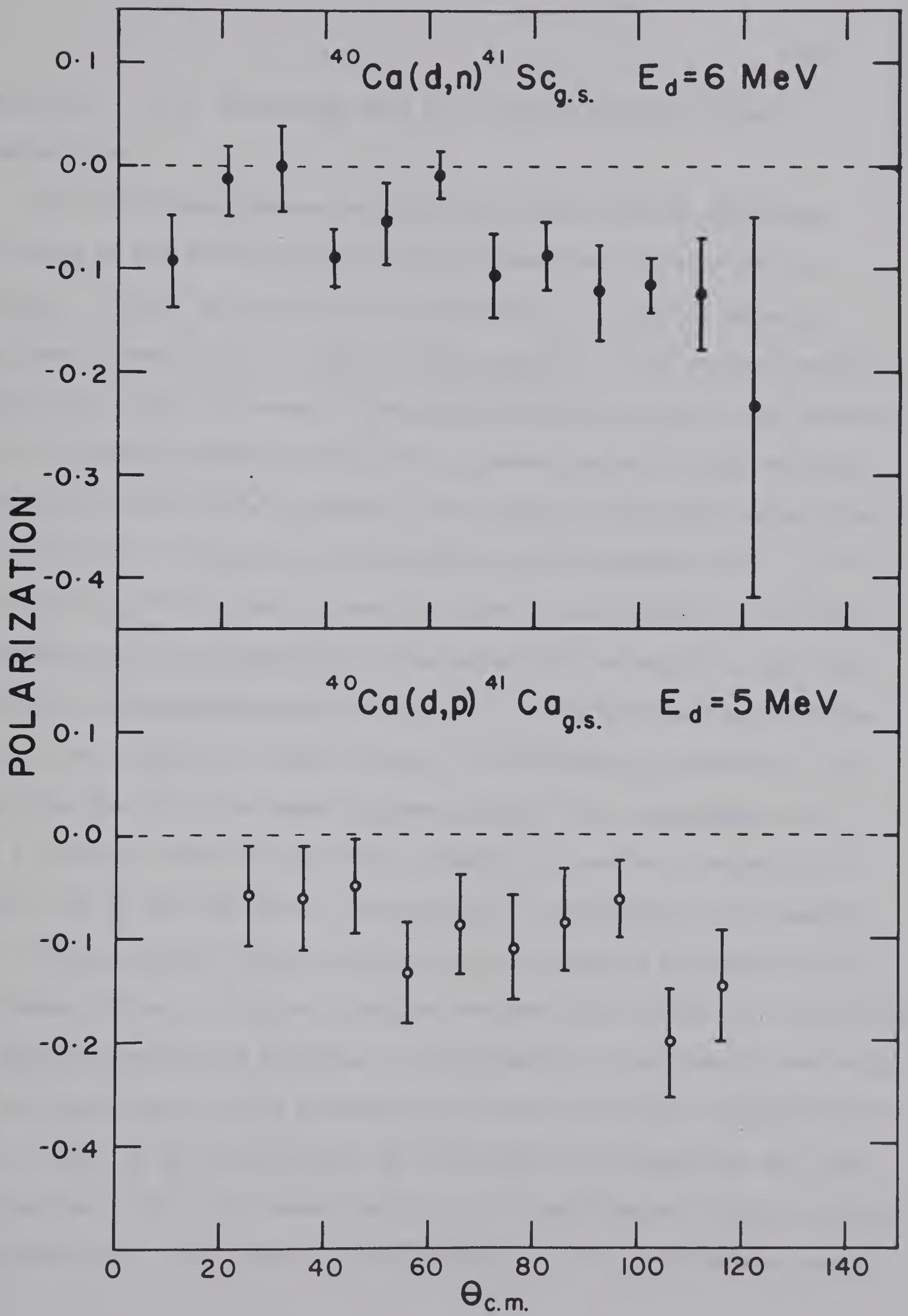
$\theta_{\text{cm}}$	$P \pm \Delta P$
25.6	- 0.057 $\pm$ 0.046
35.8	- 0.062 $\pm$ 0.049
46.0	- 0.049 $\pm$ 0.047
56.1	- 0.135 $\pm$ 0.049
66.2	- 0.087 $\pm$ 0.047
76.3	- 0.110 $\pm$ 0.051
86.3	- 0.084 $\pm$ 0.049
96.3	- 0.062 $\pm$ 0.037
106.3	- 0.201 $\pm$ 0.051
116.2	- 0.147 $\pm$ 0.054



Figure 3.16 Polarization distributions from the  $^{40}\text{Ca}(d,p)^{41}\text{Ca}$  and  $^{40}\text{Ca}(d,n)^{41}\text{Sc}$  reactions









pronounced. It is interesting that the (d,n) polarization shows a similar trend.

The proton polarization was calculated using the code DWUCK and with many of the same deuteron potentials described in the previous sections. In all of the following calculations, the proton potential was that of Buck, and the radius of the potential of the captured neutron was 1.25 F. Since the shape of the polarization distribution was insensitive to these parameters, efforts were concentrated on varying the spin-orbit part of the Set III potential, the potential parameters being given in table 3.12. It should be noticed that for the potential with  $V_s = 10$  MeV and  $W_s = 0$ ,  $W_D$  was reduced by 0.5 MeV. This change in  $W_D$  was to compensate for the introduction of the spin-orbit potential in the calculation of the deuteron elastic scattering. As the polarization distribution is not sensitive to small changes in the potential parameters, the fact that the fit is no longer optimum is not of any consequence. The No. 4 potential uses the spin-orbit potential of the No. 4 potential of Hjorth (Hj 65) but the rest of the parameters correspond to our standard set. This spin-orbit term was chosen partly because it provided the best agreement to the 14.3 MeV polarization data and partly because it introduced an imaginary spin-orbit potential. The agreement to the elastic scattering is no longer such that the spin-orbit part could be easily compensated for, but in light of the insensitivity of the results it is doubtful that this is important. Fig. 3.17 shows the fit to the polarization data and angular distributions. In all cases, it can be seen that the calculations predict



Table 3.12

Deuteron optical model parameters used for polarization calculations

Set No.	V MeV	$r_0$ F	a F	W MeV	$r_0'$ F	a' F	$V_s$ MeV	$W_s$ MeV	S
1	110	1.03	0.92	9.8	1.64	0.53	0.0	0.0	0.62
2	110	1.03	0.92	9.8	1.64	0.53	5.0	0.0	0.64
3	110	1.03	0.92	9.3	1.64	0.53	10.0	0.0	0.64
4	110	1.03	0.92	9.8	1.64	0.53	8.36	3.59	0.73

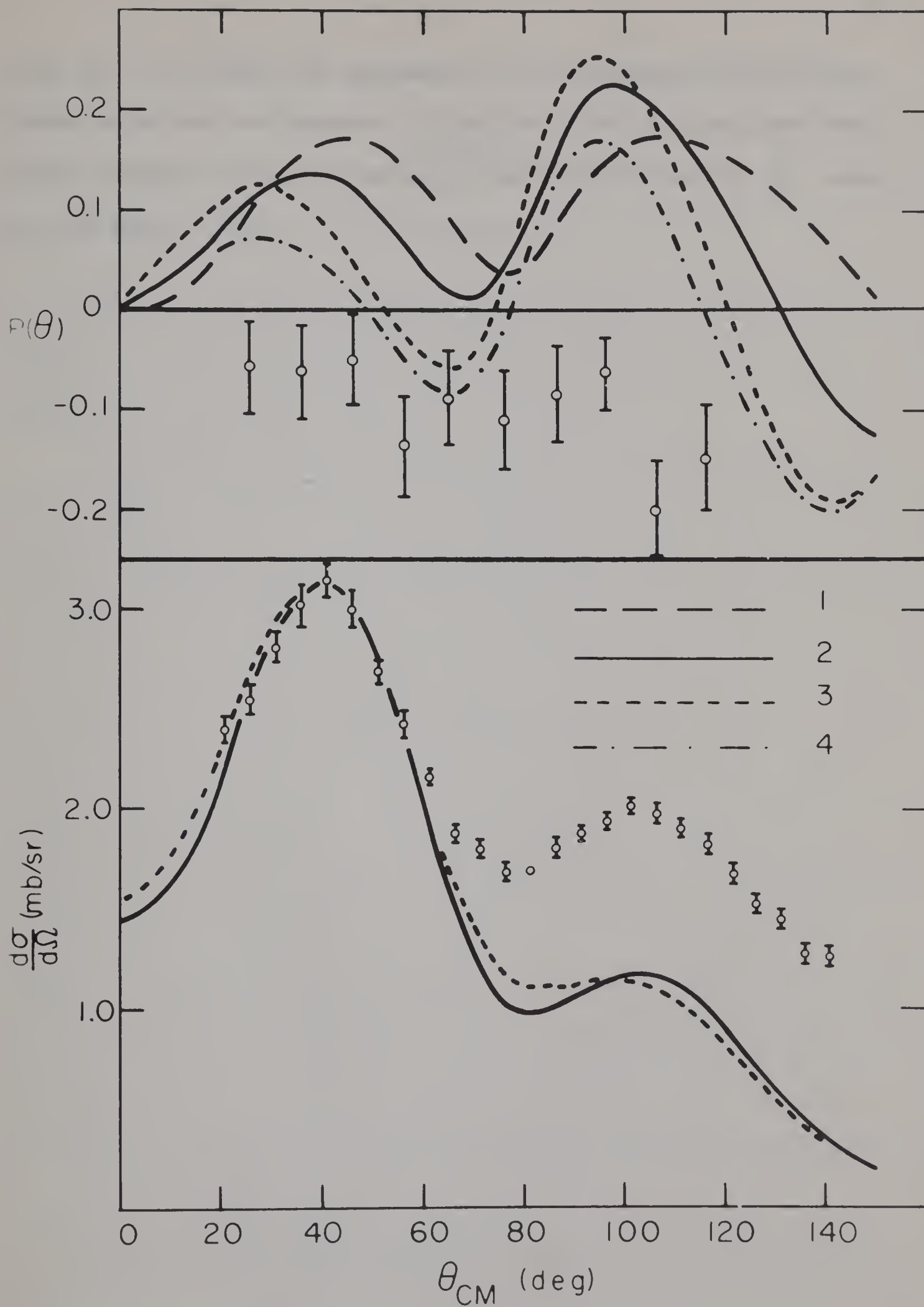






Figure 3.17 The proton polarization and angular distribution from the  $^{40}\text{Ca}(d,p)^{41}\text{Ca}_{g.s.}$  reaction at 5 MeV. The indicated errors are statistical only. The curves represent the result of DWBA calculations, the numbers refer to the potentials of table 3.12. For the sake of clarity, the angular distributions corresponding to sets 1 and 4 have been omitted







such as  $\ell = 1$ , where the agreement to the stripping distributions tends to be more satisfactory. With this in mind, plans have been made to measure the polarization of the protons from the  $\frac{3}{2}^-$  state at 1.95 MeV in  $^{41}\text{Ca}$ .





## CHAPTER 4

### CONCLUSIONS

Except for the serious disagreement between the polarization results and DWBA calculations, the results of the series of experiments described in this report are quite satisfying.

As expected, a number of sets of deuteron parameters were found that gave good fits to the elastic scattering, even though the searches were by no means exhaustive. Some of the sets (Set I) were rejected on the basis of not being able to fit the higher energy data with closely related parameters, while others (Set II), for rather obscure reasons, were unable to fit the (d,n) distributions at lower energies. Potentials were found (Set III) that did fit in fairly smoothly with the higher energy parameters. It was also possible to find a set of potentials (Set IV) that gave acceptable agreement to the whole range of elastic scattering data from 5 to 14.3 MeV only allowing the well depths to change for each potential. Furthermore, the values of the well depths did not vary widely over the whole range of energies. The parameters of this potential do not differ appreciably from the Z<sup>2</sup> potential of Bassel (Ba 64) but significantly improve the agreement to the lower energy data.

Using measured deuteron optical potentials and average proton



potentials we have found fair agreement between DWBA calculations and experimental proton distributions from some of the low lying states of  $^{41}\text{Ca}$  that show strong single-particle characteristics. The spectroscopic factors were found to be lower than would be expected on the basis of a single particle outside an inert core, and also lower than the values found from the 7 to 12 MeV study (Le 64). On the other hand, our values compare more favourably with the values found at 14.3 MeV (Hj 65). It is quite possible that in the present lower energy region, part of the error could be accounted for by the fluctuations in the cross-sections, and certainly there is the possibility of errors in the determination of the absolute cross-section. The uncertainty in the spectroscopic factors is further complicated by the coupled channels calculations of Rawitscher (Ra 67, 68a, 68b) who found excellent agreement to our absolute cross-sections but poor agreement to the measured elastic scattering distributions. This latter result is possibly due to the neglect of deuteron breakup in the calculations. Rawitscher has suggested that this effect could be investigated by performing a similar series of experiments on  $^{48}\text{Ca}$ , where the breakup effects should be unchanged but the stripping cross-sections even larger. Plans are underway to perform such experiments at this laboratory in the very near future.

The polarization results, while in agreement with the higher energy data, are in complete disagreement with the results of DWBA calculations. The calculations at 5 MeV are relatively insensitive



to the spin-orbit potential and also to the shape of the deuteron potential as can be determined from the various sets investigated in this report. This could possibly indicate the need for a tensor type of spin-orbit coupling although this was found unnecessary to fit the elastic scattering polarization measurements at 22 MeV (Ra 63). The BHMM theory (Ma 67) comes closer to fitting the polarization data at higher energies, which may indicate that modifications of the DWBA theory are required.

Whatever the ultimate answer may be, it is hoped that the experiments described here and the related neutron experiments will eventually contribute to a better understanding of the reaction processes.





## REFERENCES

- Al 66 J.L. Alty, L.L. Green, G.D. Jones and J.F. Sharpey-Schafer, Nucl. Phys. 86 (1966) 65
- Au 63 N. Austern, in Fast neutron physics, Vol. II ed. by J.B. Marion and J.L. Fowler (Interscience Publishers, New York, 1963) and references contained therein
- Ba 64 R.H. Bassel, R.M. Drisko, G.R. Satchler, L.L. Lee, Jr., J.P. Schiffer and B. Zeidman, Phys. Rev. 136 (1964) B960
- Ba 66 A.C.L. Barnard, J.B. Swint and T.B. Clegg, Nucl. Phys. 93 (1967) 164
- Ba 67a J.M. Bang and C.A. Pearson, Nucl. Phys. A100 (1967) 1
- Ba 67b J.M. Bang, C.A. Pearson and L. Pócs, Nucl. Phys. A100 (1967) 24
- Be 63 R. Beurtey et al., Compt. rend. 256 (1963) 922
- Be 63a R. Beurtey et al., Compt. rend. 257 (1963) 1477
- Be 64 R.W. Bercaw and F.B. Shull, Phys. Rev. 133 (1964) B632
- Bo 57 C.K. Bockelman and W.W. Buechner, Phys. Rev. 107 (1957) 1366
- Bo 62 E. Boschitz, in Proceedings of the Conference on Direct Interactions and Nuclear Reaction Mechanisms, Padua, 1962 (Gordon and Breach Science Publishers, Inc., New York, 1963)
- Bu 50 S.T. Butler, Phys. Rev. 80 (1950) 1095
- Bu 51 S.T. Butler, Proc. Roy. Soc. (London) A208 (1951) 559
- Bu 52 S.T. Butler, Phys. Rev. 88 (1952) 685
- Bu 57 S.T. Butler, Phys. Rev. 106 (1957) 272
- Bu 63 B. Buck, Phys. Rev. 130 (1963) 712
- Bu 65 S.T. Butler, Nature 207 (1965) 1346



- Bu 67 S.T. Butler, R.G. Hewitt, B.H.J. McKellar and R.M. May, Ann. of Phys. 43 (1967) 282  
S.T. Butler, R.G.L. Hewitt and J.S. Truelove, Phys. Rev. 162 (1967) 1061
- Co 67 E. Coffou and L.J.B. Goldfarb, Nucl. Phys. A94 (1967) 241
- Da 68 N. Davison, to be published
- Di 65 J.K. Dickens and F.G. Perey, Phys. Rev. 138 (1965) 1080
- Di 65a J.K. Dickens and F.G. Perey, Phys. Rev. 138 (1965) 1083
- Du 67 J.S. Duval, Jr., A.C.L. Barnard and J.B. Swint, Nucl. Phys. 93 (1967) 164
- Ev 61 J.E. Evans, Nucl. Phys. 27 (1961) 41
- Ge 67 D.A. Gedcke, Ph.D. Thesis, University of Alberta (1967)
- Ge 67a W.J. Gerace and A.M. Green, Nucl. Phys. 93 (1967) 110
- Ge 68 D.A. Gedcke, S.T. Lam, S.M. Tang, G.M. Stinson and J.T. Sample, to be published
- Gr 67 T.B. Grandy, Ph.D. Thesis, University of Alberta (1967)
- Gr 68 T.B. Grandy, W.J. McDonald, W.K. Dawson and G.C. Neilson, submitted for publication in Nuclear Physics
- Gu 66 D.P. Gurd, M.Sc. Thesis, University of Alberta (1966)
- Gu 68a D.P. Gurd, G. Roy and H.G. Leighton, Nucl. Inst. and Meth., in press
- Ha 64 E.C. Halbert, Nucl. Phys. 50 (1964) 353
- Hj 65 Sven A. Hjorth, J.X. Saladin and G.R. Satchler, Phys. Rev. 138 (1965) B1425
- Ho 63 P.E. Hodgson, The Optical Model of Elastic Scattering, Oxford University Press (1963)
- Jo 67 R.C. Johnson and F.D. Santos, Phys. Rev. Lett. 19 (1967) 364





- Ka 65 S. Kato, N. Takahashi, M. Takeda, T. Yamazaki and S. Yasukawa, Nucl. Phys. 64 (1965) 241
- Ku 67 P.D. Kunz, private communication
- Ku 68 K.A. Kuenhold, P.L. Beach, G.A. Bokowski and T.R. Donoghue, Bull. Am. Phys. Soc. 13 (1968) 116
- Le 64 L.L. Lee, Jr., J.P. Schiffer, B. Zeidman, G.R. Satchler, R.M. Drisko and R.H. Bassel, Phys. Rev. 136 (1964) B971
- Le 66 J.C. Legg, H.D. Scott and M.K. Mehta, Nucl. Phys. 84 (1966) 398
- Le 67 H.G. Leighton, G. Roy, D.P. Gurd and T.B. Grandy, Bull. Am. Phys. Soc. 12 (1967) 682
- Le 68a H.G. Leighton, G. Roy, D.P. Gurd and T.B. Grandy, Nucl. Phys. A109 (1968) 218
- Le 68b H.G. Leighton, G. Roy and D.P. Gurd, submitted for publication in Nuclear Physics
- Ma 65 R.M. May, Nature 207 (1965) 1348
- Ma 67 R.M. May and J. Truelove, Ann. of Phys. 43 (1967) 322
- Mo 65 S.J. Moss and W. Haeberli, Nucl. Phys. 72 (1965) 417
- Pe 62 F.G. Perey and B. Buck, Nucl. Phys. 32 (1962) 353
- Pe 63a F.G. Perey, Phys. Rev. 131 (1963) 745
- Pe 63b C.M. Perey and F.G. Perey, Phys. Rev. 132 (1963) 755
- Pe 64 F.G. Perey and D. Saxon, Phys. Lett. 10 (1964) 107
- Pe 66a F.G. Perey, page 191 in Proceedings of the 2nd International Symposium on Polarization Phenomena of Nucleons (Karlsruhe, 1965), P. Huber and H. Schopper (editors)
- Pe 66b C.M. Perey and F.G. Perey, Phys. Rev. 152 (1966) 923
- Pe 66c C.A. Pearson and M. Cóz, Nucl. Phys. 82 (1966) 533; *ibid* 82 (1966) 545; Ann. of Phys. 39 (1966) 199
- Pe 67 F.G. Perey and G.R. Satchler, Nucl. Phys. A97 (1967) 515





- Ra 63 J. Raynal, Phys. Lett. 7 (1963) 281
- Ra 67 G. Rawitscher, private communication
- Ra 68a G. Rawitscher, Phys. Rev. 163 (1967) 1223
- Ra 68b G. Rawitscher, Phys. Rev. Lett., in press
- Ro 62 L. Rosen, P. Darriulat, H. Faraggi and A. Garin, Nucl. Phys. 33 (1962) 458
- Ro 65 L. Rosen, Jerome G. Beery, A.S. Goldhaber and E.A. Auerbach, Ann. of Phys. 34 (1965) 96
- Ro 66 L. Rosen, page 253 in Proceedings of the 2nd International Symposium on Polarization Phenomena of Nucleons (Karlsruhe, 1965), P. Huber and H. Schopper (editors)
- Ro 67 G. Roy, D. Gedcke, H.G. Leighton, S.T. Lam and D.P. Gurd, Bull. Am. Phys. Soc. 12 (1967) 1183
- Sa 64 G.R. Satchler, Nucl. Phys. 55 (1964) 1
- To 61 W. Tobocman, Theory of Direct Nuclear Reactions, (Oxford University Press, New York, 1961) and references contained therein
- To 68 M.A.A. Toosi and E.V. Ivash, to be published
- Yu 67 T.J. Yule and W. Haeberli, Phys. Rev. Lett. 19 (1967) 756





**B29887**